Controls on the Sediment Geochemistry of a Low-Oxygen Precambrian Analogue

by

Kathryn I. Rico

A dissertation submitted in partial fulfillment
of the requirements for the degree of
Doctor of Philosophy
(Earth and Environmental Sciences)
in the University of Michigan
2019

Doctoral Committee:

Professor Nathan D. Sheldon, Chair
Professor Joel D. Blum
Professor G. Allen Burton, Jr.
Associate Professor Rose M. Cory
Associate Professor Greg Dick

Kathryn I. Rico

krico@umich.edu

ORCID iD: 0000-0003-2761-8663

ACKNOWLEDGEMENTS

First, I would like to thank my advisor, Nathan Sheldon, for taking me on as a student, providing me excellent mentorship and advice, and supporting me not just in terms of my career, but also in my passion for DEI-related service. I would also like to thank my committee members—Joel Blum, Greg Dick, Rose Cory, and Allen Burton—for their encouragement and constructive feedback, and my co-authors—Timothy Gallagher, Anthony Chappaz, and Lauren Kinsman-Costello—for their expertise and helpful comments that made this dissertation possible.

Thank you to all of the members of the Sheldon, Hendy, and Smith labs who have provided both professional and personal advice over the years, especially Molly Ng, Bekah Stein, Becca Dzombak, Xiaojing Du, Yi Wang, and Kelly Matsunaga. Thank you to those who helped me in the lab: Clarissa Crist, Charlotte Connop, Maggie Hammond, Amelia Jelic, Lora Wingate, Sara Nedrich, Laura Motta Medina, and Aaron Kurz. I want to thank those who had the painstaking task of joining me in field work to sample the stinkhole: Sharon Grim, Judith Klatt, Matthew Medina, and the dive team of NOAA GLERL—Russ Green, John Bright, Phil Hartmeyer, Stephanie Gandulla, Wayne Lusardi, and Tane Casserley. I would like to acknowledge the funding sources that supported my research: the National Science Foundation, the Geological Society of America, the University of Michigan Rackham Graduate School, and the Department of Earth and Environmental Sciences. I would like to thank my fellow graduate students in the Department of Earth and Environmental Sciences for many, many laughs on this

incredible journey, especially Adrianna Trusiak, Alex Tye, Derek Smith, Tristan Childress, Jenny Bowen, Meredith Calogero, YoungJae Kim, and Meg Veitch. Cheers to the “Gneiss Goal” paleo soccer team for a great winter/spring, and for trusting me as a goalie. I want to thank my fellow Sacnistas of SACNAS@UMich for providing me with a powerful sense of community. Thank you to my non-academic friends for helping to keep me sane, namely Dustin Fowler, Arielle Torres, and LeakyChat. Thank you to my family for all of your love and compassion for the past five years, but especially to Mom and Dad, my brother Danny, my soul sister Lori, and Margie and Nick Font. Finally, thank you to Eric Font for your never-ending patience with me, for being my rock each day, and for being an excellent father to BeeBee.

TABLE OF CONTENTS

LIST OF TABLES

LIST OF FIGURES

LIST OF APPENDICES

ABSTRACT

With early life presumed to have evolved in ancient oceans and lakes, identifying the availability of oxygen (e.g. redox chemistry) in these environments is necessary to establish the environmental conditions required for early biosphere evolution. However, the sediments of ancient oceans are the only relics of their existence, making sediment geochemical analyses critical tools for analyzing ancient biogeochemistry. In particular, the geochemistry of elements that are sensitive to oxygen (e.g. redox-sensitive metals, such as iron, manganese, and molybdenum) have proven useful for considering the biogeochemical cycling of modern environments. Subsequently, these geochemical tools have been considered robust proxies for identifying the redox chemistry of ancient systems such as Proterozoic (~0.5–2.3) oceans, wherein microbial life diversified and eukaryotic life evolved with limited atmospheric and aquatic oxygen. This dissertation uses a Proterozoic ocean analogue—the Middle Island Sinkhole (MIS)— to characterize the sediment geochemistry of a modern low-oxygen aquatic environment, and consider implications for the biogeochemical cycling of ancient oceans and lakes. This is achieved by 1) testing various metal redox proxies in an iron-rich environment (such as is inferred for Proterozoic oceans), and 2) assessing how the presence of a cyanobacterial microbial mat in MIS impacts macronutrient and metal burial in sediments. In **Chapter II**, I explore macronutrient and iron geochemistry in MIS sediments and a fully oxygenated Lake Huron control site (LH). Differences in redox between the two locales drive the enhanced burial of macronutrients in MIS, with iron speciation results consistent with known

water chemistry: MIS is ferruginous and LH is oxic. Given that iron speciation in MIS is only recording a small portion of the water column, these results indicate that we must take caution when using iron geochemistry to interpret water column redox in the fossil record. In **Chapter III**, I use sediment redox-sensitive trace metal contents and microbial community composition in MIS and LH to consider how trace metals do or do not reflect the presence of a microbial mat. Results indicate that bulk sediment trace metal abundance cannot be used as a biosignature for the community composition of microbial mats in the analogue site. Additionally, I establish that the relationships between trace metals and organic carbon in MIS and LH are not consistent with our expectations based on their use as paleo-redox and paleo-productivity proxies. Therefore, this work impacts how we use proxy metals to interpret redox chemistry within the fossil record. In **Chapter IV**, I compare the sediment geochemistry of MIS to that of Proterozoic lake sediment—the Nonesuch Formation (~1.1 billion years old)—in order to determine the redox chemistry of this Proterozoic lake, and to gauge whether or not the abundance of redox-sensitive metals can help to elucidate biological productivity or atmospheric oxygen levels. Iron geochemistry describes fluctuating oxic and anoxic redox chemistry within the Nonesuch Formation, with molybdenum and uranium covariation confirming that euxinia is not necessary for moderate molybdenum burial. Altogether, the comparison of Nonesuch Formation to the modern analogue data indicates that elemental abundance is unlikely to record atmospheric oxygen, with no clear indicator for abundant biological productivity. Taken together, these results demonstrate that we need critical evaluations of metal burial mechanisms in modern ferruginous environments before we can confidently use these metals as proxies to constrain paleoenvironmental biogeochemical cycling.

CHAPTER I

Introduction

The redox chemistry of aquatic paleoenvironments is directly related to the availability of macronutrients (*e.g.*, carbon and nitrogen) and micronutrients (*e.g.*, iron and molybdenum) in the biosphere. Therefore, identifying the redox chemistry of ancient aquatic systems is critical for understanding biogeochemical cycling in the geologic record and the co-evolution of life and Earth. The three common redox states include oxic conditions and two types of anoxic conditions: euxinic, defined by the presence of sulfide, and ferruginous conditions, which lack sulfide and instead are enriched in dissolved iron. One of the mechanisms by which redox chemistry is explored in modern and ancient systems is via metal proxies. With sensitivity to oxygen and sulfide availability, and relevance to micronutrient availability and biological productivity, the metal geochemistry of ancient sediments can help us to understand the diversification and evolution of life through time. Iron cycling in aquatic systems has been well characterized across a variety of different redox regimes, making iron geochemistry a robust proxy for constraining system-wide redox chemistry (*e.g.*, Figure 1.1). In addition, different trace metals respond to changes in redox and biological productivity in various ways, providing a more nuanced interpretation of aquatic redox chemistry, often at a smaller scale. Altogether, known burial mechanisms for iron (Fe) and trace metals allow these elements to be useful tools for examining the redox chemistry of ancient environments.

1.1 Constraining Paleoenvironmental Redox Chemistry Using Metals

1.1.1 Iron Speciation

Given its high abundance in aquatic systems, and sensitivity to large-scale redox transformations, Fe geochemistry is considered to be one of the most robust tools for understanding the redox chemistry of modern and ancient aquatic environments (Raiswell and Canfield, 2012; Raiswell et al., 2018). Therefore, techniques for the speciation of Fe were developed to pinpoint the presence or absence of highly reactive Fe sedimentary mineral phases (Fe_{HR}), which includes iron in carbonates (Fe_{carb}), crystalline iron oxides (Fe_{ox}), magnetite (Fe_{mag}), and iron in pyrite (Fe_{py}; Canfield et al., 1986; Poulton et al., 2004; Poulton and Canfield, 2005). The formation and dissolution of these mineral phases is highly dependent on the redox chemistry of the water column, and the vertical and lateral transport of reactive Fe throughout the water column (Figure 1.1). In oxic waters, Fe is largely present as Fe^{2+} and Fe^{3+}, as well as the reactive (and more oxidized) species Fe_{ox} and Fe_{mag} (Figure 1.1; Poulton and Canfield, 2004). Therefore, Fe_{ox} and Fe_{mag} comprise the majority of the Fe_{HR} species in oxic sediments (Figure 1.1; Table 1.1; Poulton and Canfield, 2004; Raiswell et al., 2018). In anoxic waters (both ferruginous and euxinic), Fe_{ox} is dissolved, and the more reduced species such as Fe_{carb} form (Figure 1.1; Poulton and Canfield, 2004; Raiswell et al., 2018). Particular to euxinic environments, free sulfide available in the water column allows for the formation of Fe_{py}, either from the reactivity of other Fe_{HR} species with sulfide (*e.g.*, the dissolution of Fe_{mag} and reincorporation of that Fe in Fe_{py}; Canfield and Berner, 1987), or from free Fe in the water column (Figure 1.1b; Raiswell and Berner, 1985). As a result, while all anoxic sediments will feature enrichments in Fe_{mag} and Fe_{carb}, only euxinic sediments will exhibit significant enrichments in Fe_{py} (Figure 1.1; Table 1.1; Raiswell et al., 2018).

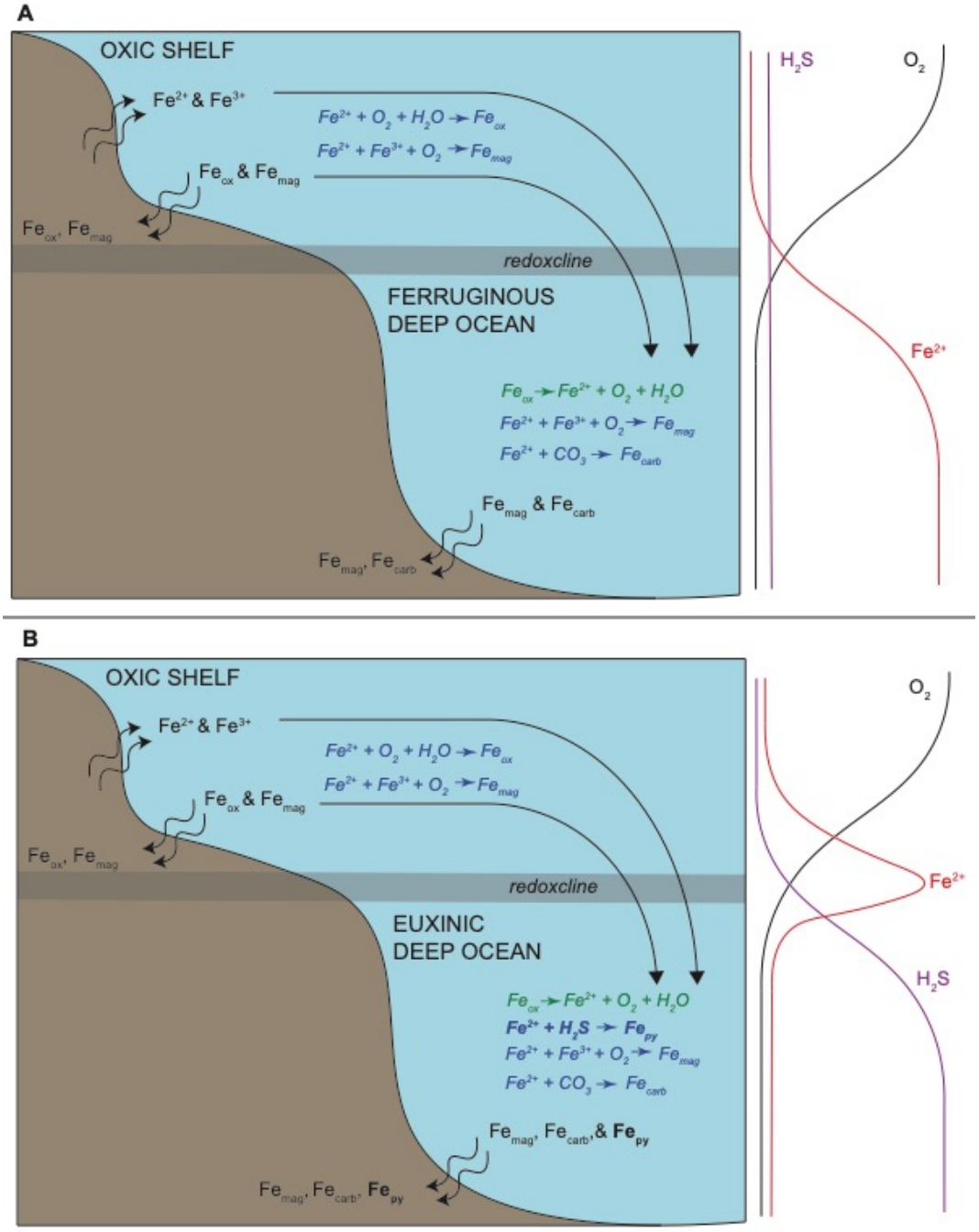

Figure 1.1 Schematic highlighting the horizontal and vertical transport of highly reactive iron in the oceans, from an oxic shelf to a A) ferruginous deep ocean and B) euxinic deep ocean, with basic water chemistry and simplified reactions for the formation (in blue) and dissolution (in green) of various Fe_{HR} species. Modeled after Lyons and Severmann (2006).

Due to our comprehensive understanding of the processes that lead to the burial of iron

under different redox regimes, iron speciation has become one of the most widely used proxies to understand oxygen and sulfide availability in paleoenvironments (Li et al., 2010; Sperling et al., 2013; Wood et al., 2015; Tessin et al., 2016; Fan et al., 2018; Rico et al., 2019) and modern systems (Anderson and Raiswell, 2004; Gomes and Hurtgen, 2013; Rico and Sheldon, 2019). However, the traditional interpretation of Fe speciation is based upon the geochemistry of iron minerals that are highly reactive towards sulfide in depositional environments with an abundance of free sulfide present such as the Black Sea (Raiswell and Canfield, 1998; Anderson and Raiswell, 2004); fewer studies use the Fe speciation method in environments with ferruginous—not sulfidic—water chemistry.

1.1.2 Trace Metal Contents

The enrichment, depletion, and fluxes of trace metals in the water column, porewater, and sediment of aquatic systems are regularly used to draw conclusions about redox and productivity of modern and ancient environments (wherein productivity is also tied to redox; Table 1.1; Tessier and Campbell, 1987; Tessier et al., 1993; Crowe et al., 2007; Chappaz et al., 2008; Wirth et al., 2013; Tessin et al., 2016; Cole et al., 2017). U and V are soluble in oxic waters, but complex strongly with organic acids under reducing (not-sulfidic) conditions, and are therefore enriched in suboxic or ferruginous sediments (Table 1.1; Klinkhammer and Palmer, 1991; Tribovillard et al., 2006). In oxic environments, Cd, Zn, Ni, and Cu act as micronutrients for aquatic organisms, and are thereby incorporated into organic matter and buried in sediments (Table 1.1; Lepp, 1992; Tribovillard et al., 2006; Moore et al., 2017). When sediments are reduced, these trace metals can become mobilized and released into the porewater and/or upwards into the water column, or complex with sulfide under euxinic conditions (Huerta-

Table 1.1 Summary of trace metals that are expected to be enriched in aquatic sediments under different water chemistry regimes.

Water Chemistry	Expected Enrichment of Highly Reactive Fe Species	Expected Trace Metal Enrichment
Oxic	Fe_{ox}, Fe_{mag}	Mn, Cd, Zn, Ni, Cu
Suboxic or Ferruginous	Fe_{mag}, Fe_{carb}	U, V
Euxinic	Fe_{mag}, Fe_{carb}, Fe_{py}	Mo, Cd, Zn, Ni, Cu

Diaz and Morse, 1992; Calvert and Pederson, 1993). Mn is predominantly found as a solid in oxic environments in the form of Mn-oxyhydroxides (Table 1.1), and is released into the water column when reduced (whether or not sulfide is present; Huerta-Diaz and Morse, 1992; Calvert and Pederson, 1993). In oxic waters, Mo can be captured by Mn-oxyhydroxides (Calvert and Pederson, 1993). However, with free sulfides present, Mo is converted into particle-reactive thiomolybdates, which are scavenged with organic matter and buried in sediments (Erickson and Helz, 2000; Tribovillard et al., 2006). As a result of this thiomolybdate formation, and given its high affinity towards sulfide relative to other trace metals (e.g. Cd, Zn, Ni, and Cu; Tribovillard et al., 2006), Mo is considered to be one of the most robust proxies for the presence of water column euxinia (Table 1.1; *e.g.,* Algeo and Lyons, 2006; Lyons et al., 2009).

Just as with Fe speciation, the burial mechanisms of these trace metals are not well constrained for sub-oxic or ferruginous environments, and are largely studied in modern euxinic environments (*e.g.*, Lake Cadagno; Wirth et al., 2013). In addition, despite being considered a proxy for euxinia (Table 1.1; *e.g.*, Algeo and Lyons, 2006; Lyons et al., 2009), recent work has indicated significant Mo burial under anoxic and non-sulfidic, and low-sulfide systems (Scholz et al., 2017; Wagner et al., 2017; Tessin et al., 2018). Therefore, a critical re-examination of the burial mechanisms of these trace metals under a variety of redox regimes is necessary in order to refine our application of trace metals as paleoredox proxies.

1.2 Oxygenation of Proterozoic Atmosphere and Oceans

One key time period where redox proxies have been used to assess biogeochemical cycling is the Proterozoic (~0.5–2.3 billion years ago), wherein which microbial life diversified and advanced, and eukaryotic life evolved. Until roughly 2.3 billion years ago, atmospheric oxygen was $<10^{-5}$ of present atmospheric levels, and oceans were anoxic and low in sulfate (<1 or 0.01% of present levels; Figure 1.2; Canfield et al., 2000; Habicht et al., 2002; Crowe et al., 2014), with euxinic conditions at least in the late Archean (Figure 1.2; Scott et al., 2011). At the onset of the Proterozoic, cyanobacterial microbial mats capable of anoxygenic and oxygenic photosynthesis are hypothesized to have been a key driver of an increase in atmospheric oxygen (the "Great Oxidation Event"; Figure 1.2; Holland, 2006; Johnston et al., 2009; Dick et al., 2018). Following this oxygenation of the atmosphere, it is thought that Proterozoic oceans had oxygenated surface waters, while the deep waters were either ferruginous or euxinic (Figure 1.2; Lyons et al., 2009; Poulton and Canfield, 2011). In the mid-Proterozoic, there is much evidence to support a ferruginous deep ocean with sulfate rather than sulfide present (Canfield et al., 2008; Planavsky et al. 2014; Sperling et al., 2015). However, recent work by Planavsky et al. (2018) uses iron speciation, trace metal, and Mo isotope data from the ~1.85 Stambaugh Formation (USA) to argue that the mid-Proterozoic oceans lacked a strong redox buffer, making the deep ocean vulnerable to brief periods of oxygenation.

Our current understanding of Proterozoic ocean chemistry is largely dependent on the geochemistry of those ancient sediments (*e.g.,* Scott et al., 2008; Reinhard et al., 2013; Sperling et al., 2015). However, those ancient sediments may or may not include evidence of an active biosphere (such as biomarkers; *e.g.*, Brocks et al., 2017), making it difficult to consider biology when interpreting geochemical data. Therefore, modern analogues for ancient ecosystems are

often used to develop hypotheses about biogeochemical cycling in the fossil record (*e.g.*, Rothschild, 1991; Hasiotis et al., 2001; Konhauser et al., 2001; Hamilton et al., 2017). In addition, modern analogue systems are excellent models for testing various paleoproductivity and paleoredox proxies, and for interpreting results in a geologic context.

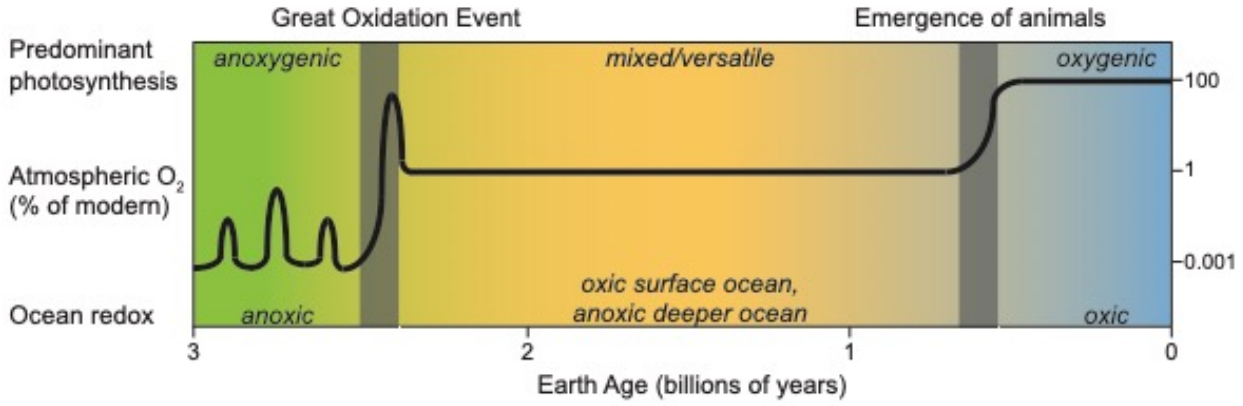

Figure 1.2 Abiotic and biotic evolution of the Earth (three billion years ago to modern), including dominant photosynthesis, atmospheric O_2 levels, and ocean redox chemistry.

1.3 Middle Island Sinkhole: a Low-Oxygen Precambrian Analogue

The Middle Island Sinkhole (MIS) is a karst feature located 23 m beneath the surface of Lake Huron (USA). Low-oxygen, high-sulfate, and high-salinity groundwater seeps into the sinkhole, creating an environment with water chemistry that differs from the overlying fully oxygenated Lake Huron waters (Figure 1.3; Ruberg et al., 2008; Biddanda et al., 2012). This groundwater layer persists <3 m above the sediment and also features an enrichment in free iron (Figure 1.3), making MIS waters ferruginous relative to the Lake Huron chemistry (Rico and Sheldon, 2019). The sinkhole water chemistry supports the growth of microbial mats at the sediment-water interface. These microbial mats include metabolically flexible cyanobacteria and sulfur-oxidizing and reducing bacteria, capable of metabolisms such as oxygenic photosynthesis,

anoxygenic photosynthesis, and chemosynthetic sulfate reduction and sulfide oxidation (Voorhies et al., 2012; Grim, 2019). With ferruginous water chemistry and microbiology similar to that inferred for the Proterozoic (*e.g.*, Figure 1.2), Middle Island Sinkhole is considered to be an analogue for Proterozoic oceans (Voorhies et al., 2012; Kinsman-Costello et al., 2017., Dick et al., 2018).

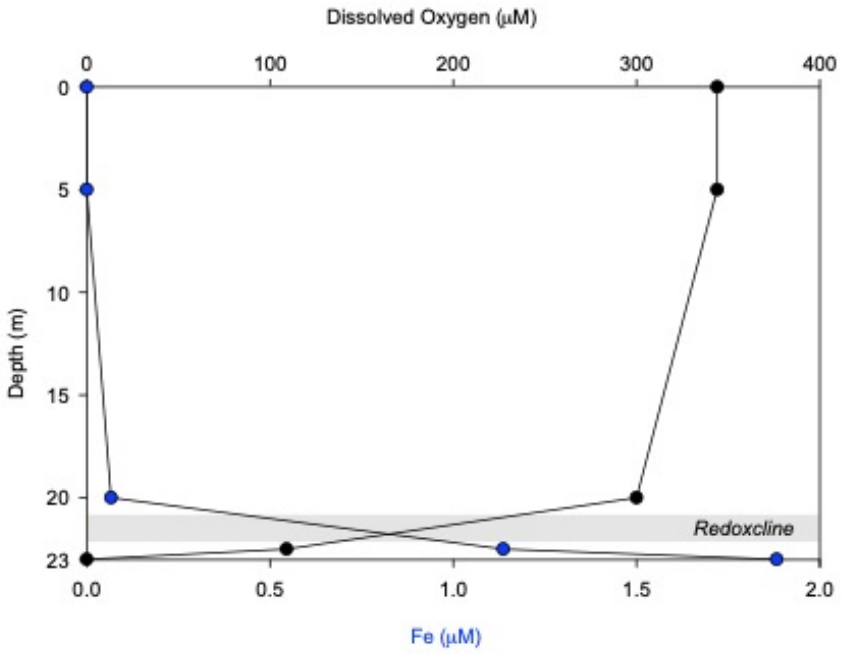

Figure 1.3 Water column dissolved oxygen (from Ruberg et al., 2008 and Biddanda et al., 2012) and dissolved Fe concentrations with depth (Rico and Sheldon, 2019), from Lake Huron surface down to the Middle Island Sinkhole sediment-water interface. Fe concentrations were measured by ICP-MS with ICP Science certified standards at the STARLAB, Central Michigan University.

This dissertation aims to refine our understanding of the biogeochemical cycling of Proterozoic ferruginous environments using MIS as a modern analogue system. I focus on the use of various metals as proxies for understanding the redox chemistry of this analogue, with implications for our understanding of Proterozoic biogeochemical cycling. In this dissertation, I

assess how various metal redox proxies do or do not reflect water column chemistry in modern aquatic systems, how significant microbiological presence impacts our interpretation of sediment metal geochemistry, and the burial mechanisms for different trace metals.

1.4 Thesis Structure

Chapter II explores whether the burial of macronutrients (C, N, P, and S) and Fe in MIS is attributed to productivity (*e.g.,* primary productivity) or preservation (*e.g.*, redox chemistry). MIS sediment geochemistry was compared to that of a fully oxygenated Lake Huron control site (LH) in order to determine how low-oxygen water chemistry and microbial mat presence in particular influence the burial of these elements. The iron speciation method is used to gauge what portion of a stratified water column is reflected in the iron geochemistry of sediments, thereby having major implications for how we interpret Fe geochemical results in the geologic record.

The relationships between microbial mat presence and redox chemistry in MIS and LH continue to be addressed using a suite of redox-sensitive trace metals in Chapter III. By considering metal-organic carbon covariation in three different biotic-abiotic regimes—oxic Lake Huron sediments, anoxic MIS sediments with microbial mat present (*i.e.*, the sediments closest to the sediment-water interface), and anoxic MIS sediments with free sulfide available (deeper MIS sediments)—we are able to consider how microbiology and redox conditions influence trace metal burial in modern systems, and how these burial mechanisms compare to what is expected based on fundamental trace metal proxy literature. In addition, considering MIS to be an analogue for Proterozoic waters, Chapter III allows us to test whether metal-organic carbon covariation can be used as a biosignature for the presence of microbial mats in the

geologic record.

A direct comparison between Proterozoic sediment geochemistry and sediment geochemistry from the modern analogue (MIS) is made in Chapter IV. In this chapter, Fe and Mo geochemistry from the ~1.1 billion year old Nonesuch Formation (Michigan and Wisconsin, USA), MIS, and LH are used to determine the redox chemistry and Mo burial mechanisms in a Proterozoic terrestrial aquatic system, and to test directly the hypothesis that euxinia, biological productivity, and atmospheric oxygenation were widespread by the mid-Proterozoic.

1.5 References

Algeo, T.J., Lyons, T.W., 2006. Mo-total organic carbon covariation in modern anoxic marine environments: Implications for analysis of paleoredox and paleohydrographic conditions. Paleoceanography 21. https://doi.org/10.1029/2004PA001112

Anderson, T.F., Raiswell, R., 2004. Sources and mechanisms for the enrichment of highly reactive iron to euxinic Black Sea sediments. Am. J. Sci. 304, 203–233.

Biddanda, B.A., Nold, S.C., Dick, G.J., Kendall, S.T., Vail, J.H., Ruberg, S.A., Green, C.M., 2012. Rock, Water, Microbes: Underwater Sinkholes in Lake Huron are Habitats for Ancient Microbial Life Characteristics of Lake Huron's Submerged Sinkholes. Nat. Educ. Knowl. 3.

Brocks, J.J., Jarrett, A.J.M., Sirantoine, E., Hallmann, C., Hoshino, Y., Liyanage, T., 2017. The rise of algae in Cryogenian oceans and the emergence of animals. Nature 548, 578–581. https://doi.org/10.1038/nature23457

Calvert, S.E., Pedersen, T.F., 1993. Geochemistry of Recent oxic and anoxic marine sediments: Implications for the geological record. Mar. Geol. 113, 67–88. https://doi.org/10.1016/0025-3227(93)90150-T

Canfield, D.E., 2000. The Archean sulfur cycle and the early history of atmospheric oxygen. Science (80). 288, 658–661. https://doi.org/10.1126/science.288.5466.658

Canfield, D.E., Poulton, S.W., Knoll, A.H., Narbonne, G.M., Ross, G., Goldberg, T., Strauss, H., 2008. Ferruginous Condition Dominated Later Neoproterozoic Deep Water Chemistry. Science (80). 321, 949–952. https://doi.org/10.1126/science.1154499

Canfield, D.E., Berner, R. A., 1987. Dissolution and pyritization of magnetite in anoxie marine sediments. Geochim. Cosmochim. Acta 51, 645–659. https://doi.org/10.1016/0016-7037(87)90076-7

Canfield, D.E., Raiswell, R., Westrich, J.T., Reaves, C.M., Berner, R. A., 1986. The use of chromium reduction in the analysis of reduced inorganic sulfur in sediments and shales. Chem. Geol. 54, 149–155. https://doi.org/10.1016/0009-2541(86)90078-1

Chappaz, A., Gobeil, C., Tessier, A., 2008. Geochemical and anthropogenic enrichments of Mo in sediments from perennially oxic and seasonally anoxic lakes in Eastern Canada. Geochim. Cosmochim. Acta 72, 170–184. https://doi.org/10.1016/j.gca.2007.10.014

Cole, D.B., Zhang, S., Planavsky, N.J., 2017. A new estimate of detrital redox-sensitive metal concentrations and variability in fluxes to marine sediments. Geochim. Cosmochim. Acta 215, 337–353. https://doi.org/10.1016/j.gca.2017.08.004

Crowe, S. a, O'Neill, a H., Weisener, C.G., Kulczycki, E., Fowle, D. A., Roberts, J. A., 2007. Reductive dissolution of trace metals from sediments. Geomicrobiol. J. 24, 157–165. https://doi.org/10.1080/01490450701457329

Crowe, S.A., Paris, G., Katsev, S., Jones, C., Kim, S.T., Zerkle, A.L., Nomosatryo, S., Fowle, D.A., Adkins, J.F., Sessions, A.L., Farquhar, J., Canfield, D.E., 2014. Sulfate was a trace constituent of Archean seawater. Science (80). 346, 735–740.

Dick, G.J., Grim, S.L., Klatt, J.M., 2018. Controls on O2 production in cyanobacterial mats and implications for Earth's oxygenation. Annu. Rev. Earth Planet. Sci. 46, 123–147. https://doi.org/10.1146/annurev-earth-082517-010035

Erickson, B.E., Helz, G.R., 2000. Molybdenum(VI) speciation in sulfidic waters: Stability and lability of thiomolybdates. Geochim. Cosmochim. Acta 64, 1149–1158. https://doi.org/10.1016/S0016-7037(99)00423-8

Fan, H., Wen, H., Han, T., Zhu, X., Feng, L., Chang, H., 2018. Oceanic redox condition during the late Ediacaran (551–541 Ma), South China. Geochim. Cosmochim. Acta 238, 343–356. https://doi.org/10.1016/j.gca.2018.07.014

Gomes, M.L., Hurtgen, M.T., 2013. Sulfur isotope systematics of a euxinic, low-sulfate lake: Evaluating the importance of the reservoir effect in modern and ancient oceans. Geology 41, 663–666. https://doi.org/10.1130/G34187.1

Grim, S., 2019. "Genomic and functional investigations into seasonally-impacted and morphologically-distinct anoxygenic photosynthetic cyanobacterial mats." Doctoral dissertation.

Habicht, K.S., Gade, M., Thamdrup, B., Berg, P., Canfield, D.E., 2002. Calibration of sulfate levels in the Archean ocean. Science (80). 298, 2372–2374. https://doi.org/10.1126/science.1078265

Hamilton, T.L., Welander, P. V., Albrecht, H.L., Fulton, J.M., Schaperdoth, I., Bird, L.R., Summons, R.E., Freeman, K.H., Macalady, J.L., 2017. Microbial communities and organic biomarkers in a Proterozoic-analog sinkhole. Geobiology 15, 784–797. https://doi.org/10.1111/gbi.12252

Hasiotis, S.T., Brake, S.S., Dannelly, H.K., Duncan, A., 2001. Eukaryote-dominated microbial communities that build iron-stromatolites in acid mine drainage, Western Indiana: An analog for Proterozoic Banded Iron Formations and oxygenation of the early atmosphere. Lunar and Planetary Sciences Conference, volume 32.

Holland, H.D., 2006. The oxygenation of the atmosphere and of the oceans. Philos. Trans. R. Soc. Lond. B. Biol. Sci. 361, 903–915. https://doi.org/10.1007/3-540-33088-7_2

Huerta-Diaz, M.A., Morse, J.W., 1992. Pyritization of trace metals in anoxic marine sediments. Geochim. Cosmochim. Acta 56, 2681–2702. https://doi.org/10.1016/0016-7037(92)90353-K

Johnston, D.T., Wolfe-Simon, F., Pearson, A., Knoll, A. H., 2009. Anoxygenic photosynthesis modulated Proterozoic oxygen and sustained Earth's middle age. Proc. Natl. Acad. Sci. 106, 16925–16929. https://doi.org/10.1073/pnas.0909248106

Kinsman-Costello, L.E., Sheik, C.S., Sheldon, N.D., Burton, G. a., Costello, D., Marcus, D.N., Uyl, P. Den, Dick, G.J., 2017. Groundwater shapes sediment biogeochemistry and microbial diversity in a submerged sinkhole. Geobiology 15, 225–239. https://doi.org/10.1038/nature04068

Klinkhammer, G.P., Palmer, M.R., 1991. Uranium in the oceans: Where it goes and why. Geochim. Cosmochim. Acta 55, 1799–1806. https://doi.org/10.1016/0016-7037(91)90024-Y

Konhauser, K.O., Phoenix, V.R., Bottrell, S.H., Adams, D.G., Head, I.M., 2001. Microbial-silica interactions in Icelandic hot spring sinter: Possible analogues for some Precambrian siliceous stromatolites. Sedimentology 48, 415–433. https://doi.org/10.1046/j.1365-3091.2001.00372.x

Lepp, N. W., 1992. Uptake and accumulation of metals in bacteria and fungi. In: Biogeochemistry of Trace Metals, ed. Adriano, D. C. Boca Raton, FL: Lewis Publishers. pp. 277–298

Li, C., Love, G.D., Lyons, T.W., Fike, D. A., Sessions, A.L., Chu, X., 2010. A Stratified Redox Model for the Ediacaran Ocean. Science (80). 328, 80–83. https://doi.org/10.1126/science.1182369

Lyons, T.W., Anbar, A.D., Severmann, S., Scott, C., Gill, B.C., 2009. Tracking Euxinia in the Ancient Ocean: A Multiproxy Perspective and Proterozoic Case Study. Annu. Rev. Earth Planet. Sci. 37, 507–534. https://doi.org/10.1146/annurev.earth.36.031207.124233

Lyons, T.W., Severmann, S., 2006. A critical look at iron paleoredox proxies: New insights from modern euxinic marine basins. Geochim. Cosmochim. Acta 70, 5698–5722. https://doi.org/10.1016/j.gca.2006.08.021

Moore, E.K., Jelen, B.I., Giovannelli, D., Raanan, H., Falkowski, P.G., 2017. Metal availability and the expanding network of microbial metabolisms in the Archaean eon. Nat. Geosci. 10, 629–636. https://doi.org/10.1038/ngeo3006

Planavsky, N.J., Asael, D., Hofmann, A., Reinhard, C.T., Lalonde, S. V, Knudsen, A., Wang, X., Ossa Ossa, F., Pecoits, E., Smith, A.J.B., Beukes, N.J., Bekker, A., Johnson, T.M., Konhauser, K.O., Lyons, T.W., Rouxel, O.J., 2014. Evidence for oxygenic photosynthesis half a billion years before the Great Oxidation Event. Nat. Geosci. 7, 283–286. https://doi.org/10.1038/ngeo2122

Planavsky, N.J., Slack, J.F., Cannon, W.F., O'Connell, B., Isson, T.T., Asael, D., Jackson, J.C., Hardisty, D.S., Lyons, T.W., Bekker, A., 2018. Evidence for episodic oxygenation in a weakly redox-buffered deep mid-Proterozoic ocean. Chem. Geol. 483, 581–594. https://doi.org/10.1016/j.chemgeo.2018.03.028

Poulton, S., Canfield, D., 2005. Development of a sequential extraction procedure for iron: implications for iron partitioning in continentally derived particulates. Chem. Geol. 214, 209–221. https://doi.org/10.1016/j.chemgeo.2004.09.003

Poulton, S.W., Canfeld, D.E., 2011. Ferruginous conditions: A dominant feature of the ocean through Earth's history. Elements 7, 107–112. https://doi.org/10.2113/gselements.7.2.107

Poulton, S.W., Krom, M.D., Raiswell, R., 2004. A revised scheme for the reactivity of iron (oxyhydr)oxide minerals towards dissolved sulfide. Geochim. Cosmochim. Acta 68, 3703–3715. https://doi.org/10.1016/j.gca.2004.03.012

Raiswell, R., Berner, R.A., 1985. Pyrite formation in euxinic and semi-euxinic sediments. Am. J. Sci. 285, 710–724. https://doi.org/10.2475/ajs.285.8.710

Raiswell, R., Hardisty, D.S., Lyons, T.W., Canfield, D.E., Owens, J.D., Planavsky, N.J., Poulton, S.W., Reinhard, C.T., 2018. The iron paleoredox proxies: A guide to the pitfalls, problems and proper practice. Am. J. Sci. 318, 491–526. https://doi.org/10.2475/05.2018.03

Raiswell, R., Canfield, D.E., 2012. The iron biogeochemical cycle past and present. Geochem. Persp. 1, 1–220. https://doi. org/10.7185/geochempersp.1.1

Raiswell, R., Canfield, D.E., 1998. Sources of iron for pyrite formation in marine sediments. Am. J. Sci. 298, 219–245. https://doi.org/10.1017/CBO9781107415324.004

Reinhard, C.T., Planavsky, N.J., Robbins, L.J., Partin, C. A., Gill, B.C., Lalonde, S. V., Bekker, A., Konhauser, K.O., Lyons, T.W., 2013. Proterozoic ocean redox and biogeochemical stasis. Proc. Natl. Acad. Sci. 110, 5357–5362. https://doi.org/10.1073/pnas.1208622110

Rico, K.I., Sheldon, N.D., 2019. Nutrient and iron cycling in a modern analogue for the redoxcline of a Proterozoic ocean shelf. Chem. Geol. 511, 42–50. https://doi.org/10.1016/j.chemgeo.2019.02.032

Rico, K.I., Sheldon, N.D., Gallagher, T.M., Chappaz, A., 2019. Redox chemistry and molybdenum burial in a Mesoproterozoic lake. Geophys. Res. Lett., 46, 5871–5878. https://doi.org/10.1029/2019GL083316

Rothschild, L.J., 1991. A model for diurnal patterns of carbon fixation in a Precambrian microbial mat based on a modern analog. BioSystems 25, 13–23. https://doi.org/10.1016/0303-2647(91)90009-A

Ruberg, S.A., Kendall, S.T., Biddanda, B.A., Black, T., Nold, S.C., Lusardi, W.R., Green, R., Casserly, T., Smith, E., Sanders, T.G., Lang, G.A., Constant, S.A., 2008. Observations of the Middle Island Sinkhole in Lake Huron – A unique hydrogeologic and glacial creation of 400 Million Years. Mar. Technol. Soc. J. 42, 12–21.

Scholz, F., Siebert, C., Dale, A.W., Frank, M., 2017. Intense molybdenum accumulation in sediments underneath a nitrogenous water column and implications for the reconstruction of paleo-redox conditions based on molybdenum isotopes. Geochim. Cosmochim. Acta 213, 400–417. https://doi.org/10.1016/j.gca.2017.06.048

Scott, C.T., Bekker, A., Reinhard, C.T., Schnetger, B., Krapež, B., Rumble, D., Lyons, T.W., 2011. Late Archean euxinic conditions before the rise of atmospheric oxygen. Geology 39, 119–122. https://doi.org/10.1130/G31571.1

Scott, C., Lyons, T.W., Bekker, A., Shen, Y., Poulton, S.W., Chu, X., Anbar, a. D., 2008. Tracing the stepwise oxygenation of the Proterozoic ocean. Nature 452, 456–459. https://doi.org/10.1038/nature06811

Sperling, E.A., Halverson, G.P., Knoll, A.H., Macdonald, F.A., Johnston, D.T., 2013. A basin redox transect at the dawn of animal life. Earth Planet. Sci. Lett. 371–372, 143–155. https://doi.org/10.1016/j.epsl.2013.04.003

Sperling, E.A., Wolock, C.J., Morgan, A.S., Gill, B.C., Kunzmann, M., Halverson, G.P., Macdonald, F.A., Knoll, A.H., Johnston, D.T., 2015. Statistical analysis of iron geochemical data suggests limited late Proterozoic oxygenation. Nature 523, 451–454. https://doi.org/10.1038/nature14589

Tessier, a., Campbell, P.G.C., 1987. Partitioning of trace metals in sediments: Relationships with bioavailability. Hydrobiologia 149, 43–52. https://doi.org/10.1007/BF00048645

Tessier, a., Coullard, Y., Campbell, P.G.C., Auclair, J.C., 1993. Modeling Cd partitioning in oxic lake sediments and Cd concentrations in the freshwater bivalve Anodonta grandis. Limnol. Oceanogr. 38, 1–17. https://doi.org/10.4319/lo.1993.38.1.0001

Tessin, A., Chappaz, A., Hendy, I., Sheldon, N., 2018. Molybdenum speciation as a paleo-redox proxy: A case study from Late Cretaceous Western Interior Seaway black shales. Geology 47, 59–62. https://doi.org/10.1130/g45785.1

Tessin, A., Sheldon, N.D., Hendy, I., Chappaz, A., 2016. Iron limitation in the Western Interior Seaway during the Late Cretaceous OAE 3 and its role in phosphorus recycling and enhanced organic matter preservation. Earth Planet. Sci. Lett. 449, 135–144. https://doi.org/10.1016/j.epsl.2016.05.043

Tribovillard, N., Algeo, T.J., Lyons, T., Riboulleau, A., 2006. Trace metals as paleoredox and paleoproductivity proxies: An update. Chem. Geol. 232, 12–32. https://doi.org/10.1016/j.chemgeo.2006.02.012

Voorhies, A.A., Biddanda, B.A., Kendall, S.T., Jain, S., Marcus, D.N., Nold, S.C., Sheldon, N.D., Dick, G.J., 2012. Cyanobacterial life at low O_2: community genomics and function reveal metabolic versatility and extremely low diversity in a Great Lakes sinkhole mat. Geobiology 10, 250–67. https://doi.org/10.1111/j.1472-4669.2012.00322.x

Wagner, M., Chappaz, A., Lyons, T.W., 2017. Molybdenum speciation and burial pathway in weakly sulfidic environments: Insights from XAFS. Geochim. Cosmochim. Acta 206, 18–29. https://doi.org/10.1016/j.gca.2017.02.018

Wirth, S.B., Gilli, A., Niemann, H., Dahl, T.W., Ravasi, D., Sax, N., Hamann, Y., Peduzzi, R., Peduzzi, S., Tonolla, M., Lehmann, M.F., Anselmetti, F.S., 2013. Combining sedimentological, trace metal (Mn, Mo) and molecular evidence for reconstructing past water-column redox conditions: The example of meromictic Lake Cadagno (Swiss Alps). Geochim. Cosmochim. Acta 120, 220–238. https://doi.org/10.1016/j.gca.2013.06.017

Wood, R.A., Poulton, S.W., Prave, A.R., Hoffmann, K.H., Clarkson, M.O., Guilbaud, R., Lyne, J.W., Tostevin, R., Bowyer, F., Penny, A.M., Curtis, A., Kasemann, S.A., 2015. Dynamic redox conditions control late Ediacaran metazoan ecosystems in the Nama Group, Namibia. Precambrian Res. 261, 252–271. https://doi.org/10.1016/j.precamres.2015.02.004

CHAPTER II

Nutrient and Iron Cycling in a Modern Analogue for the Redoxcline of a Proterozoic Ocean Shelf[1]

2.1 Abstract

Proterozoic oceans are characterized by a thin veneer of oxygenated surface waters underlain by anoxic or euxinic deeper waters, and it has been hypothesized that metabolically flexible microbes such as cyanobacteria would have thrived under these conditions. However, relatively little is known about the relationship between water chemistry, microbial mats, and the biogeochemical cycling of macronutrients (C, N, P, and S) and Fe in these redox transition zones. We investigated the burial of these elements in a modern analogue for the Proterozoic to constrain these relationships better. The low-oxygen and high sulfate water chemistry of Middle Island Sinkhole (MIS; a sinkhole within Lake Huron) allows for the proliferation of a microbial mat community with diverse metabolisms within the photic zone at the sediment-water interface similar to what has been hypothesized following the Great Oxidation Event (~2.35 Ga). Sediments from MIS were compared to those of a fully oxygenated Lake Huron control site in order to determine how water chemistry and microbial mat presence impact biogeochemical cycling. MIS sediments have a greater accumulation of macronutrients than Lake Huron, with stable C isotopes and C:N ratios demonstrating that the C buried within MIS and Lake Huron

[1]Published under the citation:
Rico, K.I., Sheldon, N.D., 2019. Nutrient and iron cycling in a modern analogue for the redoxcline of a Proterozoic ocean shelf. Chem. Geol. 511, 42–50. https://doi.org/10.1016/j.chemgeo.2019.02.032

sediments comes from the same phytoplankton source. Given that both sites bury C from the same source, the increased organic matter burial in MIS is not dependent on microbial mat presence and instead must be controlled by differences in preservation. Sequential extraction of iron indicates that MIS is ferruginous, but not euxinic, and that Lake Huron is oxic; both results are consistent with measured water chemistry. At the same time, the presence of ferruginous iron speciation in sediments under a partly oxygenated water column suggests that the sediment is recording either rapid transformations across the redoxcline rather than the whole water column, some *in situ* re-speciation of iron, or both. This has important implications for our interpretations of Fe speciation results in the geologic record. Taken together, nutrient and Fe burial in the analogue MIS site demonstrate that Proterozoic biogeochemical cycling in surficial sediments may be predominately driven by a combination of water column and porewater redox chemistry, and not microbial activity.

2.2 Introduction

Following the "Great Oxidation Event" (GOE; ~2.35 Ga) the Paleoproterozoic featured widespread ocean stratification between a thin veneer of oxygenated surface water and ferruginous (high Fe^{2+}, low oxygen) or euxinic (high sulfide, low oxygen) deeper water (Lyons et al., 2009; Poulton and Canfield, 2011). This impacted the biosphere by limiting marine ecosystems to single-celled microorganisms or microbial mats until a second rise of oxygen in the late Ediacaran and Cambrian (Nursall, 1959; Catling et al., 2005; Canfield et al, 2007; Sperling et al., 2013, 2015). However, Scott et al. (2008) found that widespread euxinia was unlikely due to a nutrient-limiting feedback, and there is much evidence to support the presence of a ferruginous deep ocean with sulfate rather than sulfide present (*e.g.,* Canfield et al., 2008;

Poulton and Canfield, 2010; Sperling et al., 2015), at least in some basins and at some times. Thus, understanding Fe cycling in modern low-oxygen environments is critical for understanding nutrient and Fe cycling and burial on Earth prior to widespread oxygenation of the atmosphere and oceans.

Iron cycling has been explored widely in marine systems, wherein reactive Fe is shuttled into anoxic or euxinic basins, and then sequestered by sediments (Anderson and Raiswell, 2004; Lyons and Severmann, 2006). In order to compare the reactivity of Fe deposited in aquatic environments, sequential extraction methods (Poulton and Canfield, 2005) have been developed to examine the speciation of Fe into sedimentary mineral phases. Iron speciation was initially calibrated primarily to investigate redox chemistry in sulfur-rich marine systems such as the äck Sea (*e.g.,* Raiswell and Canfield, 1998; Anderson and Raiswell, 2004), and has been subsequently used to determine redox chemistry of ancient systems such as: the Proterozoic ocean during termination of banded iron formations (1.8 Gya; Poulton et al., 2004b); Ediacaran ocean chemistry (635–543 Mya; Li et al., 2010; Wood et al., 2015); and Cretaceous Oceanic Anoxic Event 3 black shale deposition (~86 Ma; März et al., 2008; Tessin et al., 2016).

The cycling of Fe in aquatic systems is directly linked to the cycling of various macronutrients (*e.g.,* C, N, S, and P; Raiswell and Canfield, 2012). In this study, we explore nutrient and Fe cycling in both oxygenated and low-oxygen systems: 1) the Middle Island Sinkhole (MIS), a 23 m deep karst feature with low-oxygen bottom waters within Lake Huron; and 2) a fully oxygenated Lake Huron control site (LH) of similar depth. MIS is considered a Proterozoic analogue due to its water chemistry and microbial assemblage (*e.g.,* Voorhies et al., 2012; Figures 2.1–2.3). The low oxygen and high sulfate content of the sinkhole waters (Figure 2.1) allow microbial mat communities to flourish at the sediment-water interface. The mats

include metabolically flexible cyanobacteria capable of both oxygenic and anoxygenic photosynthesis, as well as organisms using a variety of heterotrophic metabolisms (Figure 2.3;

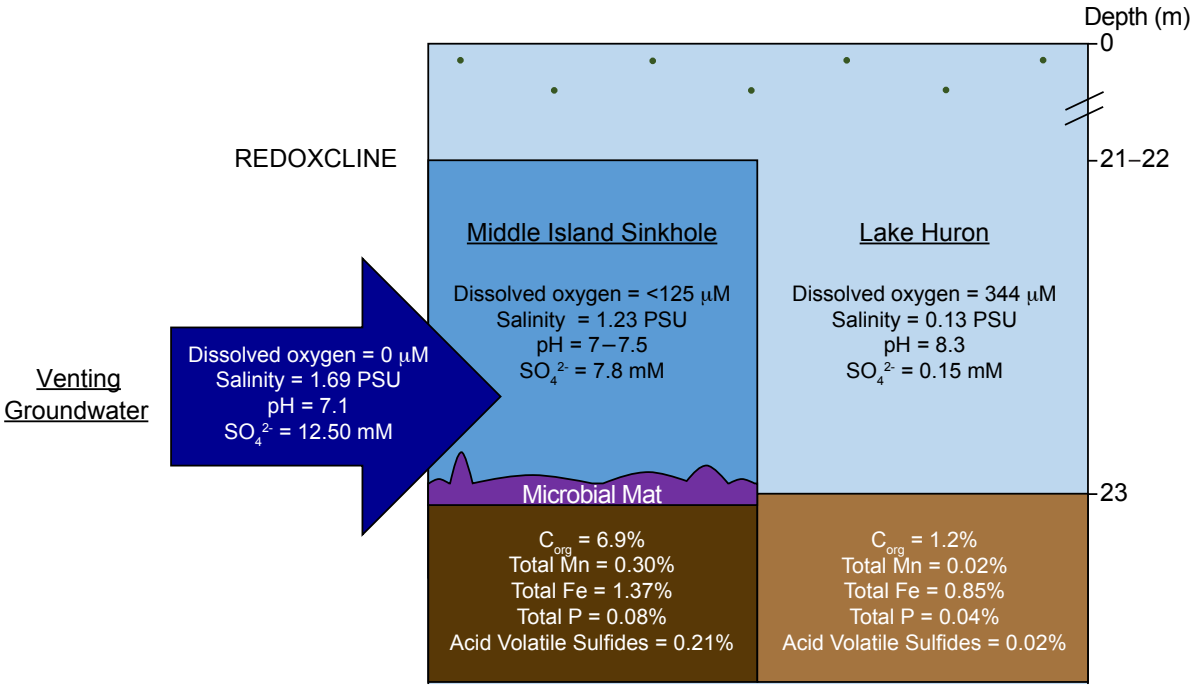

Figure 2.1 Site comparison between Middle Island Sinkhole (MIS) and the Lake Huron control site (LH). Water chemistry at the MIS is fueled by the venting of regional groundwater that is low in oxygen and high in sulfur; this creates a strong redoxcline between MIS and LH waters (Ruberg et al., 2008; Biddanda et al., 2012; Kinsman-Costello et al., 2017) and difference in metal and nutrient burial in the sediments (Kinsman-Costello et al., 2017).

Nold et al, 2010; Voorhies et al., 2012; Kinsman-Costello et al., 2017). It has been hypothesized that metabolic flexibility in cyanobacteria may have been the rule rather than the exception after the GOE and before the widespread emergence of animals (~0.54 Gya; Johnston et al., 2009).

Estimates of ocean sulfate concentrations during the mid to late Proterozoic range between <2 mM (Luo et al., 2015) up to 10 mM (Olson et al., 2016; Blättler et al., 2018, far lower than modern sulfate concentrations of 28 mM (Shen et al., 2002; Kah et al., 2004; Scott et al., 2014; Olson et al., 2016; Blättler et al., 2018). MIS water sulfate concentrations of 7.8 mM (Figure 2.1; Ruberg et al., 2008; Biddanda et al., 2012; Kinsman-Costello et al., 2017) fall within

the range of these estimated values. Additionally, surface ocean waters need to exceed dissolved oxygen concentrations of 150–200 μM in order to maintain oxygenated deep waters (Canfield, 1998). MIS falls below the low end of this dissolved oxygen range (125 μM; Figures 2.1 and 2.2; Ruberg et al., 2008, Biddanda et al., 2012; Kinsman-Costello et al., 2017), and is rich in dissolved Fe compared to LH (Figure 2.2), consistent with deeper ferruginous Proterozoic ocean waters, which are inferred to have had little to no oxygen (*e.g.,* Shen et al., 2002; Lyons et al., 2014).

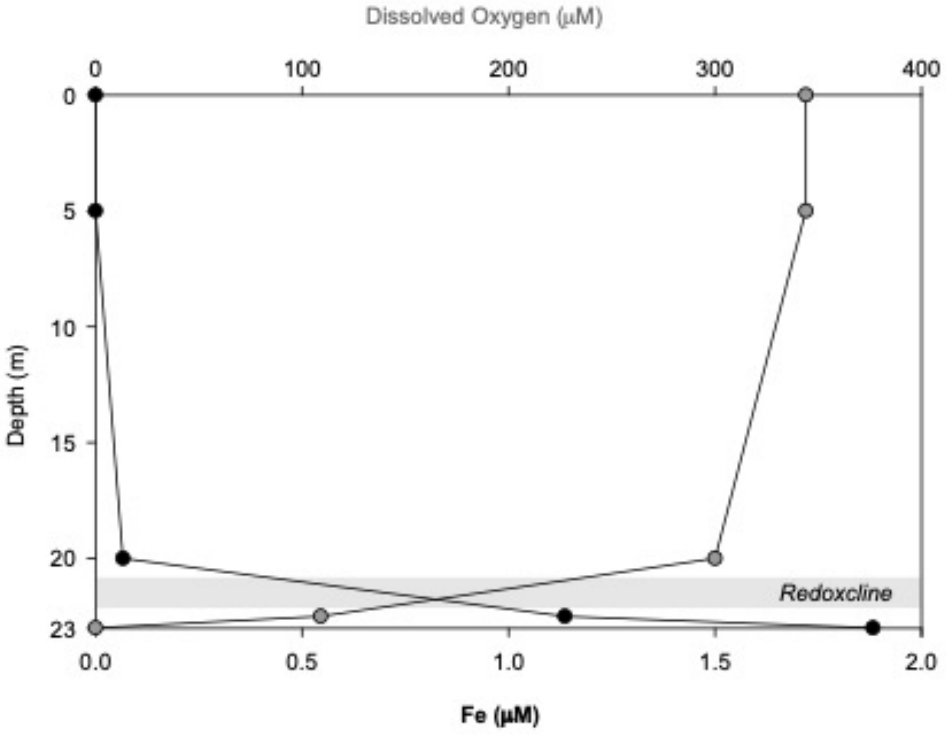

Figure 2.2 Water column dissolved oxygen (from Ruberg et al., 2008 and Biddanda et al., 2012) and dissolved Fe concentrations with depth (*this work*), from Lake Huron surface down to the Middle Island Sinkhole sediment-water interface

Although MIS is a freshwater system, its elevated sulfate and Fe concentrations, higher conductivity (*i.e.*, salinity) relative to most lakes, low dissolved oxygen concentrations, and the presence of metabolically flexible microbial mats at the sediment-water interface (Figures 2.1

and 2.2) distinguish MIS from typical freshwater systems, and are similar to what is inferred for mid-to- late Proterozoic oceans. In addition, known microbial-sediment community structure for

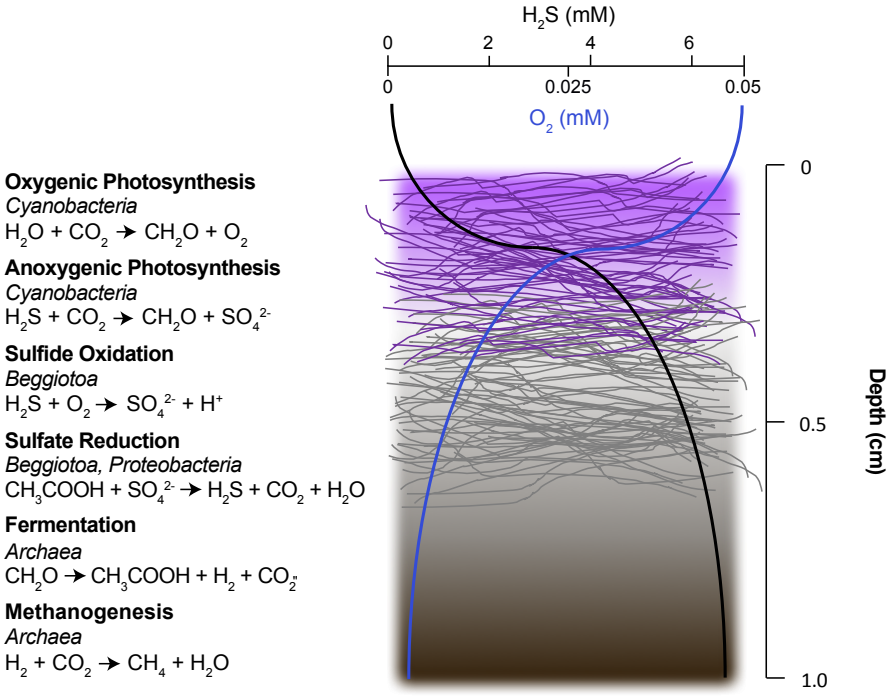

Figure 2.3 Schematic drawing of the microbial mat and upper sediment at the Middle Island Sinkhole sediment-water interface (adapted from Nold et al., 2010). The major microbial groups and their identified metabolisms at each layer are summarized (Nold et al., 2010; Voorhies et al., 2012; Kinsman-Costello et al., 2017). Sulfide-oxygen depth profiles are from Kinsman-Costello et al. (2017).

MIS and LH (Kinsman-Costello et al., 2017) allows us to consider how different microbial groups may be facilitating the transport of elements or mineral phases across the sediment-water interface. With biology and water chemistry similar to marine systems, MIS can be used as a modern analogue to help to understand the relationships between redox chemistry, microbial mat presence, and nutrient and Fe burial of low-oxygen waters overlain by oxygenated surface waters on a shallow Proterozoic ocean shelf (Figure 2.4).

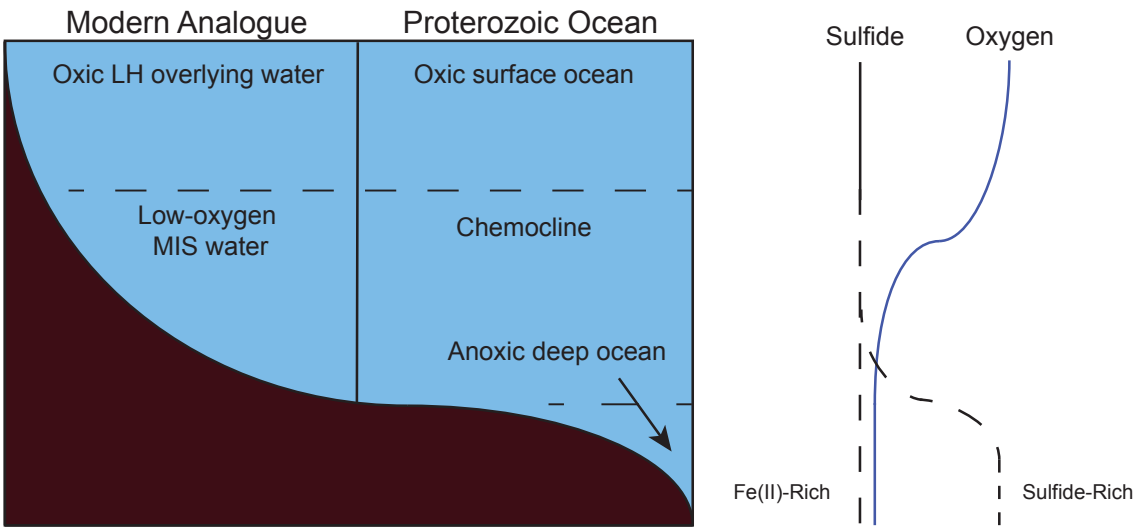

Figure 2.4 Comparison of Proterozoic ocean chemistry to its Lake Huron (LH) and Middle Island Sinkhole (MIS) counterparts, with associated oxygen and sulfide depth profiles. MIS is proposed to be an analogue for the oxic-anoxic transition on a Proterozoic ocean shelf.

2.3 Materials and Methods

2.3.1 Site Description

Near Alpena, Michigan, MIS sits ~23 m below the water surface of Lake Huron, occupying one hectare. Regional groundwater that is low in oxygen and high in sulfate seeps into the sinkhole, making MIS waters compositionally distinct from Lake Huron, and creating a strong redoxcline (Figures 2.1 and 2.2; Ruberg et al., 2008; Biddanda et al., 2012). MIS water is compositionally intermediate between the venting groundwater and Lake Huron, and has a higher conductivity and sulfate concentration, and lower dissolved oxygen than Lake Huron (Figure 2.1; Ruberg et al., 2008; Kinsman-Costello et al., 2017). The distinct water chemistry at MIS prevents multi-cellular life from flourishing and allows for the proliferation of metabolically diverse microbial mats (Figure 2.3) without any influence of herbivory, resulting in differences in the burial of nutrients and metals in the sediments preserved below the microbial mats (*e.g.,* P and Fe; Figure 2.1).

2.3.2 Sediment Collection and Core Processing

National Oceanic and Atmospheric Administration Thunder Bay National Marine Sanctuary (NOAA TBNMS) scuba divers collected sediment cores at the bottom of MIS (n = 28; 45°11.911' N, 83°19.662' W) during May and July 2013, September 2014, and May 2015. Cores were also obtained at a Lake Huron control site with comparable water depth (LH; 45°12.267' N, 83°19.831' W) in May 2015 (n = 8). Divers used 20 x 7 cm (length x inner diameter) clear polycarbonate tubes to obtain 12–16 cm of sediment per core. In May 2015, one "long core" (30 x 7 cm) was also collected at the MIS site. With each sampling trip, cores were transported upright and frozen to the University of Michigan in Ann Arbor, MI, where they were stored at -20°C. Frozen cores were sectioned according to depth (three 1 cm sections at the top, then 3 cm intervals downcore). Each of the sections was freeze-dried and homogenized for their stable isotope ($\delta^{13}C$) and elemental composition, and iron speciation.

2.3.4 Water Sample Collection and Analyses

Water column samples were collected by NOAA TBNMS scuba divers in July 2015. Fe concentrations on these samples were measured on ICP-MS (Thermo iCAPQ) at the STARLAB at Central Michigan University. Analytical precision and accuracy, determined from replicate analyses (n = 11) of a certified standard (ICP Science) were better than 3%. Porewater data that are discussed were previously published in Kinsman-Costello et al. (2017).

2.3.5 Elemental Analyzer and Stable Isotopic Analyses

For organic C and N content measurements, and stable isotopic ($\delta^{13}C$) analyses, samples were washed with 2% HCl solution to remove carbonates, and oven-dried overnight at 50°C. To

determine organic C and N content, the dried samples (n = 173 for MIS, n = 37 for LH) were loaded into tin capsules, and analyzed using a Costech ECS4010 elemental analyzer at the University of Michigan's Earth System Science Lab. C and N contents for the May and July 2013 samples were previously published in a study by Kinsman-Costello et al. (2017), and were replicated for this study. Of the 173 MIS samples, 19 samples were replicated with an average standard deviation of 0.17% for C_{org} and 0.03% for N. All 37 LH samples were replicated with an average standard deviation of 0.02% for C_{org} and 0.01% for N. The averages of each replicate are used in subsequent data analyses.

A subset of MIS samples (n = 45) were loaded into tin capsules, and analyzed using a Costech ECS4010 elemental analyzer attached to a Thermo Delta V+ isotope ratio mass spectrometer at the University of Michigan's Stable Isotope Laboratory. Acetanilide (%C = 71.09, %N = 10.36) was used to calibrate C elemental composition, and International Atomic Energy Agency (IAEA) 600 caffeine (n = 6, $\delta^{13}C$ = -27.77 ± 0.03‰) and IAEA-CH-6 sucrose (n = 6, $\delta^{13}C$ = -10.45 ± 0.09‰) standards were used to calibrate isotopic values; replicates were reproduced with an average standard deviation of 0.27‰.

LH samples (n = 37) were loaded into tin capsules, and analyzed for $\delta^{13}C$ using a Picarro G2201-*i* Cavity Ring Down Spectrometer (CRDS) at the University of Michigan's Earth Systems Science Lab. Acetanilide (%C = 71.09, %N = 10.36; n = 8, $\delta^{13}C$ = -28.32 ± 0.20‰), and International Atomic Energy Agency (IAEA) 600 caffeine (n = 6, $\delta^{13}C$ = -27.64 ± 0.12‰) and IAEA-CH-6 sucrose (n = 3, $\delta^{13}C$ = -10.45 ± 0.05‰) standards were used to calibrate isotopic values; replicates were reproduced with an average standard deviation of 0.06‰. MIS sediments run previously on the Thermo Delta V+ isotope ratio mass spectrometer were reproduced on the CRDS with a standard deviation of 0.17‰.

2.3.6 Elemental Composition

Elemental analysis (n = 56 for MIS, n = 22 for LH) was completed at ALS Laboratories in Vancouver, British Columbia. Samples were digested with perchloric, hydrofluoric, nitric, and hydrochloric acids. Concentrations for S, P, and total Fe (Fe_T) were determined by inductively coupled plasma (ICP)-atomic emission spectroscopy and ICP-mass spectroscopy. OREA-45d, MRGeo08, OGGeo08, CDN-CM-34, SARM-45, and SARM-43 internal standards were used to verify elemental concentrations. Major element uncertainty was approximately 0.2 wt.%.

2.3.7 Iron Speciation

Sequential extraction of iron for iron speciation (Table 2.1) was conducted using the three-step procedure developed by Poulton and Canfield (2005), as well as a separate extraction of iron in pyrite (Canfield et al., 1986), in order to extract the highly reactive pools of iron from MIS (n = 55) and LH (n = 21) sediments.

Table 2.1 Sequential iron extraction[1] procedure.

Extraction	Time of extraction, pH	Target Fe phases	Terminology
(1) Sodium acetate buffered with acetic acid	24 hrs, pH 4.5	Carbonate phases, *e.g.,* siderite and ankerite	Fe_{carb}
(2) Sodium dithionite buffered with acetic acid and sodium citrate	2 hrs, pH 4.8	Crystalline oxides, *e.g.,* goethite and hematite	Fe_{ox}
(3) Ammonium oxalate buffered with ammonium hydroxide	6 hrs, pH 3.2	Magnetite	Fe_{mag}
Chromous chloride sulfur reduction titrated with potassium iodate	2 hrs	Pyrite	Fe_{py}

[1]Sequential extraction protocol follows Poulton and Canfield (2005) for (1)–(3) and Canfield et al. (1986) for pyrite.

Highly reactive iron is defined as iron that is highly reactive towards sulfide (Canfield and Berner, 1987; Poulton et al., 2004a; Poulton and Canfield, 2005). The highly reactive pool of

iron (Fe_{HR}) is composed of iron in carbonates (Fe_{carb}), iron in crystalline oxides (Fe_{ox}), magnetite (Fe_{mag}), and iron in pyrite (Fe_{py}; Poulton et al., 2004b). Iron in the sequential extraction solutions (Fe_{carb}, Fe_{ox}, Fe_{mag}, Fe_{py}) were analyzed by ICP-optical emission spectroscopy at the University of Michigan (n = 76); replicate analysis for all steps gave an RSD <5%. Iron in pyrite was determined stoichiometrically following titration of sulfide (n = 76; Canfield et al., 1986); replicate analysis gave an average RSD of 12%.

2.4 Results

2.4.1 Nutrients

MIS sediments have C_{org}, N, S, and P contents greater than the LH control site sediments (Table 2.2; Figures 2.1 and 2.5). While MIS sediment C_{org} was greater than that of LH, it decreased with depth for both sites for the first ~3 cm before stabilizing with depth (Figure 2.5a). Surficial MIS sediments had the maximum C_{org} value of 20.11%, while surficial LH sediments had a maximum C_{org} of 3.15% (Table 2.2). LH sediment N was consistent with depth (averaging 0.2 ± 0.1%), while MIS N was greater and more variable (0.9 ± 0.5%; Figures 2.5b and 2.6a). MIS C:N ratios overlapped those of LH (Figure 2.5e), but LH values were more variable (Figure 2.6b), primarily driven by low N values in some samples (Table 2.2).

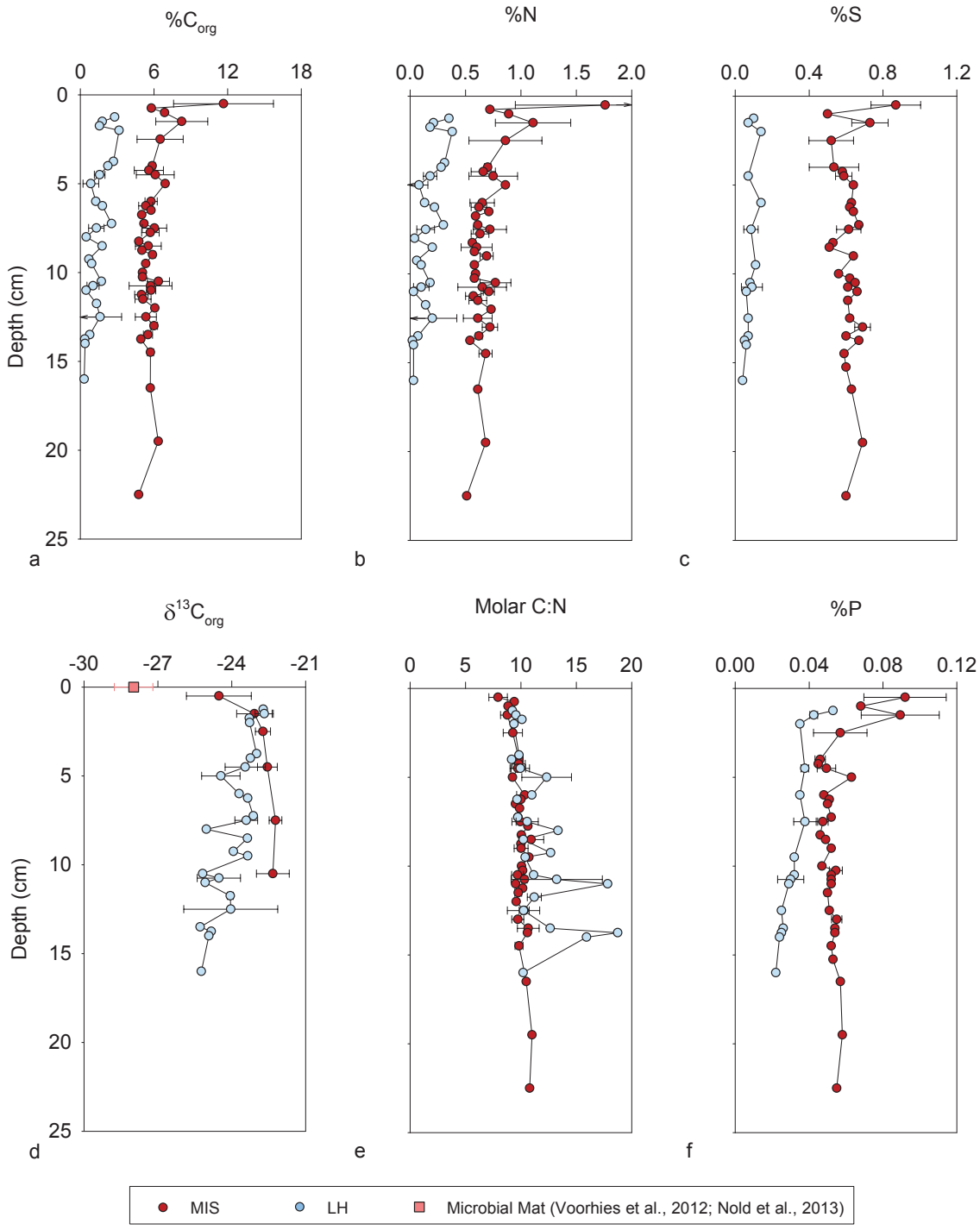

Figure 2.5 Average (a) $\%C_{org}$, (b) %N, (c) %S, (d) $\delta^{13}C_{org}$, (e) molar C:N, and (f) %P at each depth. For $\%C_{org}$, %N, molar C:N, %S, and %P, error bars represent variability (1σ) between different cores at particular depths (n = 29 for Middle Island Sinkhole, MIS; and n = 8 for Lake Huron, LH). For $\delta^{13}C_{org}$, error bars represent variability (1σ) between different cores at particular depths (n = 12 for MIS, and n = 8 for LH). Microbial mat $\delta^{13}C_{org}$ averages data from Voorhies et al. (2012; n = 5) and Nold et al. (2013; n ≥ 4).

Table 2.2 Major nutrients in sediments from MIS and LH.

	MIS			LH		
	Min.	*Max.*	*Mean*[1]	*Min.*	*Max.*	*Mean*[1]
%C_{org}	3.44	20.11	6.97 ± 2.69	0.31	3.15	1.5 ± 0.8
%N	0.36	3.47	0.90 ± 0.49	0.02	0.38	0.2 ± 0.1
Molar C:N	6.8	12.1	9.5 ± 1.0	9.1	18.7	11 ± 2
%S	0.37	0.98	0.62 ± 0.11	0.04	0.20	0.08 ± 0.04
%P	0.04	0.11	0.06 ± 0.02	0.02	0.05	0.03 ± 0.01
C:P	67	132	103 ± 14	14	66	35 ± 15
$\delta^{13}C$ (‰)	-26.0	-21.3	-22.7 ± 0.8	-25.4	-22.3	-23.8 ± 0.9

[1]Uncertainties are ± 1σ about the mean.

MIS S decreased with depth within the first ~3 cm before becoming unchanging with depth, while LH S was consistent with depth (Figure 2.5c). Surficial MIS sediments had the maximum S value of 0.98%, while surficial LH sediments averaged 0.08 ± 0.04% downcore (Table 2.2). For both MIS and LH sediment, P decreased for the first ~3 cm before becoming consistent with depth (Figure 2.5f). Maximum P of MIS surficial sediments was 0.11%, while maximum P of LH surficial sediments was 0.05% (Table 2.2).

Consistent with previous results (Nold et al., 2013), stable isotope $\delta^{13}C_{org}$ values for MIS sediments average -22.7 ± 0.8‰, decreasing with depth within the first ~3 cm before becoming unchanging with depth (Figure 2.5d. The MIS sediments are isotopically more positive relative to the surface microbial mat $\delta^{13}C_{org}$ values (-28.1 ± 1.1‰; Figure 2.5d; Voorhies et al., 2012; Nold et al., 2013). Stable isotope $\delta^{13}C_{org}$ values for LH sediments average -23.8 ± 0.9‰, overlapping the range for MIS (Figure 2.5d).

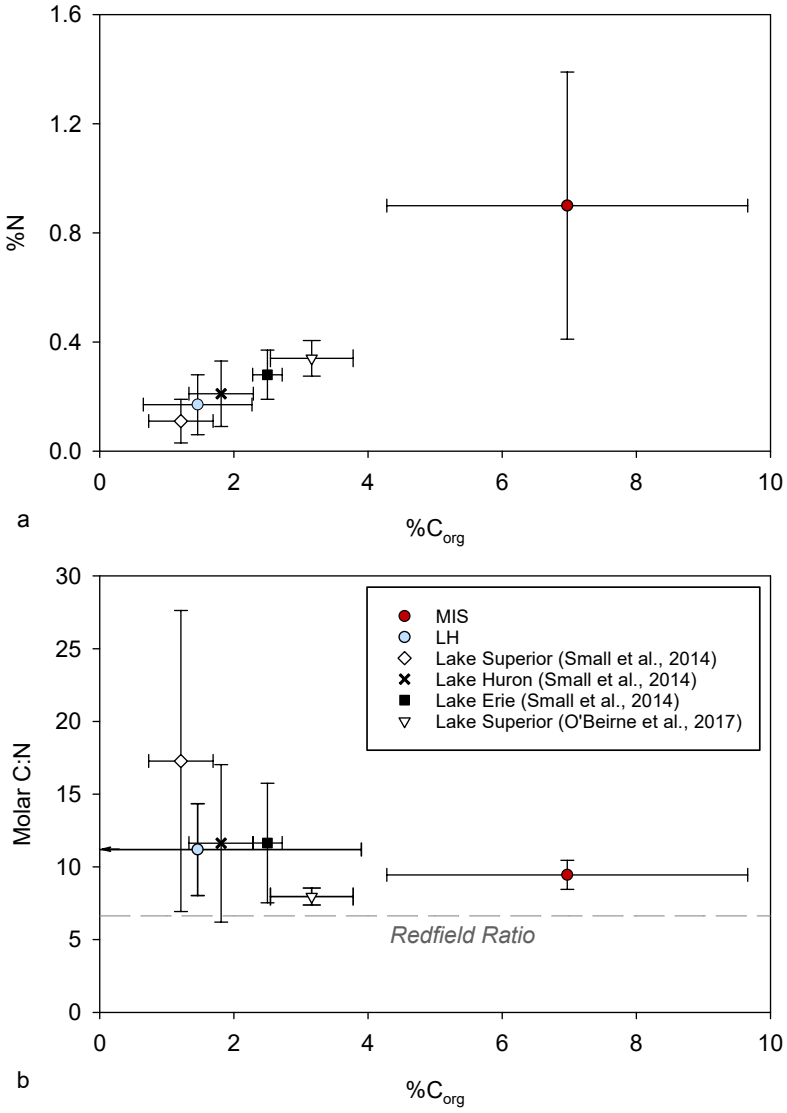

Figure 2.6 Comparative lake sediment C and N. (a) Cross plot of average $\%C_{org}$ versus %N and (b) cross plot of average $\%C_{org}$ versus molar C:N for the Middle Island Sinkhole (MIS) and Lake Huron control site (LH). Other Great Lakes data from Small et al. (2014) and O'Beirne et al. (2017). MIS and LH averages determined using all samples (n = 173 for MIS; n = 27 for LH), while error bars represent one standard deviation from these averages. Gray dashed line denotes C:N Redfield Ratio of marine particulate organic matter (106:16; Redfield, 1934).

2.4.2 Iron Speciation

MIS sediments had significantly greater Fe_T, Fe_{carb}, Fe_{ox}, Fe_{mag}, and Fe_{py} contents than LH sediments ($p < 0.01$; Table 2.3), with no trend downcore for either location (Figure A2). This drives the Fe_{py}/Fe_{HR} and Fe_{HR}/Fe_T ratios—which together are used to consider the degree of

euxinia and anoxia—significantly higher for MIS sediments than LH sediments ($p < 0.001$; Table 2.3; Figure 2.7). The schematic diagram developed by Li et al. (2010) and modified by Raiswell and Canfield (2012) uses various thresholds to designate the water chemistry of aquatic systems. The Fe_{HR}/Fe_T threshold demonstrates the upper limit for oxic deposition for modern and Phanerozoic systems ($Fe_{HR}/Fe_T \geq 0.38$; Raiswell and Canfield, 1998; Poulton and Raiswell, 2002). The Fe_{py}/Fe_{HR} threshold used here depicts the upper limit of ferruginous conditions ($Fe_{py}/Fe_{HR} = 0.7$; März et al., 2008), which incorporates full quantification of Fe_{carb} and Fe_{mag} (as in this study). Using these thresholds, MIS sediments are largely Fe(II)-rich (ferruginous), and LH sediments are oxic (Figure 2.8).

Table 2.3 Mean iron contents for each of the different iron speciation phases for MIS and LH, including probability values from a two-tailed unpaired t-test ($\alpha = 0.05$) to compare the means for each location.

	MIS[1]	LH[1]	p-value
$\%Fe_{carb}$	0.10 ± 0.03	0.03 ± 0.01	<0.001
$\%Fe_{ox}$	0.08 ± 0.04	0.06 ± 0.01	0.006
$\%Fe_{mag}$	0.07 ± 0.01	0.06 ± 0.01	<0.001
$\%Fe_{py}$	0.40 ± 0.06	0.14 ± 0.04	<0.001
$\%Fe_T$	1.45 ± 0.17	1.04 ± 0.13	<0.001
Fe_{py}/Fe_{HR}	0.63 ± 0.05	0.41 ± 0.08	<0.001
Fe_{HR}/Fe_T	0.44 ± 0.07	0.34 ± 0.05	<0.001

[1]Values given as mean ± 1σ

2.5 Discussion

2.5.1 Nutrient Cycling in Anoxic Sediments

The depth profiles of C_{org}, N, P, and S are variable within the first ~3 cm of depth before

stabilizing, with consistently higher nutrient contents in MIS than LH (Figure 2.5). Given that the mat material was not separated from the sediment when sampling cores, this surficial variability is assumed to indicate the presence of the microbial mats. The observed ranges of C_{org} and N contents are similar to prior results from MIS and LH based on smaller datasets (Table 2.2; Figure 2.5; Nold et al., 2013; Kinsman-Costello et al., 2017). These new results can also be put into context via comparison with previous work on the Great Lakes; LH values are similar to other Great Lake surficial sediments data, while MIS is distinctly higher with regards to both C_{org} and N (Figure 2.6a; Small et al., 2014; O'Beirne et al., 2017). Although reduced species such as ammonium can support additional biological productivity (leading to higher burial of organic matter), there is no evidence for enhanced ammonium in the groundwater layer relative to the rest of Lake Huron (Kinsman-Costello et al., 2017). Instead, stable isotopes shed light on the mechanism behind these differences in organic matter burial.

As demonstrated by Nold et al. (2013) and Voorhies et al. (2012), surficial microbial mat $\delta^{13}C_{org}$ values are isotopically more negative than that of Lake Huron phytoplankton. If the microbial mat was continually buried and thereby providing the bulk of the organic matter to MIS sediments, we would expect these sediments to be isotopically more negative as well. However, MIS sediments are isotopically more positive relative to the surface microbial mat, and are more similar to the Lake Huron phytoplankton $\delta^{13}C_{org}$ values (Voorhies et al., 2012; Nold et al., 2013) and to LH surficial sediments (Figure 2.5d), indicating that the buried organic matter in MIS is dominantly sourced from the water column rather than from the microbial mat. Therefore, the mat must either be routinely displaced via underwater currents and storm events (and thereby become incorporated into the sediment elsewhere), or it continually migrates to the sediment surface, recycling its own material instead of being buried. The latter hypothesis is

more likely given the observed rapid motility of the cyanobacteria in the mat (Biddanda et al., 2015), and the lack of evidence for mat burial in any sediment cores throughout the sinkhole (*e.g.,* more positive $\delta^{13}C_{org}$ values in MIS sediment, Figure 2.5d).

Although MIS has greater C_{org} and N values compared to LH, molar C:N ratios are similar between the two locales (Table 2.2; Figures 2.5d and 2.6b). With strong correlations between C_{org} and N for both MIS and LH ($p < 0.0001$; Figure A3) indicating that N in these locations is dominantly organic, C:N ratios can be used to characterize the availability of nutrients from aquatic and terrestrial inputs. Lower C:N ratios in lake sediments (*i.e.*, C:N ratios near the Redfield Ratio of marine phytoplankton: 106:16; Redfield, 1934) indicate organic matter from nonvascular aquatic material (*e.g.,* phytoplankton; Meyers and Ishiwatari, 1993). In comparison to Great Lakes surficial sediment C:N ratios from Small et al. (2014) and O'Beirne et al. (2017), LH and MIS C:N ratios are within range of those from Great Lakes surficial sediment (Figure 2.6b; Kinsman-Costello et al., 2017). However, MIS C:N ratios are consistently low, nearing that of the Redfield Ratio (Figure 2.6b).

Broadly, as C:N ratios increase, the contribution of vascular land plants to the organic matter of lake sediments increases (Meyers and Ishiwatari, 1993). However, because stable $\delta^{13}C_{org}$ values indicate that a common source of organic matter was deposited in both MIS and LH, there must be an alternative explanation for increased C:N ratios in LH. C:N ratios can also be increased by the preferential degradation of N during organic matter remineralization, via dentrification (Van Mooy et al., 2002). Enhanced denitrification in LH would explain the higher C:N ratios in LH, and still allow for the similar sources of organic matter within the two locales (as determined by $\delta^{13}C_{org}$ values). This is corroborated by the low N content of LH (Table 2.2; Figures 2.5b and 2.6a). In addition, while the gross abundance of Nitrospirae in LH sediments

(>11% by OTU; Kinsman-Costello, et al., 2017) cannot be used to determine what specific nitrogen oxidizers and/or denitrifiers are present, the broad phylogenetic group includes many denitrifying microbes. In comparison, the lack of oxygen in MIS sediments (Kinsman-Costello et al., 2017) allows for nitrogen reduction to take place (in accordance with Van Mooy et al., 2002), but the lack of apparent nitrogen loss (Table 2.2; Figures 2.5b and 2.6a) suggests that denitrification is not occurring at high rates. In contrast to many lakes that have C:N ratios that are elevated (>2x) relative to the marine Redfield Ratio (*e.g.*,, Hecky et al., 1993), most Great Lakes sediments (including MIS and LH) are only slightly elevated (Figure 2.6b), which suggests that they may have similar organic matter cycling to marine systems rather than to other lakes. For MIS in particular, this could be driven in part by elevated sulfate concentration and higher conductivity than typical freshwater systems (Figure 2.1).

The influence of the sulfate present in the water column (Figure 2.1; Ruberg et al., 2008; Biddanda et al., 2012; Kinsman-Costello et al., 2017) as well as microbial groups that cycle sulfur (*e.g.,* Cyanobacteria, Beggiatoa, and some Proteobacteria; Figure 2.3; Nold et al., 2010; Voorhies et al., 2012; Kinsman-Costello et al., 2017) results in MIS sediments having bulk S contents an order of magnitude greater than that of LH (Table 2.2). This trend is consistent with the differences in sediment acid volatile sulfides (AVS; Figure 2.1; Kinsman-Costello et al., 2017) and Fe_{py} between the two locales (Table 2.3).

Enhanced P contents in MIS relative to LH (Table 2.2; Figure 2.5f) can be explained by the uptake of P onto organic matter, which occurs to a greater degree in reducing, organic-rich sediments (Slomp et al., 1996; März et al., 2008; Kraal et al., 2015). The high content and variability of P in only the first few centimeters of sediment are attributed to microbial mat influence (Figure 2.5f). In addition, P and C_{org} are significantly correlated for both MIS and LH

sediments ($p < 0.01$; Figure 2.7); this demonstrates that P accumulation in both locales can generally be attributed to biogenic accumulation and cycling. This is further corroborated by results from Kinsman-Costello et al. (2017), who found that microbial community structure within the mat and sediment communities was significantly and highly correlated with soluble reactive phosphorus (SRP) in the porewater and total P in the sediments. In fact, dissolved phosphate profiles from Kinsman-Costello et al. (2017) do not indicate release of P into the water column, and instead indicate a decrease in porewater concentration in the presence of the microbial mat, indicating that these mats may serve as a trap for P. MIS sediments with microbial mat present (sediments 0–3 cm, as determined via $\delta^{13}C$; Voorhies et al., 2012; Nold et al., 2013), show a strong positive correlation between %P and $\%C_{org}$, whereas P contents of MIS sediments >3 cm only increase modestly with higher $\%C_{org}$ values (Figure 2.7). This suggests that the productivity of the MIS microbial mats themselves may inherently be tied to the lack of a P limitation.

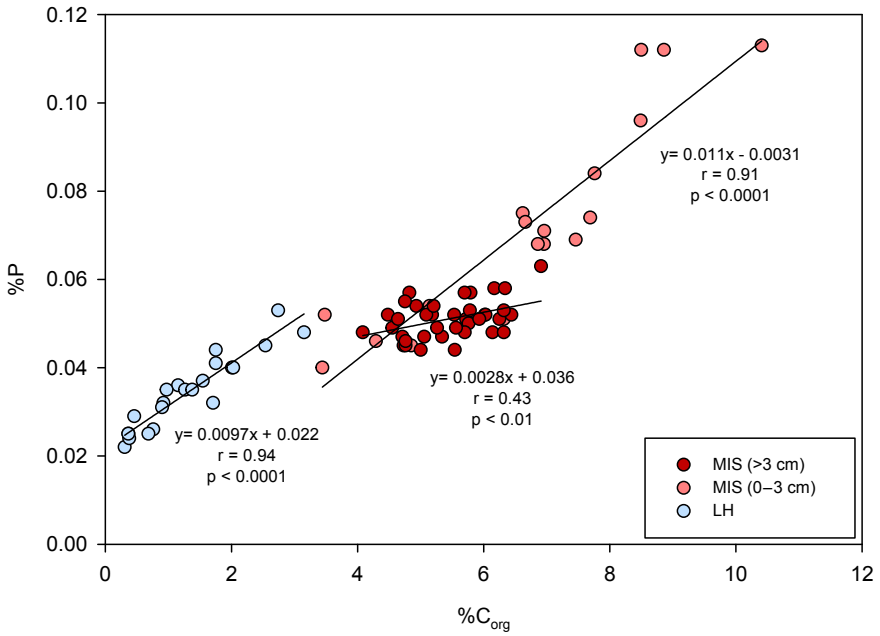

Figure 2.7 Cross plot of the %P versus $\%C_{org}$ for Middle Island Sinkhole (MIS) sediments (n = 38), MIS mat (n = 18), and Lake Huron (LH) sediments (n = 22).

C:P ratios of MIS sediments (103 ± 14) are similar to the C:P Redfield Ratio of phytoplankton (106:1; Redfield, 1934) and are >2x higher than the C:P ratios of LH sediments (35 ± 15; Table 2.2). Higher MIS C:P ratios can partially be attributed to the enhanced C preservation in MIS. In addition, bacterial storage of P can be limited by anoxic conditions (Ingall et al., 1993), which would further increase the C:P ratio at MIS. Ultimately, the similarity of MIS C:N and C:P ratios to the Redfield Ratio provides additional evidence that the dominant source of organic matter being buried is Lake Huron phytoplankton rather than microbial mat, in accordance with the $\delta^{13}C_{org}$ data of buried sediments (this study; Voorhies et al., 2012; Nold et al. 2013). As a result, microbial mat presence cannot fully explain nutrient cycling in this low-oxygen system. Instead, the primary mechanism for organic matter burial in MIS may be tied to preservation.

There are a number of mechanisms by which organic matter is preserved in modern sediments, including varying rates of organic matter decomposition under different oxygen concentrations (Hartnett et al., 1998), sorption of organic matter to mineral surfaces (*e.g.,* Keil et al., 1993), association of organic matter to reactive iron phases (*e.g.,* Lalonde et al., 2012), and organic matter sulfurization (*e.g.,* Werne et al., 2008). All of these mechanisms are dependent to varying degrees on a lack of oxygen availability in the water column above the sediment-water interface. Iron geochemistry helps to elucidate the redox chemistry of MIS and LH further.

2.5.2 Sources and Cycling of Iron

Consistent with data from Kinsman-Costello et al. (2017; Figure 2.1), Fe_T contents are significantly greater in MIS than in LH sediments ($p < 0.001$; Table 2.3). With greater dissolved Fe concentrations in the groundwater-influenced MIS water column relative to the overlying LH

water column (Figure 2.2), some of this total Fe could be sourced from the groundwater in addition to authigenic inputs. Understanding the source of each of the pools of Fe_{HR}—which are also significantly greater in MIS compared to LH ($p < 0.01$; Table 2.3)—can help to elucidate this further. Fe oxides (Fe_{ox} and Fe_{mag}) are expected to be reduced under low-oxygen conditions (*e.g.,* Ingall and Jahnke, 1994; Poulton and Raiswell, 2002), and therefore are unlikely to be sourced from the high-salinity anoxic groundwater. Comparatively, Fe_{carb} could be sourced from the regional groundwater that flows into the sinkhole is sourced from limestone/dolomite sedimentary rocks (Biddanda et al., 2006; 2012). However, Nold et al. (2013) demonstrated that the $\delta^{13}C_{inorg}$ of sediment is consistent with sedimentation and fractionation from Lake Huron dissolved inorganic carbon (DIC) and not with sedimentation and fractionation from the groundwater DIC, which suggests that carbonates (including Fe_{carb}) in MIS sediments are produced authigenically. Voorhies et al. (2012) also used X-ray diffraction (XRD) to identify a significant enrichment in carbonate just beneath the top of the mat surface at MIS, at a depth characterized by sulfide oxidation and sulfate reduction (Figure 2.3). Carbonate precipitation can be promoted by heterotrophic sulfate reduction (*e.g.,* Dupraz et al., 2009), which potentially provides a mechanism for these observations. Just as C_{org} burial is enhanced in MIS, C_{inorg} is also increased, and is available to complex with Fe(II) as Fe_{carb}.

Sulfide is present within the sediment porewater at up to 7 mM but not above the sediment-water interface, where instead dissolved O_2 rises rapidly up through the water column (Kinsman-Costello et al., 2017). This is reflected by enhanced Fe_{py} in MIS sediments relative to LH sediments (Table 2.3), but is not robust enough to drive MIS sediments into the sulfide-rich field (Figure 2.8). This indicates a sulfide limitation in MIS. Although there is unlimited water column sulfate, its transformation across the sediment-water interface by sulfate reducers

(Proteobacteria; Figure 2.3) may be equalled by or even exceeded by sulfide oxidizers (*e.g.,* Beggiatoa; Nold et al., 2010; Kinsman-Costello et al., 2017), limiting the subsequent deposition of sulfide-bearing mineral phases.

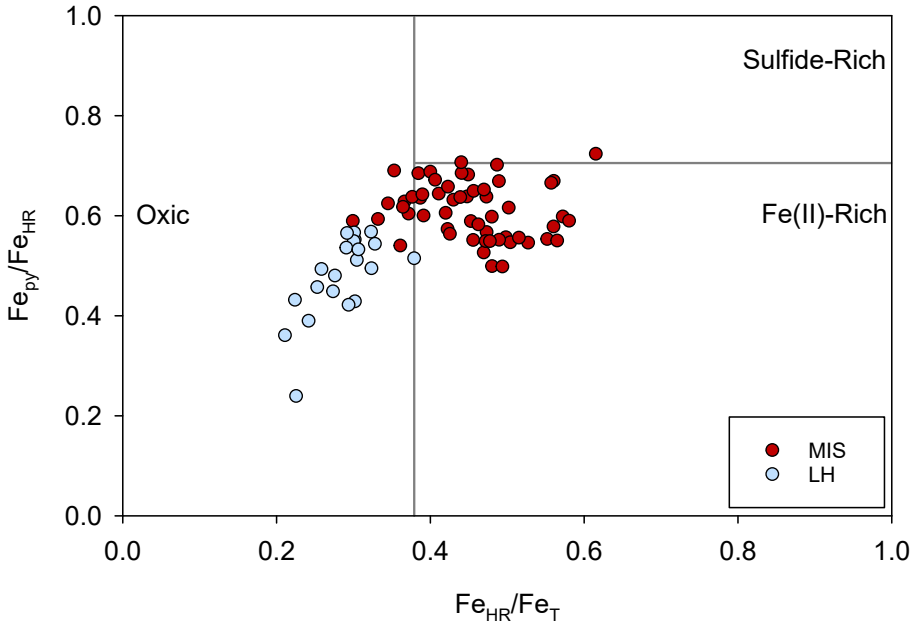

Figure 2.8 Cross plot of the ratios of iron in pyrite (Fe_{py}) to highly reactive iron (Fe_{HR}) versus Fe_{HR} to total iron (Fe_T) for Middle Island Sinkhole (MIS; n = 55) and Lake Huron (LH; n = 21). These values can distinguish aquatic environments as oxic, sulfide-rich, or iron(II)- rich (Li et al., 2010; Poulton and Canfield, 2011; Raiswell and Canfield, 2012). Vertical line determines the upper limit for ferruginous waters (März et al., 2008) while the horizontal line determines the upper limit of oxic deposition (Raiswell and Canfield, 1998; Poulton and Raiswell, 2003).

2.5.3 Iron Speciation Interpretations

Development of Fe speciation in marine, sulfide-rich systems with deep shelf-to-basin transport may potentially result in challenges when the methodology is used to interrogate basins with a shallow depth gradient. In these systems, it is difficult to discern whether this technique demonstrates the redox chemistry of the entire water column, the redoxcline above the sediment-water interface, or that of the porewater. For a system like MIS, where ~20 m of oxic water overlies a few meters of low-oxygen water, and a second chemocline occurs at the sediment-

water interface (Figure 2.1; Kinsman-Costello et al., 2017), this information is crucial. Samples from MIS indicate ferruginous conditions (Figure 2.8), consistent with the lack of dissolved oxygen and dissolved sulfide, and the availability of free Fe in the groundwater-influenced layer (Figures 2.1 and 2.2; Ruberg et al., 2008; Biddanda et al., 2012). Similarly, LH plots as oxic (Figure 2.8), which is also consistent with known water chemistry measured at different places within MIS previously (Figures 2.1 and 2.2; Ruberg et al., 2008; Biddanda et al., 2012). These Fe speciation results indicate that this method is recording Fe systematics of the low-oxygen water column just above the sediment-water interface, where sediment is deposited. Therefore, these Fe speciation results do not provide any indication of the long-range transport of Fe through the overlying oxic water column, nor the water chemistry of the porewater, which is sulfide-rich.

This suggests that Fe speciation results on ancient sediments may only provide a snapshot of water column chemistry, and therefore caution should be taken when considering the expanse of anoxic redox conditions (*i.e.*, the depth of the chemocline) in ancient oceans. In many cases, especially for pre-GOE Paleoproterozoic or Archean rocks, this distinction would not change the overall interpretation. However, for post-GOE systems where variable redox is more commonly observed, this could be critical for understanding shifts in redox chemistry across a shallow Proterozoic ocean shelf (as this study proposes MIS is an analogue for; Figure 2.4), as seen during the Mesoproterozoic (Poulton et al., 2010). Additionally, careful consideration of Fe speciation interpretations as they pertain to spatial variability allows us to examine more nuanced paleoceanographic factors such as the scale of oxygen minimum zones or carbonate compensation depth shoaling (which could shift the Fe_{carb} fraction, artificially making the system seem less reducing than it was). Continued application of the Fe speciation method on a variety

of aquatic environments would help us to define modern Fe transport dynamics better, which in turn will allow us to examine the Fe speciation results of ancient systems critically.

2.6 Conclusions

Nutrient and Fe burial is greater in MIS than LH, but $\delta^{13}C$ data reflect that the buried material is similar between the two locales, likely reflecting primary pelagic production rather than *in situ* production by the microbial mat system present only at MIS. Therefore, the differences in organic matter and Fe burial must be due to differences in preservation, which is attributed to varied redox chemistry. Iron speciation was used to explore this further. This test of the applicability of a marine-calibrated technique to a freshwater lake clearly differentiated between oxic and ferruginous locales, in line with known water chemistry. Fe speciation results are consistent with either or both of rapid speciation in the redoxcline between oxygenated surface and ferruginous deep waters or some re-speciation of Fe in the sediments themselves. However, given the presence of porewater sulfide in the MIS sediments, the former mechanism can be considered more likely or of relatively great importance. This has important implications for our understanding of what Fe speciation of geologic materials means, because it may reflect a strong redoxcline rather than the whole water column. Finally, in shallow ferruginous settings, redox chemistry may control biogeochemical cycling more than microbial activity, potentially limiting primary productivity at some times and/or in some basins.

2.7 Acknowledgements

We would like to thank the NOAA Thunder Bay National Marine Sanctuary dive team and ship captains for their aide in field site access and sampling. Thanks to Rebecca Dzombak

and Clarissa Crist for their help in sample processing, C and N analysis, and Fe speciation measurements. We appreciate the water column Fe analysis done by Dr. Anthony Chappaz of STARLAB at Central Michigan University, the ICP-OES Fe analysis by Sara Nedrich in the laboratory of Dr. Allen Burton at the University of Michigan for ICP-OES Fe analysis, and the $\delta^{13}C_{org}$ work done by Lora Wingate in the Stable Isotope Prep Lab at the University of Michigan. This research was funded by the NSF GRFP to KIR, a University of Michigan Department of EES Turner Award to KIR, a 2015 GSA Research Grant to KIR, and a Sokol Foundation grant to NDS.

2.8 References

Anderson, T.F., Raiswell, R., 2004. Sources and mechanisms for the enrichment of highly reactive iron in euxinic Black Sea sediments. Am. J. Sci. 304, 203–233. https://doi.org/10.2475/ajs.304.3.203

Biddanda, B. A., Coleman, D.F., Johengen, T.H., Ruberg, S. A., Meadows, G. A., Van Sumeren, H.W., Rediske, R.R., Kendall, S.T., 2006. Exploration of a submerged sinkhole ecosystem in Lake Huron. Ecosystems 9, 828–842. https://doi.org/10.1007/s10021-005-0057-y

Biddanda, B. A., McMillan, A.C., Long, S. A., Snider, M.J., Weinke, A.D., 2015. Seeking sunlight: rapid phototactic motility of filamentous mat-forming cyanobacteria optimize photosynthesis and enhance carbon burial in Lake Huron's submerged sinkholes. Front. Microbiol. 6, 1–13. https://doi.org/10.3389/fmicb.2015.00930

Biddanda, B.A., Nold, S.C., Dick, G.J., Kendall, S.T., Vail, J.H., Ruberg, S.A., Green, C.M., 2012. Rock, Water, Microbes: Underwater Sinkholes in Lake Huron are Habitats for Ancient Microbial Life Characteristics of Lake Huron's Submerged Sinkholes. Nat. Educ. Knowl. 3.

Bjerrum, C.J., Canfield, D.E., 2002. Ocean productivity before about 1.9 Gyr ago limited by phosphorus adsorption onto iron oxides. Nature 417, 159–162. https://doi.org/10.1016/j.tecto.2003.08.024

Blättler, C.L., Claire, M.W., Prave, A.R., Kirsimäe, K., Higgins, J.A., Medvedev, P. V., Romashkin, A.E., Rychanchik, D. V., Zerkle, A.L., Paiste, K., Kreitsmann, T., Millar, I.L., Hayles, J.A., Bao, H., Turchyn, A. V., Warke, M.R., Lepland, A., 2018. Two-billion-year-

old evaporites capture Earth's great oxidation. Science (80). 360, 320–323. https://doi.org/10.1126/science.aar2687

Canfield, D.E., Poulton, S.W., Narbonne, G.M., 2007. Late-Neoproterozoic deep-ocean oxgenation and the rise of animal life. Science (80). 315, 3–6. https://doi.org/10.1126/science.1135013

Canfield, D.E., 1998. A new model for Proterozoic ocean chemistry. Nature 396, 1–4.

Canfield, D.E., Poulton, S.W., Knoll, A.H., Narbonne, G.M., Ross, G., Goldberg, T., Strauss, H., 2008. Ferruginous Condition Dominated Later Neoproterozoic Deep Water Chemistry. Science (80). 321, 949–952. https://doi.org/10.1126/science.1154499

Canfield, D.E., Berner, R. A., 1987. Dissolution and pyritization of magnetite in anoxie marine sediments. Geochim. Cosmochim. Acta 51, 645–659. https://doi.org/10.1016/0016-7037(87)90076-7

Canfield, D.E., Raiswell, R., Westrich, J.T., Reaves, C.M., Berner, R. A., 1986. The use of chromium reduction in the analysis of reduced inorganic sulfur in sediments and shales. Chem. Geol. 54, 149–155. https://doi.org/10.1016/0009-2541(86)90078-1

Catling, D.C., Glein, C.R., Zahnle, K.J., McKay, C.P., 2005. Why O_2 is required by complex life on habitable planets and the concept of planetary "oxygenation time." Astrobiology 5, 568–574.

Dupraz, C., Reid, R.P., Braissant, O., Decho, A.W., Norman, R.S., Visscher, P.T., 2009. Processes of carbonate precipitation in modern microbial mats. Earth-Science Rev. 96, 141–162. https://doi.org/10.1016/j.earscirev.2008.10.005

Hartnett, H.E., Keil, R.G., Hedges, J.I., Devol, A.H., 1998. Influence of oxygen exposure time on organic carbon preservation in continental margin sediments. Nature 391, 2–4.

Hecky, R.E., Campbell, P., Hendzel, L.L., 1993. The stoichiometry of carbon, nitrogen, and phosphorus in particulate matter of lakes and oceans. Limnol. Oceanogr. 38, 709–724. https://doi.org/10.4319/lo.1993.38.4.0709

Ingall, E.D., Bustin, R.M., Van Cappellen, P., 1993. Influence of water column anoxia on the burial and preservation of carbon and phosphorus in marine shales. Geochim. Cosmochim. Acta 57, 303–316. https://doi.org/10.1016/0016-7037(93)90433-W

Ingall, E., Jahnke, R., 1994. Evidence for enhanced phosphorus regeneration from marine sediments overlain by oxygen depleted waters. Geochim. Cosmochim. Acta 58, 2571–2575. https://doi.org/10.1016/0016-7037(94)90033-7

Johnston, D.T., Wolfe-Simon, F., Pearson, A., Knoll, a. H., 2009. Anoxygenic photosynthesis modulated Proterozoic oxygen and sustained Earth's middle age. Proc. Natl. Acad. Sci. 106, 16925–16929. https://doi.org/10.1073/pnas.0909248106

Jones, C., Nomosatryo, S., Crowe, S.A., Bjerrum, C.J., Canfield, D.E., 2015. Iron oxides, divalent cations, silica, and the early earth phosphorus crisis. Geology 43, 135–138. https://doi.org/10.1130/G36044.1

Kah, L.C., Lyons, T.W., Frank, T.D., 2004. Low marine sulphate and protracted oxygenation of the Proterozoic biosphere. Nature 431, 834–838. https://doi.org/10.1038/nature02974

Kinsman-Costello, L.E., Sheik, C.S., Sheldon, N.D., Burton, G. A., Costello, D., Marcus, D.N., Uyl, P. Den, Dick, G.J., 2017. Groundwater shapes sediment biogeochemistry and microbial diversity in a submerged sinkhole. Geobiology 15, 225–239. https://doi.org/10.1038/nature04068

Lalonde, K., Mucci, A., Ouellet, A., Gélinas, Y., 2012. Preservation of organic matter in sediments promoted by iron. Nature 483, 198–200. https://doi.org/10.1038/nature10855

Li, C., Love, G.D., Lyons, T.W., Fike, D. a., Sessions, A.L., Chu, X., 2010. A stratified redox model for the Ediacaran ocean. Science (80). 328, 80–83. https://doi.org/10.1126/science.1182369

Luo, G., Ono, S., Huang, J., Algeo, T.J., Li, C., Zhou, L., Robinson, A., Lyons, T.W., Xie, S., 2015. Decline in oceanic sulfate levels during the early Mesoproterozoic. Precambrian Res. 258, 36–47. https://doi.org/10.1016/j.precamres.2014.12.014

Lyons, T.W., Reinhard, C.T., Planavsky, N.J., 2014. The rise of oxygen in Earth's early ocean and atmosphere. Nature 506, 307–15. https://doi.org/10.1038/nature13068

Lyons, T.W., Anbar, A.D., Severmann, S., Scott, C., Gill, B.C., 2009. Tracking euxinia in the ancient ocean: A multiproxy perspective and Proterozoic case study. Annu. Rev. Earth Planet. Sci. 37, 507–534. https://doi.org/10.1146/annurev.earth.36.031207.124233

Lyons, T.W., Severmann, S., 2006. A critical look at iron paleoredox proxies: New insights from modern euxinic marine basins. Geochim. Cosmochim. Acta 70, 5698–5722. https://doi.org/10.1016/j.gca.2006.08.021

März, C., Poulton, S.W., Beckmann, B., Küster, K., Wagner, T., Kasten, S., 2008. Redox sensitivity of P cycling during marine black shale formation: Dynamics of sulfidic and anoxic, non-sulfidic bottom waters. Geochim. Cosmochim. Acta 72, 3703–3717. https://doi.org/10.1016/j.gca.2008.04.025

Nold, S.C., Bellecourt, M.J., Kendall, S.T., Ruberg, S. A., Sanders, T.G., Klump, J.V., Biddanda, B. A., 2013. Underwater sinkhole sediments sequester Lake Huron's carbon. Biogeochemistry 115, 235–250. https://doi.org/10.1007/s10533-013-9830-8

Nold, S.C., Pangborn, J.B., Zajack, H. A., Kendall, S.T., Rediske, R.R., Biddanda, B.A., 2010. Benthic bacterial diversity in submerged sinkhole ecosystems. Appl. Environ. Microbiol. 76, 347–351. https://doi.org/10.1128/AEM.01186-09

Nursall, J.R., 1959. Oxygen as a prerequisite to the origin of the metazoa. Nature 183, 1170–1172.

O'Beirne, M.D., Werne, J.P., Hecky, R.E., Johnson, T.C., Katsev, S., Reavie, E.D., 2017. Anthropogenic climate change has altered primary productivity in Lake Superior. Nat. Commun. 8, 15713. https://doi.org/10.1038/ncomms15713

Olson, S.L., Reinhard, C.T., Lyons, T.W., 2016. Limited role for methane in the mid-Proterozoic greenhouse. Proc. Natl. Acad. Sci. 113, 11447–11452. https://doi.org/10.1073/pnas.1608549113

Poulton, S., Canfield, D., 2005. Development of a sequential extraction procedure for iron: implications for iron partitioning in continentally derived particulates. Chem. Geol. 214, 209–221. https://doi.org/10.1016/j.chemgeo.2004.09.003

Poulton, S.W., Canfeld, D.E., 2011. Ferruginous conditions: A dominant feature of the ocean through Earth's history. Elements 7, 107–112. https://doi.org/10.2113/gselements.7.2.107

Poulton, S.W., Fralick, P.W., Canfield, D.E., 2010. Spatial variability in oceanic redox structure 1.8 billion years ago. Nat. Geosci. 3, 486–490. https://doi.org/10.1038/ngeo889

Poulton, S.W., Fralick, P.W., Canfield, D.E., 2004. The transition to a sulphidic ocean, 1.84 billion years ago. Nature 431, 173–177. https://doi.org/10.1038/nature02863.1.

Poulton, S.W., Krom, M.D., Raiswell, R., 2004. A revised scheme for the reactivity of iron (oxyhydr)oxide minerals towards dissolved sulfide. Geochim. Cosmochim. Acta 68, 3703–3715. https://doi.org/10.1016/j.gca.2004.03.012

Poulton, S.W., Raiswell, R., 2002. The low-temperature geochemical cycle of iron: From continental fluxes to marine sediment deposition. Am. J. Sci. 302, 774–805.

Raiswell, R., Canfield, D.E., 1998. Sources of iron for pyrite formation in marine sediments. Am. J. Sci. 298, 219–245. https://doi.org/10.1017/CBO9781107415324.004

Raiswell R. and Canfield D. E., 2012. The iron biogeochemical cycle past and present. Geochem. Perspectives 1, 1–220.

Redfield, A. C., 1934. On the proportions of organic derivatives in sea water and their relation to the composition of plankton. James Johnstone memorial volume. University press of Liverpool. pp. 176–192.

Rozanov A. G., Volkov I. I. and Yagodinskaya T. A., 1974. Forms of iron in surface layer of

Black Sea sediments. In: The Black Sea—Geology, Chemistry, and Biology, eds. E. T. Degens and D. A. Ross. The American Association of Petroleum Geologists, Tulsa, Oklahoma. pp. 532–541.

Ruberg, S.A., Kendall, S.T., Biddanda, B.A., Black, T., Nold, S.C., Lusardi, W.R., Green, R., Casserly, T., Smith, E., Sanders, T.G., Lang, G.A., Constant, S.A., 2008. Observations of the Middle Island Sinkhole and Glacial Creation of 400 Million Years. Mar. Technol. Soc. J. 42, 12–21.

Scott, C., Lyons, T.W., Bekker, A., Shen, Y., Poulton, S.W., Chu, X., Anbar, A. D., 2008. Tracing the stepwise oxygenation of the Proterozoic ocean. Nature 452, 456–459. https://doi.org/10.1038/nature06811

Scott, C., Wing, B. A., Bekker, A., Planavsky, N.J., Medvedev, P., Bates, S.M., Yun, M., Lyons, T.W., 2014. Pyrite multiple-sulfur isotope evidence for rapid expansion and contraction of the early Paleoproterozoic seawater sulfate reservoir. Earth Planet. Sci. Lett. 389, 95–104. https://doi.org/10.1016/j.epsl.2013.12.010

Shen, Y., Canfield, D.E., Knoll, A.H., 2002. Middle Proterozoic Ocean Chemistry: Evidence from the McArthur Basin, Northern Australia. Am. J. Sci. 302, 1–27. https://doi.org/10.1126/science.3.53.32

Slomp, C.P., Van Der Gaast, S.J., Van Raaphorst, W., 1996. Phosphorus binding by poorly crystalline iron oxides in North Sea sediments. Mar. Chem. 52, 55–73. https://doi.org/10.1016/0304-4203(95)00078-X

Small, G.E., Cotner, J.B., Finlay, J.C., Stark, R. A., Sterner, R.W., 2013. Nitrogen transformations at the sediment–water interface across redox gradients in the Laurentian Great Lakes. Hydrobiologia 731, 95–108. https://doi.org/10.1007/s10750-013-1569-7

Sperling, E.A., Halverson, G.P., Knoll, A.H., Macdonald, F.A., Johnston, D.T., 2013. A basin redox transect at the dawn of animal life. Earth Planet. Sci. Lett. 371–372, 143–155. https://doi.org/10.1016/j.epsl.2013.04.003

Sperling, E. A., Wolock, C.J., Morgan, A.S., Gill, B.C., Kunzmann, M., Halverson, G.P., Macdonald, F. A., Knoll, A.H., Johnston, D.T., 2015. Statistical analysis of iron geochemical data suggests limited late Proterozoic oxygenation. Nature 523, 451–454. https://doi.org/10.1038/nature14589

Tessin, A., Sheldon, N.D., Hendy, I., Chappaz, A., 2016. Iron limitation in the Western Interior Seaway during the Late Cretaceous OAE 3 and its role in phosphorus recycling and enhanced organic matter preservation. Earth Planet. Sci. Lett. 449, 135–144. https://doi.org/10.1016/j.epsl.2016.05.043

Van Mooy, B. A. S., Keil, R.G., Devol, A.H., 2002. Impact of suboxia on sinking particulate organic carbon: Enhanced carbon flux and preferential degradation of amino acids via

denitrification. Geochim. Cosmochim. Acta 66, 457–465. https://doi.org/10.1016/S0016-7037(01)00787-6

Voorhies, A.A., Biddanda, B.A., Kendall, S.T., Jain, S., Marcus, D.N., Nold, S.C., Sheldon, N.D., Dick, G.J., 2012. Cyanobacterial life at low O(2): community genomics and function reveal metabolic versatility and extremely low diversity in a Great Lakes sinkhole mat. Geobiology 10, 250–67. https://doi.org/10.1111/j.1472-4669.2012.00322.x

Werne, J.P., Lyons, T.W., Hollander, D.J., Schouten, S., Hopmans, E.C., Sinninghe Damsté, J.S., 2008. Investigating pathways of diagenetic organic matter sulfurization using compound-specific sulfur isotope analysis. Geochim. Cosmochim. Acta 72, 3489–3502. https://doi.org/10.1016/j.gca.2008.04.033

Wood, R.A., Poulton, S.W., Prave, A.R., Hoffmann, K.H., Clarkson, M.O., Guilbaud, R., Lyne, J.W., Tostevin, R., Bowyer, F., Penny, A.M., Curtis, A., Kasemann, S.A., 2015. Dynamic redox conditions control late Ediacaran metazoan ecosystems in the Nama Group, Namibia. Precambrian Res. 261, 252–271. https://doi.org/10.1016/j.precamres.2015.02.004

Xu, H., Ai, L., Tan, L., An, Z., 2006. Stable isotopes in bulk carbonates and organic matter in recent sediments of Lake Qinghai and their climatic implications 235, 262–275. https://doi.org/10.1016/j.chemgeo.2006.07.005

CHAPTER III

Associations Between Redox-Sensitive Trace Metals and Microbial Communities in a Proterozoic Ocean Analogue

3.1 Abstract

Constraints on Precambrian ocean chemistry—and, subsequently, atmospheric oxygenation—are dependent upon sediment geochemistry. However, ancient sediments may or may not include biomarker evidence, making it difficult to consider biology when interpreting geochemical data. Instead, modern analogues for ancient ecosystems can be useful tools for identifying how sediment geochemistry records an active biosphere. The Middle Island Sinkhole (MIS) in Lake Huron is an analogue for shallow Proterozoic waters due to its low oxygen, moderate sulfate, high salinity water chemistry, and microbial communities that exhibit diverse metabolic functions at the sediment-water interface. This study uses sediment trace metal contents and microbial community composition in MIS sediments and at a fully oxygenated Lake Huron control site (LH) to infer mechanisms for abiotic and biotic controls on trace metal burial. Notably, relationships between trace metals and organic matter do not follow expected trends based on our conventional understanding of how the trace metals are buried. For metals that serve as paleo-proxies, such as Mo, this has major implications for our interpretations of Mo abundance and Mo isotope systematics in the geologic record. Additionally, while there are key microbial groups for each of the sampling locales (*e.g.*, cyanobacteria in the MIS microbial mat), LH and MIS ultimately have similar relationships between microbial assemblages and metal

associations with organic carbon burial, making it difficult to link trace metal burial to specific microbial metabolisms. Together, these results indicate that bulk sediment trace metal composition does not capture microbiological processes. Trace metal abundance cannot be used as a biosignature for the presence of microbial mats in the fossil record. Instead, more robust trace metal geochemistry such as isotopes and speciation may be critical for understanding the intersections between microbiology and sediment geochemistry.

3.2 Introduction

Partial oxygenation of the atmosphere 2.34 Ga (the Great Oxidation Event; GOE) is widely accepted due to the disappearance of non-mass-dependent $\Delta^{33}S$ anomalies (Farquhar et al., 2000) as well as a variety of other observations from the sedimentary record such as the appearance of oxidized soils on land and the loss of pyrite from ancient stream beds (see Lyons et al., 2014, for review). The relationship between atmospheric oxygenation and biological evolution during the Proterozoic (2.5 to 0.5 Ga) is relatively well understood, with anoxygenic photosynthesis dominating prior to the GOE (Johnston et al., 2009), and oxygenic photosynthesis by cyanobacteria hypothesized to be one of the primary drivers of the GOE (Kopp et al., 2005; Holland, 2005). Ancient oceans also responded to the shifts in atmospheric oxygen, in that (at least surficial) ocean oxygenation only occurred after the GOE, in comparison to dominantly anoxic Archean oceans (Lyons et al., 2014; Planavsky et al., 2018). However, the relationships between microbial consortia, redox, and biogeochemical cycling of elements in shallow Proterozoic oceans is not well understood.

The majority of evidence for biota in the Proterozoic comes from stromatolites, which both diversified and became more abundant in the Paleoproterozoic and Mesoproterozoic

(Awramik and Sprinkle, 1999; Noffke and Awramik, 2013). However, not all microbial systems become lithified to form stromatolites (Awramik and Sprinkle, 1999), and stromatolites can form abiotically (Grotzinger and Rotheman, 1996). Organic biomarkers have been interpreted as evidence of microbial life in the Precambrian, yet these can be contaminated by hydrocarbons of surficial sampling materials (Brocks et al., 2008; Brocks, 2011; Brocks et al., 2017). Carbon isotope fractionation and discrimination corresponds to specific enzymatic pathways for the assimilation of CO_2 of different microbial metabolisms (*e.g.*, Quandt et al., 1977; Zyakun et al., 2009; Posth et al., 2017), but this signal is subject to diagenetic alteration (*e.g.*, Imbus et al., 1992), as well as significant overlaps in C isotopes between different metabolisms (Schidlowski and Aharon, 1992). Therefore, it is critical to explore alternative methods for recognizing the presence of microbial mats and of their respective metabolic consortia in the fossil record.

Conventionally, trace metal (*e.g.*, Mo, U) sediment geochemistry is considered a robust tool for constraining the redox chemistry of ancient oceans (*e.g.*, Algeo and Lyons, 2006; Tessin et al., 2018; Planavsky et al., 2018). In addition to its application as a paleoredox proxy, trace metal geochemistry has also been used to infer microbial activity and/or the potential for biological evolution in the fossil record. For example, Parnell et al. (2015) argue that Mo enrichments in the 1.18 Ga Stoer Group (UK) indicate widespread nutrient availability and the potential for biological evolution. In addition, Zhang et al. (2016) have identified sufficient oxygen for animal respiration based depletions in V concurring with Mo and U enrichments in 1.4 Ga shales. Finally, iron and trace metal contents of Banded Iron Formations (BIF) have been used to demonstrate how iron oxidizing bacteria had a major role in the formation of these temporally expansive Precambrian deposits (Konhauser et al., 2002; Kappler and Pasquero, 2005; Canfield et al., 2018; Konhauser et al., 2018).

This work aims to use an analogue for the Proterozoic to test whether or not sediment trace metal geochemistry has the potential to serve as a biomarker for the presence of a cyanobacterial microbial mat. The Middle Island Sinkhole (MIS), located 23 m below the surface of Lake Huron, has biotic and abiotic characteristics that make it an appropriate analogue for shallow Proterozoic ocean sites (Table 3.1). MIS has lower oxygen, elevated sulfate concentration, higher conductivity (*i.e.*, salinity) relative to typical lakes (Table 3.1; Ruberg et al., 2008; Biddanda et al., 2012), with dissolved oxygen, iron, and sulfate values similar to those reconstructed for shallow Proterozoic ocean waters (Rico and Sheldon, 2019). This water chemistry allows for the proliferation of microbial communities of diverse metabolic functions at the sediment-water interface. These microbial mats include cyanobacteria that conduct both anoxygenic and oxygenic photosynthesis, sulfur oxidizers and reducers, and Archaea (Biddanda et al., 2012; Voorhies et al., 2012; Kinsman-Costello et al., 2017).

Table 3.1 Summary of select water column and sediment parameters, comparing the Middle Island Sinkhole (MIS) to the Lake Huron control site (LH).

		MIS	LH
Water Column Parameters	**Dissolved oxygen concentration (μM)**[1,2]	<125	344
	Salinity (PSU) [1,2]	1.23	0.13
	Dissolved sulfate concentration (mM) [1,2]	7.8	0.15
	Dissolved iron concentration (μM) [3]	1–2	<0.1
Sediment Parameters	**Organic C (%)**[3]	7	1.5
	Total Fe (%)[3]	1.5	1.0

[1]from Ruberg et al., 2008 and Biddanda et al., 2012
[2]from Rico and Sheldon, 2019

Placing sediment trace metal contents within the context of known redox chemistry, nutrient availability, and microbial community composition of both MIS and a fully oxygenated Lake Huron control site (LH), can elucidate how trace metals respond to different abiotic (*i.e.*,

redox) and biotic controls. Relationships between organic matter and different types of metals—organically-complexed, micronutrient, oxide-forming, and sulfide-complexed—in oxic LH and anoxic MIS serve as a test to gauge whether or not these metals are responding as expected based on their use as paleoredox and paleoproductivity proxies. Additionally, considering MIS as an analogue for Proterozoic oceans (Biddanda et al., 2012; Voorhies et al., 2012; Rico and Sheldon, 2019), MIS microbial mats can be used to determine if relationships between trace metals and microbial communities can be used as a biosignature for microbial activity in the fossil record.

3.3 Methods

3.3.1 Sample Collection and Processing

National Oceanic Administration Thunder Bay National Marine Sanctuary (NOAA TBNMS) scuba divers collected surficial sediment cores from MIS (n = 9; 45°11.911′ N, 83°19.662′) and LH (n = 8; 45°12.267′ N, 83°19.831′ W) during September 2014 and May 2015. Sediments were collected in 20 x 7 cm (length x inner diameter) clear polycarbonate tubes. In May 2015, one "long core" (30 x 7 cm) was also collected at MIS. Cores were immediately frozen and transported upright to the University of Michigan in Ann Arbor, MI, where they were stored at -20°C. Frozen cores were sectioned via a solvent-cleaned table saw according to depth (three 1 cm sections at the top, then 3 cm intervals downcore), freeze-dried, and homogenized.

3.3.2. Elemental Analysis

MIS (n = 56) and LH (n = 22) samples were analyzed for metal (U, V, Cd, Zn, Ni, Cu, Fe, Mn, Mo, Al) and macronutrient (S, P) contents at ALS Laboratories in Vancouver, British Columbia (Mo and U contents previously reported in Rico et al., 2019; Fe, S, and P contents

were previously reported in Rico and Sheldon, 2019). Samples were digested with perchloric, hydrofluoric, nitric, and hydrochloric acids, and concentrations were determined by inductively coupled plasma (ICP)-atomic emission spectroscopy and ICP-mass spectroscopy. OREA-45d, MRGeo08, OGGeo08, CDN-CM-34, SARM-45, and SARM-43 internal standards were used to verify elemental concentrations. Major element uncertainty was typically 0.2 wt.% and trace element uncertainties were variable, but typically on the order of a few ppm.

3.3.3 Trace Element Organization

Trace metals are presented as normalized to Al content in order to represent authigenic concentrations of target elements (Van der Weijden, 2002). Al was chosen because Al contents across MIS and LH had less variability other immobile elements (*i.e.*, Ti and Zr; Van der Weijden, 2002). The metals selected (U, V, Cd, Zn, Ni, Cu, Mn, Mo) were divided into four categories based upon their respective uses as redox and productivity proxies: organically-complexed metals that accumulate under sub-oxic to anoxic conditions (U and V; Klinkhammer and Palmer, 1991; Algeo and Maynard, 2004; Tribovillard et al., 2006); metals that act as micronutrients, especially as incorporated into microbial metabolisms (Zn, Cd, Ni, and Cu; Lepp, 1992; Tribovillard et al., 2006; Jelen et al., 2016; Moore et al., 2017), oxide-forming metals (*e.g.*, Mn; Calvert and Pederson, 1993; Tribovillard et al., 2006), and sulfide-complexed trace metals (*e.g.*, Mo; Erickson and Helz, 2000; Zheng et al., 2000). Although Fe geochemistry is also considered to be one of the most robust tools for understanding the redox chemistry of aquatic environments (Raiswell and Canfield, 2012; Raiswell et al., 2018), Fe could be placed the various categories of metals explored in this study (*e.g.*, Fe forms oxides, is reactive to sulfide, and can be used as enzymatic cofactor across a variety of microbial metabolisms; Huerta-Diaz

and Morse, 1992; Tessier et al., 1996; Moore et al., 2017). In addition, the Fe geochemistry of MIS and LH has already been explored in Rico and Sheldon (2019). Hence, discussion of Fe in this study is limited.

3.3.4 Microbial Community Composition

Relative abundances of microbial communities for MIS sediments and mat (n = 87), MIS mat (n = 17, wherein mat is defined as 0–1 cm depth), and LH sediments (n = 11) were previously published by Kinsman-Costello et al. (2017); see methods therein for complete information on DNA extraction, quantification, amplification, sequencing, and operational taxonomic unit (OTU) clustering.

3.3.5 Ordination Methods

Principal Component Analysis (PCA) was performed using Past 3.14 (Hammer et al., 2001) in order to a) represent how different trace metals and macronutrients are associated with MIS mat and sediment, and LH sediment, and b) how trace metal and macronutrient geochemistry are related to the relative abundances of major biological groups. In order to demonstrate true variance in the data and account for different unit scales, all variables were standardized by z-score (see supplemental materials for details).

3.4 Results and Discussion

3.4.1 Broad Controls on Trace Metal Burial

Independent of water column oxygen iron measurements, the iron geochemistry of MIS and LH sediments have corroborated known water chemistries of the two locales, providing a

redox-based mechanism for the enhanced burial of macronutrients and the abundance of different species of Fe in MIS sediments (Table 3.1; Rico and Sheldon, 2019). Similarly, these differences in redox chemistry can impact trace metal burial. Trace metal contents do not vary between the MIS mat and MIS sediments, but are generally higher than those of the LH sediments, with Mn as the only exception (Table 3.2). In MIS sediments, downcore trace metal contents do not change with depth for U, V, Ni, Cu, and Fe (Figures 3.1 and B1), increase in Cd and Zn with depth (Figures 3.1 and B1), and decrease with depth for Mo (Figure 3.1). Trace metal contents of LH sediments show a pattern of decreasing abundance with depth after 10 cm, however Mn also decreases with depth in the first 3 cm (Figure 3.1). Principal Component and correlative analyses help to determine how variable redox chemistry between LH and MIS has an impact on trace metal burial.

Table 3.2 Average[1] Al-normalized trace metal contents for MIS sediments (n = 38), MIS mat (n = 18), and LH (n = 22) sediments.

	MIS Sediments	MIS Mat	LH
U/Al (μmol mol^{-1})	6.13 ± 0.49	6.55 ± 0.56	3.85 ± 0.70
V/Al (μmol mol^{-1})	28.7 ± 2.3	30.6 ± 2.6	18.0 ± 3.3
Cd/Al (μmol mol^{-1})	4.99 ± 0.73	4.36 ± 0.79	3.03 ± 0.86
Zn/Al (mmol mol^{-1})	0.79 ± 0.07	0.75 ± 0.12	0.47 ± 0.12
Ni/Al (mmol mol^{-1})	0.34 ± 0.03	0.31 ± 0.04	0.19 ± 0.05
Cu/Al (mmol mol^{-1})	0.30 ± 0.02	0.30 ± 0.05	0.13 ± 0.04
Fe/Al (mol mol^{-1})	0.25 ± 0.01	0.25 ± 0.02	0.16 ± 0.02
Mn/Al (mmol mol^{-1})	5.15 ± 0.68	4.33 ± 0.48	4.40 ± 1.42
Mo/Al (μmol mol^{-1})	4.73 ± 0.74	5.57 ± 0.93	2.27 ± 0.54[2]

[1]Uncertainties are 1σ about the mean.
[2]One outlier removed for this average.

The PCA incorporates trace metals, macronutrients, and relative abundances of major biological groups based on depth bins in LH and MIS sediments. The first two components

account for ~87% of the total variance; PC1 accounts for 58.2% of the variability, while PC2 accounts for 28.4%. MIS sediments and LH sediments load separately across PC1, with PC1

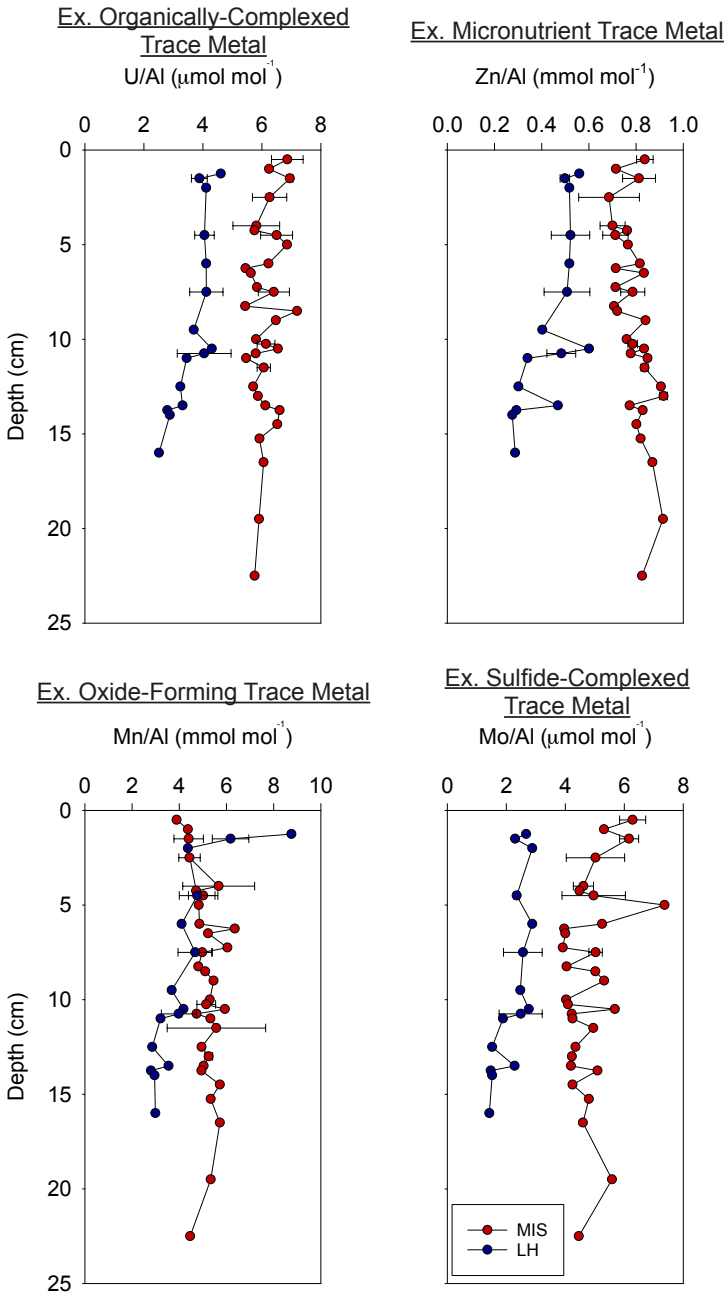

Figure 3.1 Al-normalized depth profiles of the four different forms of trace metals explored in this study—organically-complexed metals (e.g. U), micronutrient trace metals (e.g. Zn), oxide-forming trace metals (e.g. Mn), and sulfide-complexed trace metals (e.g. Mo)—for Middle Island Sinkhole (MIS) and Lake Huron (LH). Values for a given depth are reported as means, with error bars representing variability (1σ) between different cores at particular depths (n = 9 for MIS, and n = 8 for LH).

separating LH sediments by their depth bins and PC2 separating MIS sediments by depth (Figure 3.2). With the exception of Mn, trace metals and macronutrients load positively with the MIS mat and sediments (Figure 3.2). PC2 separates the macronutrients and the trace metals across the MIS sediments, with trace metals loading positively with deeper MIS sediments, and macronutrients loading negatively with shallower MIS sediments and MIS mat (0–1 cm; Figure 3.2). For both PCAs, PC1 therefore effectively resolves a gradient from oxic (LH) to low-oxygen (MIS) settings, while PC2 divides the two mechanisms for enhanced trace metal burial at MIS: loading positively for trace metal burial in association with deeper MIS sediments, and loading negatively for organic matter contents associated with microbial mat presence.

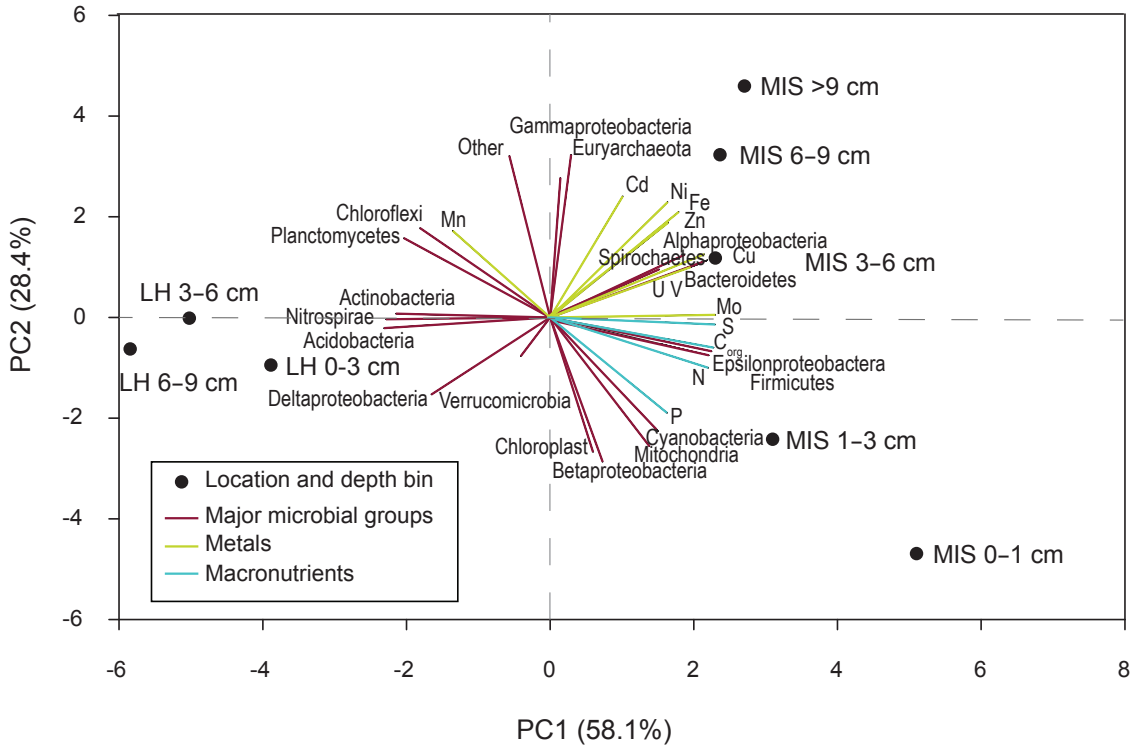

Figure 3.2 Principal component analysis demonstrating associations between trace metals and macronutrients, and relative abundances of major biological groups for Middle Island Sinkhole (MIS; n = 56) and Lake Huron (LH; n = 22) sediments. LH and MIS sediments grouped by depth bins, and individual variable vectors are extended 10x for visualization. Macronutrient and Fe data from Rico and Sheldon (2019). Mo and U data from Rico et al. (2019). Relative abundance data are from Kinsman-Costello et al. (2017).

In addition to PCA, Redundancy Analysis (RDA) was considered to determine which major microbiological groups explain most of the variance in sediment geochemistry (Figure B2). RDA results indicate that the relative abundance of six microbial groups constrains 19% of the variability in sediment geochemistry. The orientation of MIS and LH depth bins, microbial groups, macronutrients, and trace metals are similar between the RDA and the PCA (Figures 3.2 and B2); RDA did not yield additional insight about the relationships between trace metal burial and microbial community assemblage in MIS and LH. Instead, the relationships between trace metal burial and organic matter become clearer with direct correlative analyses.

Table 3.3 Pearson correlation coefficient (r) and significance (p-value) for Al-normalized trace metal contents versus organic C contents for MIS sediments (n = 38), MIS mat (n = 18), and LH (n = 22) sediments. Relationships with significance < 0.05 are in bold.

	MIS Sediments		**MIS Mat**		**LH**	
	r	**p**	**r**	**p**	**r**	**p**
U/Al	0.1	0.6	**0.75**	**<0.0005**	**0.91**	**<0.0001**
V/Al	0.1	0.6	**0.75**	**<0.0005**	**0.91**	**<0.0001**
Cd/Al	**0.36**	**<0.05**	**0.88**	**<0.0001**	**0.90**	**<0.0001**
Zn/Al	**0.45**	**<0.05**	**0.87**	**<0.0001**	**0.91**	**<0.0001**
Ni/Al	**0.45**	**<0.005**	**0.95**	**<0.001**	**0.93**	**<0.0001**
Cu/Al	**0.50**	**<0.005**	**0.95**	**<0.0001**	**0.94**	**<0.0001**
Fe/Al	**0.43**	**<0.01**	**0.90**	**<0.0001**	**0.96**	**<0.0001**
Mn/Al	0.2	0.3	0.2	0.5	**0.76**	**<0.0001**
Mo/Al	**0.41**	**<0.01**	**0.75**	**<0.0005**	**0.79**[1]	**<0.0001**[1]

[1]One outlier removed for these statistics

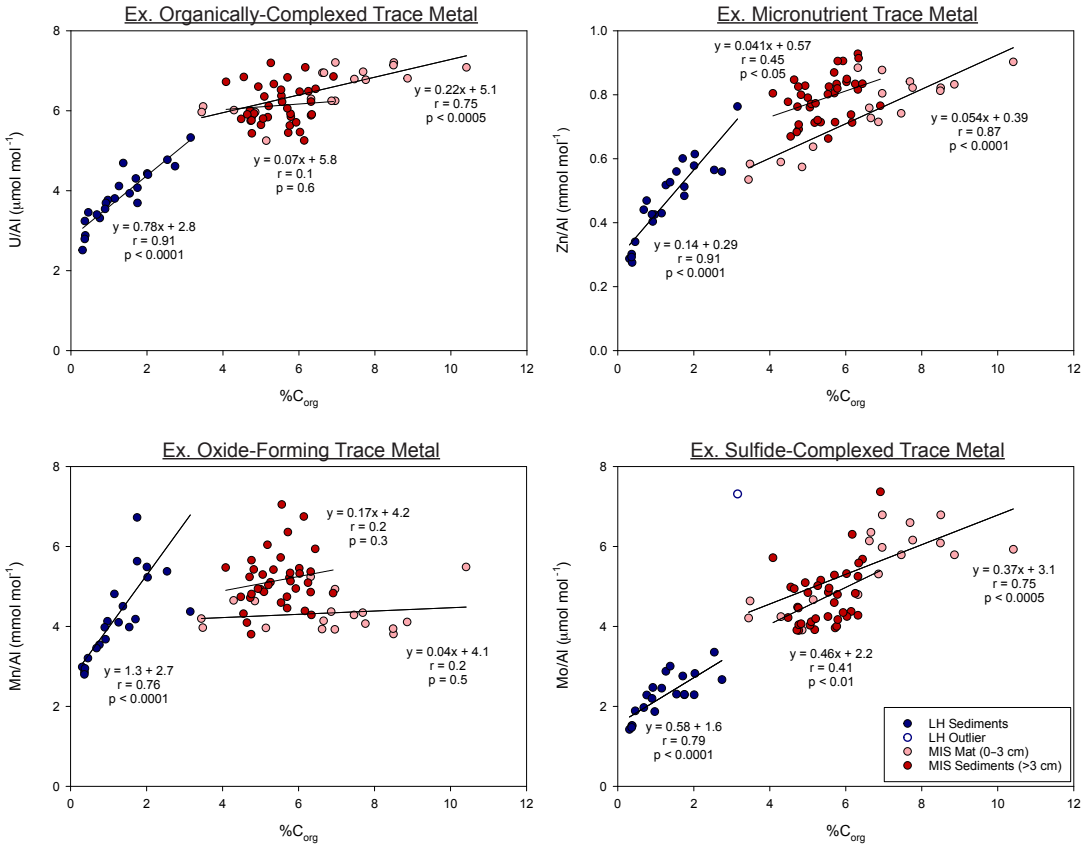

Figure 3.3 Correlations between Al-normalized trace metals and C_{org} for the four different forms of trace metals explored in this study—organically-complexed metals (e.g. U), micronutrient trace metals (e.g. Zn), oxide-forming trace metals (e.g. Mn), and sulfide-complexed trace metals (e.g. Mo)—in Lake Huron (LH) sediments, Middle Island Sinkhole (MIS) sediments, and MIS mat. Mo/Al LH outlier is not included in presented statistics. C_{org} data from Rico and Sheldon (2019).

Strong correlations between trace metals and organic C in LH ($p < 0.0005$; Table 3.3; Figures 3.3 and B3) indicate that metal burial is tied to organic matter burial in this oxic environment. Given that redox chemistry drives enhanced nutrient burial in MIS sediments relative to LH sediments (Rico and Sheldon, 2019), and that the bulk of the trace metals are correlated with organic C in MIS mat and sediments (Table 3.3; Figures 3.3 and B3), redox is also a key control on enhanced trace metal burial for MIS. For most trace metals, there are difference in slopes between the LH sediments, and the MIS mat and sediments (Table 3.3;

Figures 3.3 and B3). Although both slopes are positive, the different slopes provide quantitative evidence of different metal-C_{org} relationships for the various abiotic-biotic redox regimes. Whether or not this is attributable to different redox chemistries (*e.g.*, Rico and Sheldon, 2019), or a threshold value of organic C (~4%; Figures 3.3 and B3) is unclear, however the presence of a break in slope indicates that in MIS mat and sediments, fewer metals are buried for the same amount of organic matter. By dividing select trace metals into four categories based upon their respective uses as redox and productivity proxies, we are able to differentiate the abiotic and biotic mechanisms for their burial in these freshwater environments.

3.4.2 Trace Metals as Redox and Productivity Proxies

3.4.2.1 Organically-Complexed Trace Metals

In oxic sediments, U and V present mainly as dissolved U(VI) and V(V), respectively, and are presumed to be dissociated from organic matter (*e.g.,* Klinkhammer and Palmer, 1991; Tribovillard et al., 2006). However, the strong correlation in LH sediments between both U/Al and V/Al and organic C ($r = 0.91$, $p < 0.0001$) suggest that some oxic sediments may also allow for U and V to be buried readily via the formation of organometallic ligands in humic and fulvic acids (Figures 3.3 and B3). Alternatively, these correlations could be evidence for some reducing sediments beneath the oxic water column, which is partially corroborated by a depletion in porewater NO_3^- with depth in LH (Kinsman-Costello et al., 2017).

In mildly to strongly reducing environments, U and V are both removed to sediments via the formation of organometallic ligands, particularly in the presence of bacterial sulfate reduction and subsequent free sulfide availability (Klinkhammer and Palmer, 1991; Algeo and Maynard, 2004; Tribovillard et al., 2006). Increased U and V content in MIS mat and sediment indicates

bacterial sulfate reduction (and resulting free sulfide presence) occurring to a greater degree in MIS than LH, which is in accordance with community genomics studies of the MIS microbial mat (Voorhies et al., 2012) and geochemical data (*e.g.*, Acid Volatile Sulfide (AVS) measurements; Kinsman-Costello et al., 2017). This relationship also explains why there is a significant correlation between U and V and C_{org} where the bulk of the MIS bacterial sulfate reduction is taking place (*e.g.*, in the anoxic microbial mat; $r = 0.75$, $p < 0.0005$; Figures 3.3 and B3). In comparison, U and V covariation with C_{org} is expected to be disrupted in sediments with free sulfides present (Algeo and Maynard, 2004). With no significant correlation between U or V and C_{org} in MIS sediments ($r = 0.1$, $p = 0.6$), it appears that the sulfide contents in the MIS sediments are high enough (up to 7 mM in porewaters; Kinsman-Costello et al., 2017) to disrupt the covariation with C_{org}.

Given that U and V serve similar roles as redox proxies—complexing strongly with organic acids under reducing conditions—they are expected to have similar responses to redox. Correlative statistics (Figures 3.3 and B3) and PCA loadings (Figure 3.2) for U and V are identical, indicating that the same redox and productivity processes are influencing U and V burial. Of all the trace metals assessed except for Mo, U and V are also most associated with the macronutrients in the PCA plots, demonstrating their strong relationship with organic matter and reflecting the generally reducing conditions of MIS (Figure 3.2).

3.4.2.2 Micronutrient Trace Metals

In oxic environments, Cd, Zn, Ni, and Cu can act as micronutrients, and are thus incorporated into organic matter or complex with humic/fulvic acids (Calvert and Pederson, 1993; Tribovillard et al., 2006). These metals act as expected in the oxic LH sediments, with

contents strongly correlating to organic C ($p < 0.0001$; Figures 3.3 and B3). In reducing sediments, they are mobilized and released into the water column during organic matter degradation, and can complex with sulfide with bacterial sulfate reduction (Huerta-Diaz and Morse, 1992; Calvert and Pederson, 1993). Although MIS mats are reducing, and therefore Cd, Zn, Ni, and Cu would be expected to be released into the water column (*i.e.*, not associated with organic matter), there are still significant correlations between these metals and C_{org} ($p < 0.0001$). This indicates that these metals are serving as micronutrients to the microbial mat itself, and/or otherwise incorporated into the organic matter of the microbial mat. Significant relationships were also found in MIS sediments ($p < 0.05$; Figures 3.3 and B3), where sulfide availability would be expected to facilitate the formation of metal-sulfide complexes above metal-organics complexes. Alternatively, with enhanced organic C burial relative to LH and other Great Lakes sediments (Nold et al., 2013; Kinsman-Costello et al., 2017; Rico and Sheldon, 2019) MIS sediments may be sequestering and preserving organic matter efficiently enough that Cd, Zn, Ni, and Cu remain in metal-organic complexes.

Cd, Zn, Ni, and Cu all plot in similar PC1 and PC2 space (Figure 3.2), which is expected because all of those elements are biotic micronutrients (Lepp, 1992; Tribovillard et al., 2006; Moore et al., 2017). The use of these metals as enzymatic cofactors is highly variable across taxa and metabolisms (*e.g.*, Moore et al., 2017). This variability in microbial requirement of metals and the susceptibility of metal preservation to shifts in redox regimes (Campbell and Tessier, 1996; Tribovillard et al., 2006) can explain the spread of these trace metals across PCA space in Figure 3.2. Bacterial cells have specific mechanisms taking up Cu, Ni, and Zn (Lepp, 1992). In contrast, Cd is a nonessential element for bacteria with no specific uptake mechanism (Silver, 1998), providing a biological mechanism for the nearly orthogonal placement of Cd with regards

to the microbial mat in Figure 3.2. Conversely, the metal contributing most closely associated to the microbial mat is Cu (Figure 3.2). Cu is critical in enzymes that catalyze microbial metabolisms such as nitrification, denitrification, aerobic oxidation of ammonia, and aerobic respiration (Jelen et al., 2016). This critical demand for Cu and its availability during the GOE (*e.g.,* Chi Fru et al., 2016) makes the use of Cu as an ideal metal for the evolution of aerobic metabolisms (Moore et al., 2017). Given the breadth of metabolisms present in the MIS microbial mat (*e.g.,* anoxygenic photosynthesis, oxygenic photosynthesis, and chemosynthesis; Voorhies et al., 2012; Kinsman-Costello et al., 2017), the association of Cu in the PCA with respect to the other micronutrient trace metals (Figure 3.2) may be indicative of its use by various metabolisms in the microbial mat.

3.4.2.3 Manganese: An Oxide-Complexing Trace Metal

Oxidized Mn is predominantly found as a solid in the form of Mn-oxyhydroxides (MnO_2 and MnOOH; Calvert and Pederson, 1993; Tribovillard et al., 2006). These Mn-oxyhydroxides can trap organic matter and trace metals (Tessier et al., 1996), providing a mechanism for the correlation between Mn and C_{org} in the oxic LH sediments ($r = 0.76$; $p < 0.0001$) as well as a potential explanation for the correlations between trace metals and C_{org} in oxic LH sediments (Figures 3.3 and B3). In reducing environments, any Mn-oxyhydroxides are dissolved, and Mn is released into the water column as Mn(II) (Huerta-Diaz and Morse, 1992; Tribovillard et al., 2006). The dissolution of Mn-oxyhydroxides under reducing conditions explains why Mn contents in MIS sediments and MIS are not enriched relative to LH sediments (Figure 3.1; Table 3.2) nor correlated to C_{org} (Figure 3.3). Thus, the burial of Mn in LH, MIS sediments, and MIS mat is in accordance with the current understanding of Mn-oxyhydroxide formation and

dissolution across different redox regimes.

The formation of Mn-oxyhydroxides in the LH sediments (and dissolution of these oxides in the MIS environments) provides an abiotic mechanism for why Mn is most associated to LH sediments of all of the trace metals in the PCA (Figure 3.2). There may also be a biological mechanism for this: Mn is required by oxygenic photosynthesis in the oxygen-evolving complex of photosystem II (Ferreira et al., 2004), and some of the microbial groups in high (>5%) abundance in LH sediments (*e.g.*, Actinobacteria and Acidobacteria; Kinsman-Costello et al., 2017) have the capability to conduct aerobic respiration. Regardless, this work demonstrates that Mn is serving as an indicator of oxygenation in freshwater environments.

3.4.2.4 Molybdenum: A Proxy for Sulfidity

In oxic waters, Mo is present as the unreactive molybdate anion (MnO_4^{2-}) and can be scavenged by Fe and oxyhydroxides (Calvert and Pederson, 1993). With free sulfides present, Mo is converted into particle-reactive thiomolybdates ($MoO_xS_{(4-x)}^{2-}$), and scavenged with organic matter (Erickson and Helz, 2000; Tribovillard et al., 2006; Vorlicek et al., 2015). As a result, a strong covariation between Mo and C_{org} has been demonstrated in euxinic basins and euxinic black shales (Algeo and Lyons, 2006; Lyons et al., 2009; Helz and Vorlicek, 2019). However, despite ranging from oxic to sulfidic, LH sediments, MIS mat, and MIS sediments, all have significant correlations between Mo and organic C ($p < 0.01$; Figure 3.3). In LH, this could be explained by the capture of Mo in Mn-oxyhydroxides, which also sequester organic carbon (Tessier et al., 1996). MIS sediments have sulfide concentrations up to 7 mM (Kinsman-Costello et al., 2017), which is near the threshold for thiomolybdate formation. Formation of particle reactive thiomolybdates could explain the relationship between Mo and C_{org} (Figure 3.3) as seen

in euxinic basins (Algeo and Lyons, 2006; Lyons et al., 2009; Helz and Vorlicek, 2019). However, there is no significant relationship between Mo and S in the MIS sediments (Figure 3.4), as would be expected if Mo burial was attributable to thiomolybdate formation.

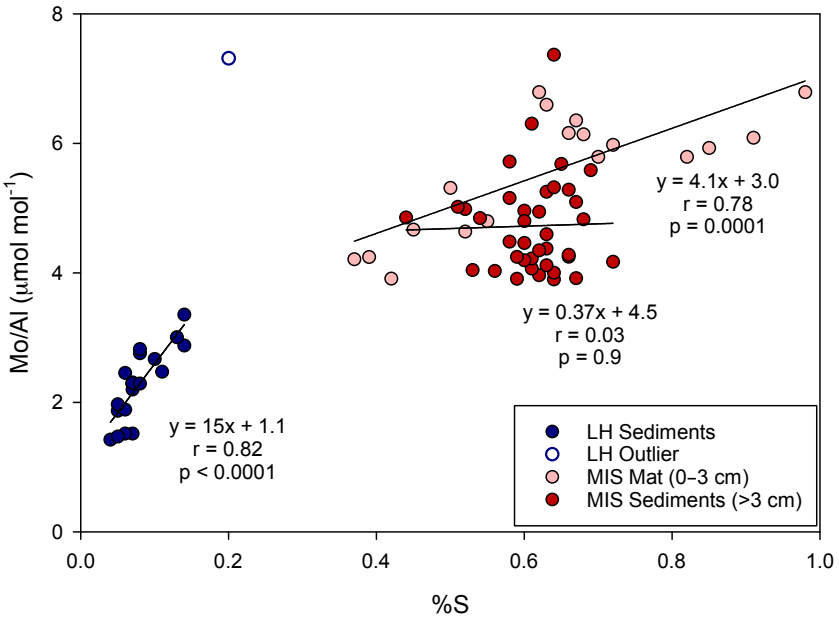

Figure 3.4 Correlations between Mo/Al and S for in Lake Huron (LH) sediments, Middle Island Sinkhole (MIS) sediments, and MIS mat. Mo/Al LH outlier is not included in presented statistics. Mo and S data from Rico and Sheldon (2019).

Additionally, there is a relationship between Mo and C_{org} in the MIS mat, where conditions are too reducing for Mn-oxyhydroxide formation, and where porewaters lack significant sulfide concentrations (Figure 3.3; Kinsman-Costello et al., 2017). Correlations between Mo and C_{org} regardless of Mn-oxyhydroxide or free sulfide availability suggest a mechanism for Mo burial that is independent of thiomolybdate formation, and instead may be related to organic matter burial. These results are consistent with the findings of Rico et al. (2019), which indicated that LH and MIS Mo burial may follow the "particulate shuttle" pathway—wherein authigenic Mo is adsorbed to Mn- and Fe-(oxy)hydroxides and buried in sediments—as opposed to a burial pathway associated with euxinia. In fact, despite conventional interpretations of Mo enrichments

(*i.e.*, free sulfide availability and euxinic conditions), there has been evidence for alternative processes of Mo burial in reducing, non-sulfidic environments (*e.g.,* Algeo and Tribovillard, 2009; Sholz et al., 2017; Tessin et al., 2018). For example, recent findings suggest that in reducing sediments without abundant sulfide, moderate to abundant Mo can be buried as a complex with organic matter, separate from thiomolybdate formation (Wagner et al., 2017).

Given that enhanced Mo burial and Mo and C_{org} covariation has been used as evidence for euxinia in modern and ancient aquatic environments (*e.g.*, Algeo and Lyons, 2006; Lyons et al., 2009), evidence for this covariation in non-euxinic environments complicates our use of Mo geochemistry as a paleoredox proxy. Furthermore, current understanding of Mo isotope systematics is dependent on the thiomolybdate burial pathway of Mo in euxinic environments (*e.g.*, Neubert et al. 2008; Helz et al., 2011; Nägler et al., 2011); the possibility of a Mo burial mechanism tied to organic matter burial shifts our understanding of Mo geochemical cycling and necessitates a reinterpretation of Mo isotope ratios in sediments.

3.4.3 Relating Microbiology to Trace Metal Burial

Comparing the major microbial groups with relative abundances greater than 5% for MIS mat (0–1 cm; n = 17), MIS sediments (>1 cm; n = 87) and LH sediments (n = 11) demonstrates substantial taxonomic overlap at the phylum level (*e.g.*, Bacteroidetes, Betaproteobacteria, Verrucomicrobia) between the three sample regimes, irrespective of redox chemistry (Figure 3.5; Kinsman-Costello et al., 2017, Moore et al., 2017). Together, organisms represented by these phyla are capable of an extensive list of microbial metabolisms (Moore et al., 2017). This overlap could just be attributed to similar microbial assemblages across freshwater environments, or could in part be attributed to groundwater influence—groundwater directly interacts with MIS

mat and sediments from above the sediment-water interface, whereas there is some subsurface groundwater influence in LH sediments (as indicated by porewater ion chemistry; Kinsman-Costello et al., 2017).

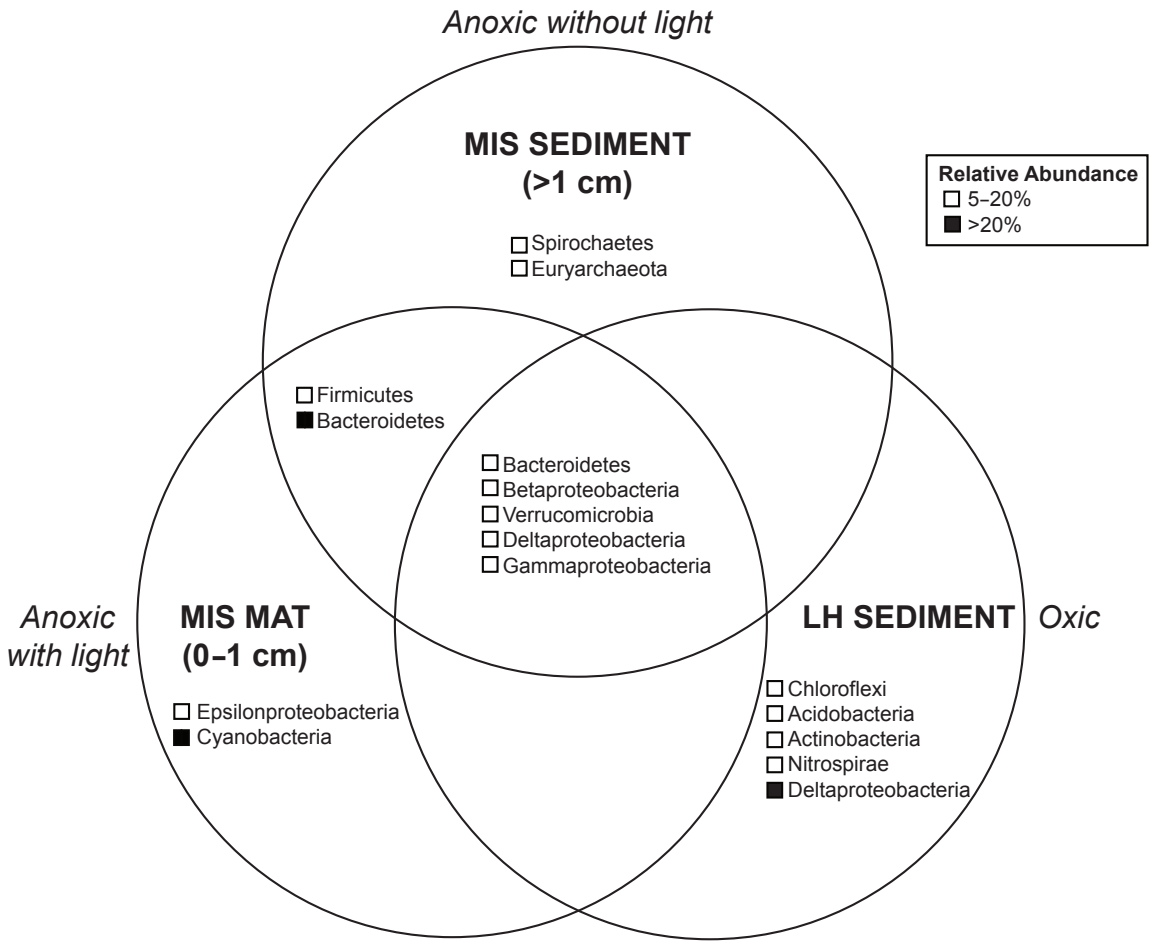

Figure 3.5 Venn diagram depicting the relative abundances of major microbial groups within the Middle Island Sinkhole (MIS) mat (0–1 cm; n = 17), MIS sediments (>1 cm; n = 87), and Lake Huron (LH) sediments (n = 11). Different symbols adjacent to the microbial groups represent varying relative abundance in their respective locations. Relative OTU abundances are from Kinsman-Costello et al. (2017).

Despite substantial taxonomic overlap between LH, MIS mat, and MIS sediments (Figure 3.5), there are some key phyla that are prominent for each of the environments. For example, as evident in Figures 3.2 and 3.5, relative abundances of the major phyla Nitrospirae,

Actinobacteria, and Acidobacteria are the most associated to LH sediments; these are in high (>5%) abundance only in LH sediments (Figure 3.5; Kinsman-Costello et al., 2017). Additionally, Deltaproteobacteria is abundant only LH sediments (>20%). In comparison, the MIS microbial mats include cyanobacteria (>20% abundance; Figure 3.5; Kinsman-Costello et al., 2017), which is corroborated by the strong association between cyanobacteria and MIS sediments where the active or buried microbial mat is present (0–3 cm depth; Figure 3.2; Voorhies et al., 2012; Nold et al., 2013; Rico and Sheldon, 2019). Additionally, the only phylum of Archaea with substantial presence —Euryarchaeota—is at relatively high abundance (>5%) in the MIS sediments (Figure 3.5), and is particularly associated with deeper MIS sediments (Figure 3.2). Euryarchaeota notably includes methanogens, which explains the production of methane in MIS sediments (Biddanda et al., 2012; Kinsman-Costello et al., 2017).

While metagenomics and metatranscriptomics work by Medina (2016) and Grim (2019) demonstrate greater metabolic diversity—and diversity in the use of electron acceptors—in MIS than in LH, this diversity is not evident when assessing phylum-level community assemblages, making it difficult to correlate trace metal burial to specific metabolic processes (*e.g.*, the spread in microbial groups across Figure 3.2). At this biological scale, and considering total trace metal content (as opposed to speciation of metals), the direct relationships between microbial assemblages and metal burial in LH and MIS remain unresolved.

3.4.4 Trace Metals as a Biosignature in the Fossil Record

There are a number of mechanisms by which ancient microbial assemblages leave physical and geochemical evidence of their presence (*e.g.*, stromatolites, organic biomarkers). This work aimed to test whether or not sediment trace metal geochemistry has the potential to

serve as a biomarker for microbial mat presence. With similar microbial presence and water chemistry as has been inferred for the Proterozoic (Biddanda et al., 2012; Voorhies et al., 2012; Kinsman-Costello et al., 2017; Rico and Sheldon, 2019), the Middle Island Sinkhole is a useful modern analogue to consider the relationships between sediment trace metal geochemistry and microbial communities. Based on the presumed mechanisms behind trace metal burial in aquatic environments, and subsequently the ways in which trace metal geochemistry in ancient environments are used as paleoredox and paleoproductivity proxies, it was expected that the three abiotic/biotic regimes—oxic LH sediments, anoxic MIS mat, and anoxic MIS sediments with free sulfides present—would yield different relationships between trace metals and organic matter. This would indicate that the abiotic and biotic controls on trace metal burial in these three environments were distinctive enough to make trace metal burial a useful biosignature for microbial mat presence in the fossil record. However, most trace metals deviated from expectation in terms of their relationship to organic matter, and, as a result, there was significant overlap in their relationship with organic matter between the three regimes (Figures 3.3 and 3.6). Notably, there are no trace metal categories that feature significant correlations to C_{org} for only the MIS mat, nor for the MIS sediments. Despite the differences in oxygen availability, sulfide availability, and microbial mat presence, there is no evidence that the relationships between trace metals and organic matter alone can be used as a biosignature for microbial mats. These results contrast the models presented by Parnell et al. (2015) and Zhang et al. (2016), which used trace metal abundance to suggest biological productivity in the fossil record. Instead, metal abundance alone may be insufficient to reconstruct an ancient biosphere. Considering the ways in which sediment metal geochemistry records biological processes may necessitate examining how biology influences tools such as metal speciation and metal isotope systematics.

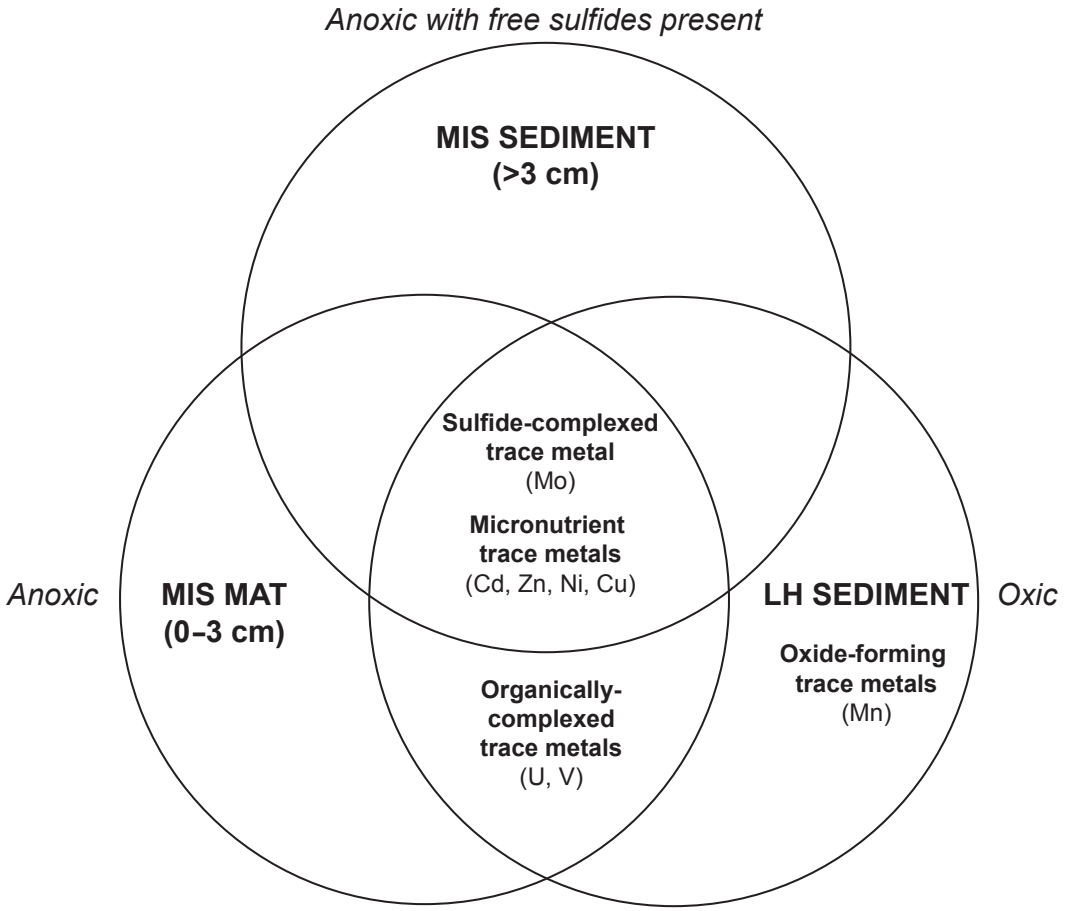

Figure 3.6 Venn diagram depicting the significant correlations ($p < 0.05$) between trace metals and C_{org} for the Middle Island Sinkhole (MIS) mat (0–3 cm; n = 18), MIS sediments (>3 cm; n = 38), and LH sediments (n = 22).

3.5 Conclusions

Trace metal data from MIS and LH reveal that the relationships between trace metals and organic matter are not consistent with what is expected from their use as paleoredox and paleoproductivity proxies. Of the types of trace metals assessed, Mn was the most consistent with expectations for burial mechanisms, and is an appropriate proxy for oxygenation of the water column. In comparison, for some trace metals such as the organically-complexed U and V, and the micronutrient metals Cd, Zn, Ni, and Cu, there were correlations between the metals and C_{org} in LH despite oxic conditions, directly contradicting the hypothesized model of Algeo and

Maynard (2004) and Tribovillard et al. (2006), which assumed no enrichment nor correlation under oxic-suboxic conditions. Given that U accumulation is often used to reflect suboxic-anoxic (but not euxinic) environments in ancient environments (*e.g.*, Algeo & Tribovillard, 2009), the accumulation of this metal in oxic environments has implications for how we interpret U geochemical data in the fossil record. Additionally, Mo (and, in particular, Mo-C_{org} covariation) is considered one of the most robust proxies for euxinia in paleoceanography. Covariation between Mo and C_{org} across LH sediments, and MIS mat and sediments regardless of free sulfide availability suggests a mechanism for Mo burial that is tied to organic matter burial, not euxinia. Notably, Mo relates to organic matter in a way similar to the micronutrient trace metals, as opposed to being an indicator of S content in MIS sediments. Considering a Mo burial mechanism that is tied to productivity instead of redox impacts our understanding of Mo geochemistry of ancient environments and uses as a paleoredox indicator (*e.g.*, Algeo and Lyons, 2006; Lyons et al., 2009), as well as obfuscating our current understanding of Mo isotope systematics (*e.g.*, Neubert et al., 2008; Helz et al., 2011; Nägler et al., 2011). Altogether, these results demonstrate a need for a greater understanding of the burial mechanisms for redox-sensitive trace metals under a variety of redox regimes that include suboxic and anoxic settings as well as euxinic ones, with special consideration for environments with significant microbiological presence.

3.6 Acknowledgements

We would like to thank the NOAA Thunder Bay National Marine Sanctuary dive team for their help with core sampling. Thanks to Rebecca Dzombak and Clarissa Crist for their help in sample processing. This research was funded by the NSF GRFP to KIR, a University of

Michigan Department of EES Turner Award to KIR, a 2015 GSA Research Grant to KIR, and a Sokol Foundation grant to NDS.

3.7 References

Algeo, T.J., Tribovillard, N., 2009. Environmental analysis of paleoceanographic systems based on molybdenum-uranium covariation. Chem. Geol. 268, 211–225. https://doi.org/10.1016/j.chemgeo.2009.09.001

Algeo, T.J., Lyons, T.W., 2006. Mo-total organic carbon covariation in modern anoxic marine environments: Implications for analysis of paleoredox and paleohydrographic conditions. Paleoceanography 21. https://doi.org/10.1029/2004PA001112

Algeo, T.J., Maynard, J.B., 2004. Trace-element behavior and redox facies in core shales of Upper Pennsylvanian Kansas-type cyclothems. Chem. Geol. 206, 289–318. https://doi.org/10.1016/j.chemgeo.2003.12.009

Awramik, S.M., Sprinkle, J., 1999. Proterozoic stromatolites: The first marine evolutionary biota. Hist. Biol. 13, 241–253. https://doi.org/10.1080/08912969909386584

Biddanda, B.A., Nold, S.C., Dick, G.J., Kendall, S.T., Vail, J.H., Ruberg, S.A., Green, C.M., 2012. Rock, Water, Microbes: Underwater Sinkholes in Lake Huron are Habitats for Ancient Microbial Life Characteristics of Lake Huron's Submerged Sinkholes. Nat. Educ. Knowl. 3.

Brocks, J.J., 2011. Millimeter-scale concentration gradients of hydrocarbons in Archean shales: Live-oil escape or fingerprint of contamination? Geochim. Cosmochim. Acta 75, 3196–3213. https://doi.org/10.1016/j.gca.2011.03.014

Brocks, J.J., Grosjean, E., Logan, G.A., 2008. Assessing biomarker syngeneity using branched alkanes with quaternary carbon (BAQCs) and other plastic contaminants. Geochim. Cosmochim. Acta 72, 871–888. https://doi.org/10.1016/j.gca.2007.11.028

Brocks, J.J., Jarrett, A.J.M., Sirantoine, E., Hallmann, C., Hoshino, Y., Liyanage, T., 2017. The rise of algae in Cryogenian oceans and the emergence of animals. Nature 548, 578–581. https://doi.org/10.1038/nature23457

Calvert, S.E., Pedersen, T.F., 1993. Geochemistry of Recent oxic and anoxic marine sediments: Implications for the geological record. Mar. Geol. 113, 67–88. https://doi.org/10.1016/0025-3227(93)90150-T

Campbell, P. G., Tessier, A., 1996. Ecotoxicology of metals in the aquatic environment: geochemical aspects. In: Ecotoxicology: A Hierarchical Treatment, eds. Newman, M. C.,

and Jagoe, C. H. Boca Raton, FL: Lewis Publishers. pp. 11–58.

Canfield, D.E., Zhang, S., Wang, H., Wang, X., Zhao, W., Su, J., Bjerrum, C.J., Haxen, E.R., Hammarlund, E.U., 2018. A Mesoproterozoic iron formation. Proc. Natl. Acad. Sci. 115, E3895–E3904. https://doi.org/10.1073/pnas.1720529115

Chi Fru, E., Rodriguez, N.P., Partin, C. A., Lalonde, S. V., Andersson, P., Weiss, D.J., El Albani, A., Rodushkin, I., Konhauser, K.O., 2016. Cu isotopes in marine black shales record the Great Oxidation Event. Proc. Natl. Acad. Sci. 113, 4941–4946. https://doi.org/10.1073/pnas.1523544113

Erickson, B.E., Helz, G.R., 2000. Molybdenum(VI) speciation in sulfidic waters: Stability and lability of thiomolybdates. Geochim. Cosmochim. Acta 64, 1149–1158. https://doi.org/10.1016/S0016-7037(99)00423-8

Farquhar, J., Bao, H., Thiemens, M., 2000. Atmospheric Influence of Earth's Earliest Sulfur Cycle. Science (80). 289, 756–758. https://doi.org/10.1126/science.289.5480.756

Ferreira, K.N., Iverson, T.M., Maghlaoui, K., Barber, J., Iwata, S., 2004. Architecture of the photosynthetic oxygen-evolving venter. Science (80). 303, 1831–1839.

Grim, S., 2019. "Genomic and functional investigations into seasonally-impacted and morphologically-distinct anoxygenic photosynthetic cyanobacterial mats." Doctoral dissertation, University of Michigan.

Grotzinger, J.P., Rothman, D.H., 1996. An abiotic model for stromatolite morphogenesis.pdf. Nature 383, 423–425.

Hammer, Ø., Harper, D.A.T., Ryan, P.D., 2001. PAST: Paleontological Statistics Software Package for Education and Data Analysis. Paleontol. Electron. 4, 1–9.

Helz, G.R., Bura-Nakić, E., Mikac, N., Ciglenečki, I., 2011. New model for molybdenum behavior in euxinic waters. Chem. Geol. 284, 323–332. https://doi.org/10.1016/j.chemgeo.2011.03.012

Helz, G.R., Vorlicek, T.P., 2019. Precipitation of molybdenum from euxinic waters; role of organic matter. Chem. Geol. 509, 178–193. https://doi.org/10.1016/j.chemgeo.2019.02.001

Huerta-Diaz, M.A., Morse, J.W., 1992. Pyritization of trace metals in anoxic marine sediments. Geochim. Cosmochim. Acta 56, 2681–2702. https://doi.org/10.1016/0016-7037(92)90353-K

Imbus, S.W., Macko, S.A., Douglas Elmore, R., Engel, M.H., 1992. Stable isotope (C, S, N) and molecular studies on the Precambrian Nonesuch Shale (Wisconsin-Michigan, U.S.A.): Evidence for differential preservation rates, depositional environment and hydrothermal influence. Chem. Geol. 101, 255–281. https://doi.org/10.1016/0009-2541(92)90007-R

Jelen, B.I., Giovannelli, D., Falkowski, P.G., 2016. The role of microbial electron transfer in the coevolution of the biosphere and geosphere. Annu. Rev. Microbiol. 70, 45–62. https://doi.org/10.1146/annurev-micro-102215-095521

Johnston, D.T., Wolfe-Simon, F., Pearson, A., Knoll, A. H., 2009. Anoxygenic photosynthesis modulated Proterozoic oxygen and sustained Earth's middle age. Proc. Natl. Acad. Sci. 106, 16925–16929. https://doi.org/10.1073/pnas.0909248106

Kappler, A., Pasquero, C., 2005. Deposition of banded iron formations by anoxygenic phototrophic Fe (II) -oxidizing bacteria. Geology 865–868. https://doi.org/10.1130/G21658.1

Kinsman-Costello, L.E., Sheik, C.S., Sheldon, N.D., Burton, G. A., Costello, D., Marcus, D.N., Uyl, P. Den, Dick, G.J., 2017. Groundwater shapes sediment biogeochemistry and microbial diversity in a submerged sinkhole. Geobiology 15, 225–239. https://doi.org/10.1038/nature04068

Klinkhammer, G.P., Palmer, M.R., 1991. Uranium in the oceans: Where it goes and why. Geochim. Cosmochim. Acta 55, 1799–1806. https://doi.org/10.1016/0016-7037(91)90024-Y

Konhauser, K.O., Hamade, T., Raiswell, R., Morris, R.C., Grant Ferris, F., Southam, G., Canfield, D.E., 2002. Could bacteria have formed the Precambrian banded iron formations? Geology 30, 1079. https://doi.org/10.1130/0091-7613(2002)030<1079:cbhftp>2.0.co;2

Konhauser, K.O., Robbins, L.J., Alessi, D.S., Flynn, S.L., Gingras, M.K., Martinez, R.E., Kappler, A., Swanner, E.D., Li, Y.L., Crowe, S.A., Planavsky, N.J., Reinhard, C.T., Lalonde, S. V., 2018. Phytoplankton contributions to the trace-element composition of Precambrian banded iron formations. Bull. Geol. Soc. Am. 130, 941–951. https://doi.org/10.1130/B31648.1

Kopp, R.E., Kirschvink, J.L., Hilburn, I.A., Nash, C.Z., 2005. The Paleoproterozoic snowball Earth: A climate disaster triggered by the evolution of oxygenic photosynthesis. Proc. Natl. Acad. Sci. 102, 11131–11136. https://doi.org/10.1073/pnas.0504878102

Lepp, N. W., 1992. Uptake and accumulation of metals in bacteria and fungi. In: Biogeochemistry of Trace Metals, ed. Adriano, D. C. Boca Raton, FL: Lewis Publishers. pp. 277–298

Lyons, T.W., Reinhard, C.T., Planavsky, N.J., 2014. The rise of oxygen in Earth's early ocean and atmosphere. Nature 506, 307–15. https://doi.org/10.1038/nature13068

Lyons, T.W., Anbar, A.D., Severmann, S., Scott, C., Gill, B.C., 2009. tracking euxinia in the ancient ocean: A multiproxy perspective and Proterozoic case study. Annu. Rev. Earth Planet. Sci. 37, 507–534. https://doi.org/10.1146/annurev.earth.36.031207.124233

Medina, M, 2016. “Genomic and transcriptomic evidence for niche partitioning among sulfate-reducing bacteria in redox-stratified cyanobacterial mats of the Middle Island Sinkhole.” Master’s thesis, University of Michigan.

Moore, E.K., Jelen, B.I., Giovannelli, D., Raanan, H., Falkowski, P.G., 2017. Metal availability and the expanding network of microbial metabolisms in the Archaean eon. Nat. Geosci. 10, 629–636. https://doi.org/10.1038/ngeo3006

Nägler, T.F., Neubert, N., Böttcher, M.E., Dellwig, O., Schnetger, B., 2011. Molybdenum isotope fractionation in pelagic euxinia: Evidence from the modern Black and Baltic Seas. Chem. Geol. 289, 1–11. https://doi.org/10.1016/j.chemgeo.2011.07.001

Neubert, N., Heri, A.R., Voegelin, A.R., Nägler, T.F., Schlunegger, F., Villa, I.M., 2011. The molybdenum isotopic composition in river water: Constraints from small catchments. Earth Planet. Sci. Lett. 304, 180–190. https://doi.org/10.1016/j.epsl.2011.02.001

Noffke, N., Awramik, S.M., 2013. Stromatolites and MISS-Differences between relatives. GSA Today 23, 4–9. https://doi.org/10.1130/GSATG187A.1

Nold, S.C., Bellecourt, M.J., Kendall, S.T., Ruberg, S. A., Sanders, T.G., Klump, J.V., Biddanda, B. A., 2013. Underwater sinkhole sediments sequester Lake Huron’s carbon. Biogeochemistry 115, 235–250. https://doi.org/10.1007/s10533-013-9830-8

Parnell, J., Spinks, S., Andrews, S., Thayalan, W., Bowden, S., 2015. High Molybdenum availability for evolution in a Mesoproterozoic lacustrine environment. Nature Comm. 6, 6996. https://doi.org/10.1038/ncomms7996

Planavsky, N.J., Slack, J.F., Cannon, W.F., O’Connell, B., Isson, T.T., Asael, D., Jackson, J.C., Hardisty, D.S., Lyons, T.W., Bekker, A., 2018. Evidence for episodic oxygenation in a weakly redox-buffered deep mid-Proterozoic ocean. Chem. Geol. 483, 581–594. https://doi.org/10.1016/j.chemgeo.2018.03.028

Posth, N.R., Bristow, L.A., Cox, R.P., Habicht, K.S., Danza, F., Tonolla, M., Frigaard, N.U., Canfield, D.E., 2017. Carbon isotope fractionation by anoxygenic phototrophic bacteria in euxinic Lake Cadagno. Geobiology 15, 798–816. https://doi.org/10.1111/gbi.12254

Quandt, L., Gottschalk, G., Ziegler, H., Stichler, W., 1977. Isotope discrimination by photosynthetic bacteria. Fems Microbiol. Lett. 1, 125–128.

Raiswell, R., Canfield, D.E., 2012. The iron biogeochemical cycle past and present. Geochem. Persp. 1, 1–220. https://doi. org/10.7185/geochempersp.1.1

Raiswell, R., Hardisty, D.S., Lyons, T.W., Canfield, D.E., Owens, J.D., Planavsky, N.J., Poulton, S.W., Reinhard, C.T., 2018. The iron paleoredox proxies: A guide to the pitfalls, problems and proper practice. Am. J. Sci. 318, 491–526. https://doi.org/10.2475/05.2018.03–

Rico, K.I., Sheldon, N.D., 2019. Nutrient and iron cycling in a modern analogue for the redoxcline of a Proterozoic ocean shelf. Chem. Geol. 511, 42–50. https://doi.org/10.1016/j.chemgeo.2019.02.032

Rico, K.I., Sheldon, N.D., Gallagher, T.M., Chappaz, A., 2019. Redox chemistry and Molybdenum burial in a Mesoproterozoic lake. Geophys. Res. Lett. 41, 5871–5878. https://doi.org/10.1029/2019GL083316

Ruberg, S.A., Kendall, S.T., Biddanda, B.A., Black, T., Nold, S.C., Lusardi, W.R., Green, R., Casserly, T., Smith, E., Sanders, T.G., Lang, G.A., Constant, S.A., 2008. Observations of the Middle Island Sinkhole and glacial creation of 400 million years. Mar. Technol. Soc. J. 42, 12–21.

Schidlowski M., Aharon P., 1992. Carbon cycle and carbon isotope record: Geochemical impact of life over 3.8 Ga of Earth history. In: Early Organic Evolution, eds. Schidlowski, M., Golubic, S., Kimberley, M.M., McKirdy, D.M., and Trudinger, P.A. Berlin, Germany: Springer, Berlin, Heidelberg. pp. 147–175.

Scholz, F., Siebert, C., Dale, A.W., Frank, M., 2017. Intense molybdenum accumulation in sediments underneath a nitrogenous water column and implications for the reconstruction of paleo-redox conditions based on molybdenum isotopes. Geochim. Cosmochim. Acta 213, 400–417. https://doi.org/10.1016/j.gca.2017.06.048

Silver, S., 1998. Genes for all metals--a bacterial view of the Periodic Table. J. Ind. Microbiol. Biotechnol. 20, 1–12. https://doi.org/10.1038/sj.jim.2900483

Tessier, A., Fortin, D., Belzile, N., DeVitre, R.R., Leppard, G.G., 1996. Metal sorption to diagenetic iron and manganese oxyhydroxides and associated organic matter: Narrowing the gap between field and laboratory measurements. Geochim. Cosmochim. Acta 60, 387–404. https://doi.org/10.1016/0016-7037(95)00413-0

Tessin, A., Chappaz, A., Hendy, I., Sheldon, N., 2018. Molybdenum speciation as a paleo-redox proxy: A case study from Late Cretaceous Western Interior Seaway black shales. Geology 47, 59–62. https://doi.org/10.1130/g45785.1

Tribovillard, N., Algeo, T.J., Lyons, T., Riboulleau, A., 2006. Trace metals as paleoredox and paleoproductivity proxies: An update. Chem. Geol. 232, 12–32. https://doi.org/10.1016/j.chemgeo.2006.02.012

Van der Weijden, C.H., 2002. Pitfalls of normalization of marine geochemical data using a common divisor. Mar. Geol. 184, 167–187.

Voorhies, A.A., Biddanda, B.A., Kendall, S.T., Jain, S., Marcus, D.N., Nold, S.C., Sheldon, N.D., Dick, G.J., 2012. Cyanobacterial life at low O(2): community genomics and function reveal metabolic versatility and extremely low diversity in a Great Lakes sinkhole mat. Geobiology 10, 250–67. https://doi.org/10.1111/j.1472-4669.2012.00322.x

Vorlicek, T.P., Chappaz, A., Groskreutz, L.M., Young, N., Lyons, T.W., 2015. A new analytical approach to determining Mo and Re speciation in sulfidic waters. Chem. Geol. 403, 52–57. https://doi.org/10.1016/j.chemgeo.2015.03.003

Wagner, M., Chappaz, A., Lyons, T.W., 2017. Molybdenum speciation and burial pathway in weakly sulfidic environments: Insights from XAFS. Geochim. Cosmochim. Acta 206, 18–29. https://doi.org/10.1016/j.gca.2017.02.018

Zhang, S., Wang, X., Wang, H., Bjerrum, C.J., Hammarlund, E.U., Costa, M.M., Connelly, J.N., Zhang, B., Su, J., Canfield, D.E., 2016. Sufficient oxygen for animal respiration 1,400 million years ago. Proc. Natl. Acad. Sci. 113, 1731–1736. https://doi.org/10.1073/pnas.1523449113

Zheng, Y., Anderson, R.F., Van Geen, A., Kuwabara, J., 2000. Authigenic molybdenum formation in marine sediments: A link to pore water sulfide in the Santa Barbara Basin. Geochim. Cosmochim. Acta 64, 4165–4178. https://doi.org/10.1016/S0016-7037(00)00495-6

Zyakun, A.M., Lunina, O.N., Prusakova, T.S., Pimenov, N. V., Ivanov, M. V., 2009. Fractionation of stable carbon isotopes by photoautotrophically growing anoxygenic purple and green sulfur bacteria. Microbiology 78, 757–768. https://doi.org/10.1134/S0026261709060137

CHAPTER IV

Redox Chemistry and Molybdenum Burial in a Mesoproterozoic Lake[2]

4.1 Abstract

While marine sediments have been used to constrain a history of redox chemistry throughout the Precambrian, far fewer data have been generated from lakes. With major biological innovations thought to have occurred in Proterozoic lakes, understanding their chemistry is critical for understanding the evolution of eukaryotic life. We use sediment geochemistry to characterize the redox conditions of the Nonesuch Formation (~1.1 Ga) and a modern analogue for the Proterozoic: the Middle Island Sinkhole in Lake Huron (USA). Iron speciation, Mo contents, and Mo-U covariation demonstrate oxic and anoxic—not euxinic—environments, with no clear indicators of enhanced biological productivity in the Nonesuch Formation. Moderate Mo enrichments observed in the Nonesuch Formation are not attributed to euxinia, but instead to an authigenic particulate shuttle. We suggest that the Fe and Mo sediment geochemistry of these lacustrine systems reflect only local water column and sediment burial conditions and not atmospheric oxygenation.

---

[2]Published under the citation:
Rico, K.I., Sheldon, N.D., Gallagher, T.M., Chappaz, A., 2019. Redox Chemistry and Molybdenum Burial in a Mesoproterozoic Lake. Geophys. Res. Lett. 41, 5871–5878. https://doi.org/10.1029/2019GL083316

4.2 Introduction

Geochemical characterizations of ancient marine sediments have been used successfully to investigate shifts in atmospheric oxygenation throughout the Precambrian (*e.g.,* Farquhar et al., 2000). For the mid-Proterozoic, ocean redox chemistry and atmospheric oxygenation has been hotly debated, with geochemical methods indicating variable marine redox conditions, and subsequently, various interpretations of atmospheric oxygenation (*e.g.*, Sperling et al., 2014; Planavsky et al., 2018). In comparison, fewer geochemical data have been generated from Proterozoic lakes to constrain the redox chemistry of terrestrial environments. However, there is increasing evidence that Proterozoic lakes—not oceans— may have been critical habitats for biological evolutions (*e.g.*, the diversification of cyanobacteria and early eukaryotic life; Blank and Sánchez-Baracaldo, 2009; Strother et al., 2011; Blank, 2013). As a result, it becomes increasingly important to understand the habitats wherein these major evolutions took place. Constraining the geochemistry of Proterozoic lake environments can help to characterize the conditions wherein multicellular life may have evolved. Molybdenum (Mo), a redox-sensitive trace element, has been intensively used as a paleo redox proxy, mostly to identify periods of past anoxia (Chappaz et al., 2018; Hardisty et al., 2018). In presence of sulfide ($\sum S(-II) = H_2S + HS^- + S^{2-}$), Mo can be scavenged in sediment via two pathways: (1) through association with Fe-S minerals (*e.g.*, Chappaz et al., 2014; Helz and Vorlicek, 2019) and (2) through interactions with organic matter (*e.g.*, Ardakani et al., 2016; Tessin et al., 2018; Wagner et al., 2017). As a consequence, Mo enrichments can exceed crustal levels by 2 orders of magnitude when $\sum S(-II)$ is present within the water column (euxinia; Scott and Lyons, 2012). In addition, Mo is a cofactor in many metabolic pathways and has consequently played a key role in biospheric evolution (Lyons et al., 2014). Geobiologically speaking, Mo is an essential micronutrient

strongly integrated into the nitrogen cycle, including vital roles in N2 fixation and fixed nitrogen assimilation, and is a key element limiting primary productivity in lakes (Goldman, 1960; Howarth & Cole, 1985; Glass et al., 2012).

The relationship between geochemistry and biological evolution in Mesoproterozoic lakes has been studied using the Stoer Group (1.18 Ga) of the Torridonian Supergroup, UK (Parnell et al., 2010; Parnell et al., 2015). Based upon ample burial of Mo in Stoer Group sediments, Parnell et al. (2015) concluded that oxygenation of terrestrial environments increased oxidative weathering and sulfate delivery to lakes, allowing for widespread euxinia to develop and for abundant nutrients that spurred enhanced biological productivity. However, Mo and Sr isotope data indicate that much of the Stoer Group is marine or marine-influenced, and not strictly lacustrine (Stüeken et al., 2017). Therefore, if the Stoer Group is not appropriate for understanding redox chemistry Proterozoic lakes, we must consider other systems to investigate Mesoproterozoic lacustrine geochemistry. Here we examine the Fe and Mo geochemistry of the Nonesuch Formation (~1.1 Ga; Figure 4.1a) of the Keweenaw Supergroup, as well as two modern analogues for Proterozoic waters—the low-oxygen Middle Island Sinkhole (MIS) and an oxic Lake Huron (LH) control site (Figure 4.1b)—to test the conclusions made by Parnell et al. (2015) and to assess whether euxinia and enhanced biological productivity were widespread during the Mesoproterozoic in terrestrial environments.

4.3 Site Descriptions

4.3.1 The Nonesuch Formation

The Nonesuch Formation is composed of sandstones, mudstones, and rare limestone interbeds that were deposited as part of the Midcontinent Rift System (Elmore et al., 1989). This

formation—which is bookended by alluvial fan and fluvial depositional environments, and incorporates one or possibly a series of rift lakes (Suszek, 1997)—includes diverse freshwater phytoplankton microfossils (Wellman & Strother, 2015). Further, the Nonesuch Formation interfingers in places with the Copper Harbor Conglomerate (1.09 Ga), which features alluvial fan and fluvial facies, and lacustrine stromatolite mounds (Elmore, 1983; Fedorchuk et al., 2016; Wilmeth et al., 2014). Therefore, there is an abundance of evidence that the Nonesuch Formation is composed of fluctuating freshwater environments and lacks significant marine influence. This work uses samples from cores DO-6, PI-2, and WPB-4 (Figure 1a), incorporating shore-proximal and shore-distal lacustrine units possibly from two different lake subbasins (Suszek, 1997). This work includes samples from mudstone beds with consistent stratigraphic spacing (roughly every 1–5 m) for each of these three cores. Nonesuch Formation geochemical data and interpretations of redox chemistry are compared to that of core PI-1 (Cumming et al., 2013), and DO-8 and WC-9 (Slotznick et al., 2018), which also may also encompass additional lake subbasins.

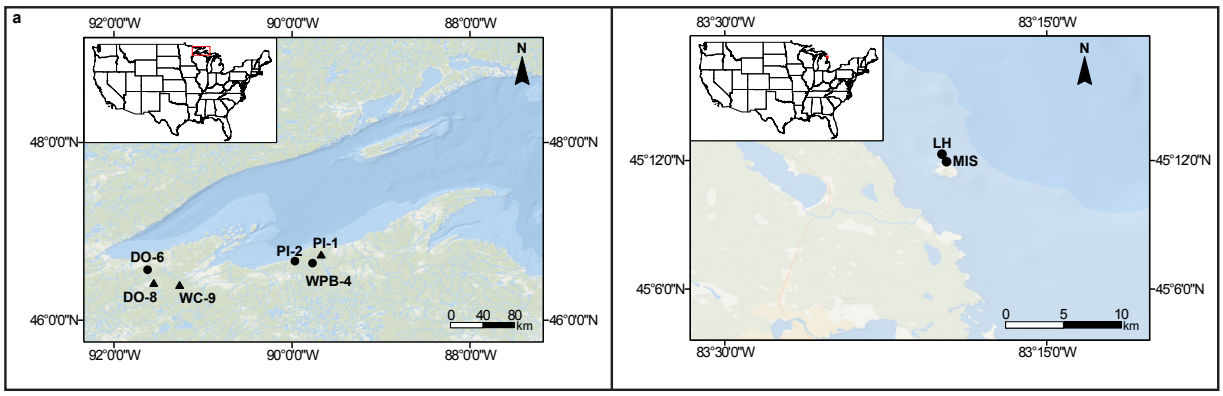

Figure 4.1 Sample localities for the (a) DO-6, PI-2, and WPB-4 cores of the Nonesuch Formation and (b) Middle Island Sinkhole and Lake Huron control site. The PI-1 core was previously examined for Fe speciation by Cumming et al. (2013), and the DO-8 and WC-9 cores were previously examined by Slotznick et al. (2018).

4.3.2 The MIS

Located in LH (Figure 4.1b), the MIS is a 23-m-deep karst feature wherein low-oxygen high-sulfate groundwater seeps into the sinkhole, resulting in low (<5%) dissolved oxygen and 7.8 mM sulfate that persists 1–3 m above the sediment-water interface (Ruberg et al., 2008). This water chemistry is comparable to proposed levels for mid-Proterozoic waters, which are inferred to have little to no oxygen (*e.g.*, Lyons et al., 2014; Shen et al., 2002), and sulfate concentrations in the range of <2 to ~10 mM (Blättler et al., 2018; Olson et al., 2016). As a result of this water chemistry, dynamic microbial mats grow at this interface, including cyanobacteria that conduct both oxygenic and anoxygenic photosynthesis (Voorhies et al., 2012), and are therefore similar to the versatile cyanobacteria proposed to have dominated Proterozoic aquatic systems (Johnston et al., 2009; Voorhies et al., 2012). Redox chemistry of MIS allows for the burial of nutrient- and metal-rich sediments below the microbial mat (Kinsman-Costello et al., 2017; Nold et al., 2013; Rico and Sheldon, 2019). With water chemistry and microbiology similar to what has been inferred for the Proterozoic, MIS has been considered an analogue to interpret biogeochemical cycling in shallow Proterozoic waters (Kinsman-Costello et al., 2017; Rico and Sheldon, 2019; Voorhies et al., 2012).

A LH control site of comparable depth to MIS is used to provide an oxic end-member. LH, which is 0.6 km away from MIS (Figure 4.1b), is composed of mudstones like MIS but has limited groundwater influence and no evidence of a microbial mat at the sediment water interface (Kinsman-Costello et al., 2017). Porewater and sediment geochemistry, and microbial community assemblage, differ between MIS and LH (Kinsman-Costello et al., 2017; Rico and Sheldon, 2019). For MIS and LH, samples encompass surficial sediments (<25-cm depth).

4.4 Methods

MIS (n = 56), LH (n = 22) Mo, U, and Al contents and Nonesuch Formation (n = 113) Mo, Fe, U, Al, S, and P concentrations were analyzed at ALS Laboratories in Vancouver, British Columbia, where samples were digested with perchloric, hydrofluoric, nitric, and hydrochloric acids, and concentrations were determined by inductively coupled plasma (ICP)-optical emission spectrometry and ICP-mass spectrometry (MS) calibrated using internal standards. Major element precision was better than 0.2 wt.%. A single outlier for LH with respect to Mo was excluded from this work. To compare the respective enrichments of Mo and U in the study locations, trace metal concentrations are given in the form of enrichment factors (EFs), which were calculated as

$$X_{EF} = [(X/Al)_{sample}/(X/Al)_{background}] \quad (1)$$

where X and Al represent the weight percent concentrations of elements X and Al, respectively. For the Nonesuch Formation, samples are normalized using the post-Archean average shale compositions of Taylor and McLennan (1985). LH and MIS samples were normalized using average LH background values of Mo (0.25 ± 0.05 ppm), U (1.02 ± 0.15 ppm), and Al (3.1 ± 1.1 wt. %; after Chappaz et al., 2008). While there are potential pitfalls with any normalization (*e.g.*, post-Archean average shale may not be representative of local sediments; Van der Weijden, 2002), because this study aims to compare respective enrichments of Mo and U, the differences in reference material between our study sites should not have major implications for our overall interpretations.

For total organic carbon analyses, Nonesuch Formation samples (n = 112) were washed

with a 1–2N HCl solution to remove carbonates, rinsed, and oven-dried overnight at 50°C. In order to get total organic carbon of the bulk sample, acidified and unacidified sample pairs were loaded into tin capsules, and analyzed using a Costech ECS4010 elemental analyzer in UM's Earth System Science Lab. Acetanilide (%C = 71.09, %N = 10.36) was used to calibrate elemental composition.

Fe speciation for the Nonesuch Formation (n = 55) samples was determined using a three-step sequential extraction developed by Poulton and Canfield (2005). Pyrite concentrations were stoichiometrically determined via titration of chromium reducible sulfide precipitated as ZnS (Canfield et al., 1986). The total highly reactive pool of iron (iron that is highly reactive toward sulfide; FeHR; Poulton & Canfield, 2005) represents the sum of these four extractions. Detailed methods are given in Table S1 in the supporting information. Iron in the Nonesuch Formation sequential extraction solutions were analyzed by ICP-MS within the STARLAB at Central Michigan University. Uncertainties for all Fe pools were less than 0.2 wt.%. All of the sediment geochemical data (this work) are presented in Tables S2 and S3 in the Data Repository.

To calibrate "normal" distributions of Mo and U in large lakes, water column samples were collected at three stations in August 2014 at 10 different depths using Niskin bottles aboard R/V Blue Heron in Lake Superior. Within 1 hr and in a clean environment, all water samples were filtered with 0.45-μm syringe nylon filters and transferred into 50-ml high-density polyethylene (previously acid washed) tubes filled with 1 ml of HNO3 high purity (Optima, 2% v/v). Molybdenum and U concentrations were determined at the STARLAB at Central Michigan University using ICP-MS analysis and external calibration.

4.5 Results and Discussion

4.5.1 Redox Chemistry of the Nonesuch Formation

Analysis of Fe speciation uses Fe_{HR}/Fe_T and Fe_{py}/Fe_{HR} to differentiate between oxic, ferruginous (Fe (II) within the water column), anoxic ($\sum$S(–II) only present in the porewater), and euxinic conditions (*e.g.*, Tessin et al., 2016). Previous Fe speciation data for the Nonesuch Formation from a nearby core (Figure 4.1) to the ones examined herein indicate predominantly ferruginous conditions (Cumming et al., 2013; Figure C1 in the supporting information). In contrast, magnetic Fe mineralogy and petrographic data from two cores in Northern Wisconsin have been interpreted to indicate that the Nonesuch Formation there featured oxic water columns (Slotznick et al., 2018). Thus, one possibility for this discrepancy is that the proxies are not reliably recording water column oxygenation. However, modern sequential Fe extraction results appropriately define MIS as ferruginous and LH as oxic (Figure 4.2; Rico and Sheldon, 2019), matching their known oxygen levels, so we consider the Fe-based proxies to be reliable. The new Nonesuch Formation data mostly indicate oxic or possibly anoxic conditions (Figure 4.2), with significant overlap between individual cores (DO-6, PI-2, and WPB-4; Figure C1). Notably, Fe speciation results indicate that the oxic LH sediments are more anoxic than the majority of the Nonesuch Formation samples. This is driven by an Fe limitation in LH; there is a much higher relative abundance (~5x LH) of Fe_T in the Nonesuch Formation. As cautioned by Raiswell et al. (2018), this work suggests that discrepancies in local Fe enrichments need to be considered when comparing Fe speciation results for spatially or temporally separate aquatic systems.

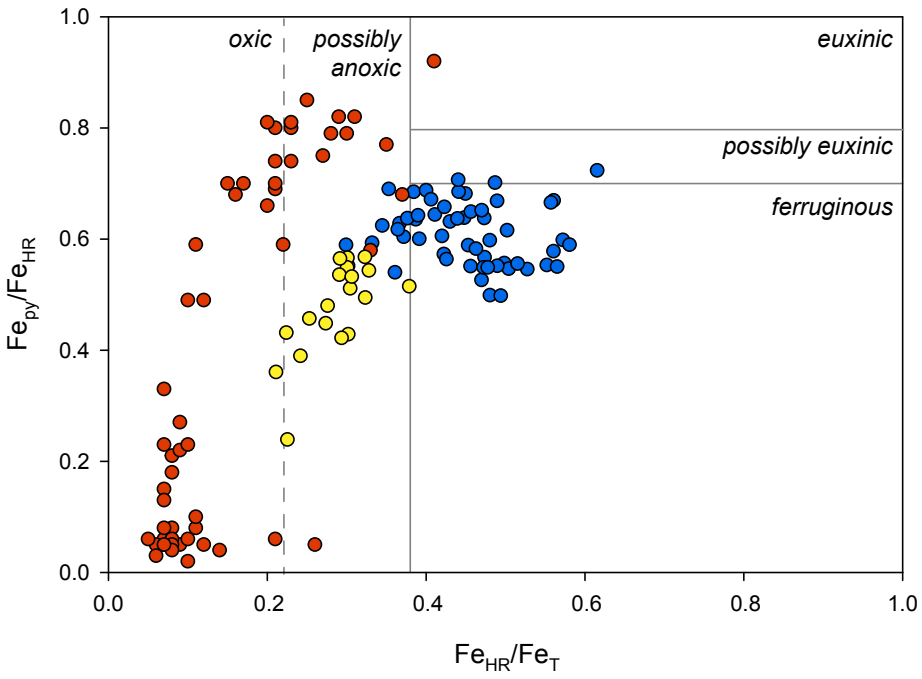

Figure 4.2 Cross plot of the ratios of iron in pyrite (Fe_{py}) to highly reactive iron (Fe_{HR}) versus Fe_{HR} to total iron (Fe_T) for Middle Island Sinkhole (dark blue circles) Lake Huron (yellow circles), and Nonesuch Formation (red circles) sediments. These Fe ratios can distinguish the redox chemistries of aquatic environments as oxic, ferruginous, or euxinic (Raiswell and Canfield, 2012; Raiswell et al., 2018). The solid gray lines are recommended boundaries, the whereas dashed gray line is suggested only for ancient sediments (after Raiswell et al., 2018). Middle Island Sinkhole and Lake Huron data are from Rico and Sheldon (2019).

Iron speciation results for much of the Nonesuch Formation sediments indicate a high degree of pyritization with oxic deposition (Figure 4.2), which is rare for modern systems (Tables C2 and C3). However, especially with limited oxygen availability in the mid-Proterozoic (*e.g.*, Planavsky et al., 2018), reduced chemical species such as pyrite are to be expected when oxygen is consumed. In contrast, MIS does not display a high degree of pyritization, likely attributed to a sulfide limitation in porewater (which fluctuates between 0–7 mM H_2S; Kinsman-Costello et al., 2017). Given that the Nonesuch Formation is likely composed of a series of rift basins (Suszek, 1997), data from this study could incorporate separate lake systems that overlap with those of previously published data from Cumming et al. (2013) and Slotznick et al. (2018). Taken together, variability in interpretations of Fe geochemistry in the Nonesuch Formation

could in part reflect real spatial and temporal variability in water chemistries and depths of the sedimentary environments.

4.5.2 Molybdenum Burial in the Nonesuch Formation

The modern anoxic analogue and oxic lake sediments exhibit a large range in organic C contents (0.3–10.4%), whereas their Mo contents are consistently low (<1 ppm; Figure 4.3), regardless of redox conditions. In comparison, the Nonesuch Formation samples exhibit a smaller range in organic C (0–1.7%) but feature higher Mo concentrations (0.12–40 ppm; Figure 4.3). However, both the modern systems and the Nonesuch Formation exhibit Mo contents far below what is anticipated for euxinic conditions (*e.g.*, as in the Stoer Group; Figure 4.3).

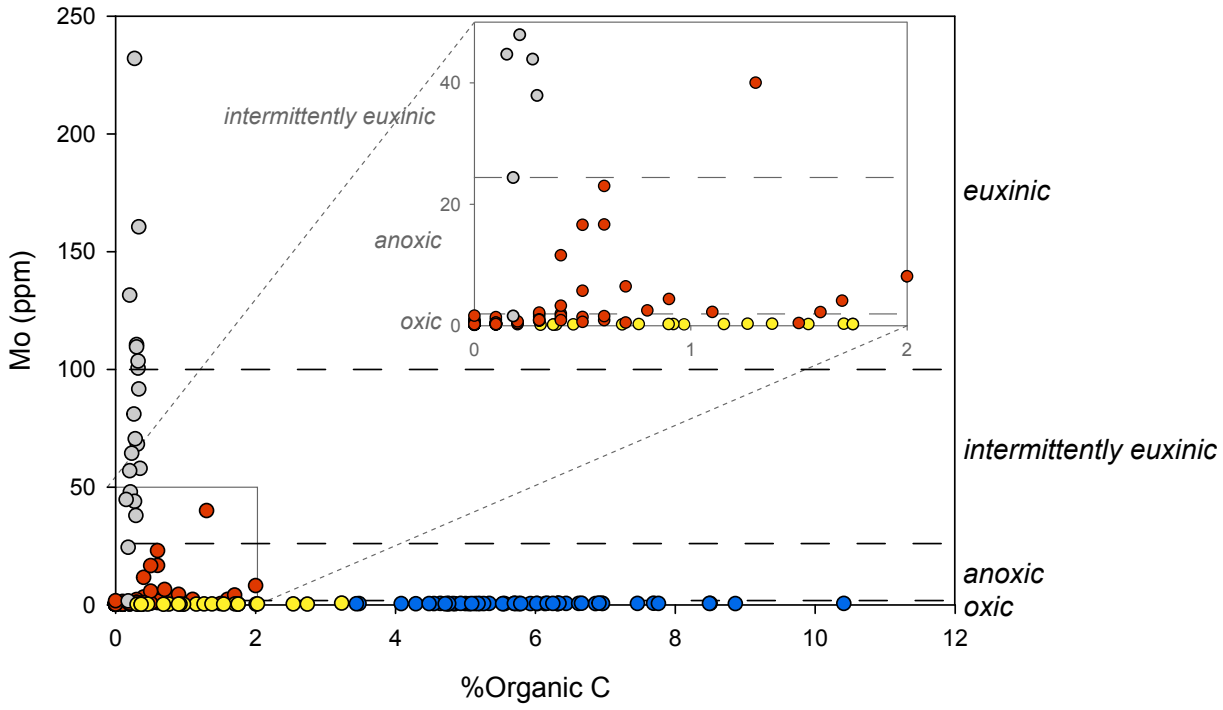

Figure 4.3 Mo (ppm) versus $\%C_{org}$ contents for Middle Island Sinkhole (blue circles), Lake Huron (yellow circles), and Nonesuch Formation (red circles). Stoer Group data (gray circles; Parnell et al., 2015) are also included as a comparative euxinic end-member. The dashed lines indicate thresholds for oxic, anoxic, and euxinic conditions based upon Mo enrichments (Scott and Lyons, 2012). Inset plot highlights Lake Huron and Nonesuch Formation data. Middle Island Sinkhole and Lake Huron organic C data are from Rico and Sheldon (2019).

The highest accumulation of authigenic Mo is conventionally attributed to the presence of free sulfide (∑S(–II); *i.e.*, euxinic conditions) and subsequent formation of thiomolybdates (Erickson and Helz, 2000; Vorlicek et al., 2015). Some Nonesuch Formation samples exhibit Mo enrichments relative to the modern systems (Figure 4.3), yet there is no evidence for persistent euxinia in any of the lake environments (Table 4.1 and Figures 4.2 and 4.3). To refine the mechanisms that could control Mo burial, the Mo-U covariation was evaluated across all of our sites.

Table 4.1 Percentage of Fe speciation data indicative of a given redox regime

Location	Percent oxic (%)	Percent possibly anoxic (%; ancient sediments only)	Percent ferruginous (%)	Percent possibly euxinic (%)	Percent euxinic (%)
Middle Island Sinkhole	16	--	78	5	0
Lake Huron	100	--	0	0	0
Nonesuch Formation[1]	73(40)	25(45)	0(14)	0	<1(<1)

[1]Values are given for Middle Island Sinkhole, Lake Huron, and the Nonesuch Formation from *this work*, with parenthetical values including both *this work* and previously published data from Cumming et al. (2013; Figure C1).

Trends in Mo-U covariation for modern and ancient marine systems have been linked to the controls on Mo deposition in sediments (Algeo and Tribovillard, 2009; Tribovillard et al., 2012). Molybdenum enrichments can occur (1) via a "particulate shuttle" wherein authigenic Mo is scavenged by metal hydroxides (*e.g.*, Mn and Fe), transported through the water column, and buried in sediments (authigenic U does not get scavenged in this process, resulting in a high Mo_{EF} and comparably low U_{EF}) or (2) via a shift from suboxic to anoxic to euxinic water chemistry, enabling an enrichment in U under suboxia, and then enhanced burial of Mo in the presence of free sulfide (*i.e.*, the "unrestricted marine" trend wherein U_{EF} increases then Mo_{EF}

increases; Algeo and Tribovillard, 2009). The Mo_{EF}/U_{EF} method uses mass ratios from modern seawater to designate threshold concentrations that can be related to depositional processes. Average seawater concentrations for Mo and U are 10.6 and 3.1 ppb, respectively (Mo/U = 3.4 Algeo and Tribovillard, 2009). Throughout the entire water column at three different stations in Lake Superior (max depth of 315 m), average concentrations for Mo and U are 0.13 and 0.04 ppb, respectively (n = 30; Mo/U = 3.3; Table C4). Given that the Mo_{EF}/U_{EF} method is based on ratios (not total concentration), the fact that $Mo/U_{seawater}$ is almost identical to the $Mo/U_{Lake\ Superior}$ (3.4 versus 3.3) implies that the approach developed by Algeo and Tribovillard (2009) can be applied to our lacustrine systems.

As a fully oxygenated system, LH sediments are anticipated to have little Mo and U enrichment; this is corroborated by low EFs in Figure 4.4. MIS sediments are more enriched in Mo and U relative to LH sediments, with no overlap, and may follow the particulate shuttle pathway of Mo burial (Figure 4.3). In comparison, ~30% of the Nonesuch Formation data are enriched (EF > 1) for Mo and U, with only a few samples exhibiting substantial enrichment (EF > 10). However, the samples that are enriched fall along the particulate shuttle pathway (Figure 4.4). This suggests that for the Nonesuch Formation, euxinic conditions are not directly causing Mo enrichments. Instead, the dominant burial mechanism for Mo is the particulate shuttle pathway; enrichments in Fe_T and Fe_{ox} (Table C3) may have favored Mo enrichments via this pathway relative to MIS and LH.

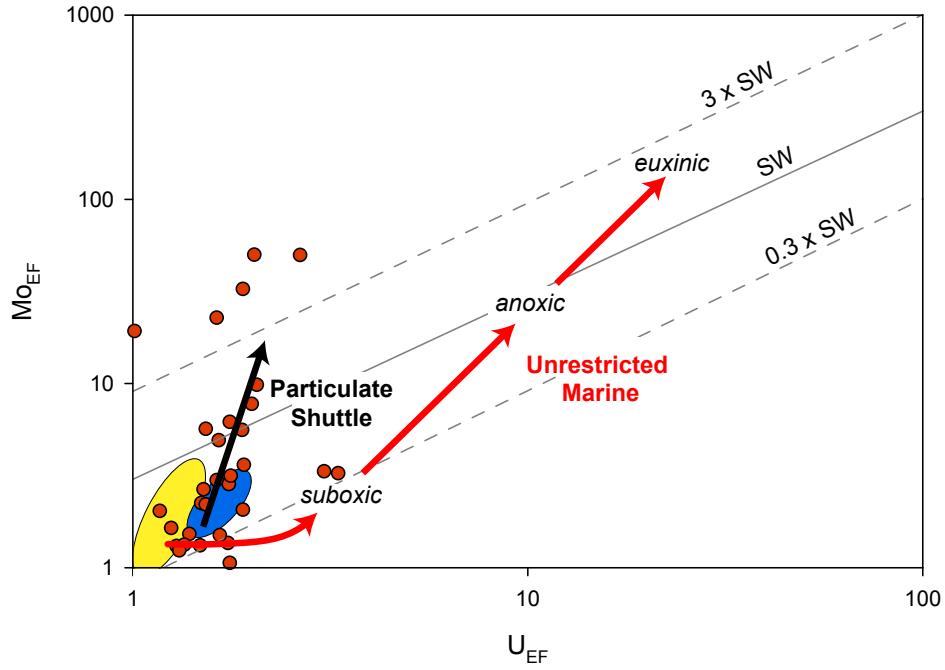

Figure 4.4 Cross plot of the enrichment factors (EFs) of Mo and U for the Nonesuch Formation sediments (red circles), Middle Island Sinkhole sediments (blue field) and Lake Huron sediments (yellow field) for samples enriched in Mo and U relative to their reference value (EF > 1). The diagonal lines represent the Mo:U ratio of present-day seawater and fractions thereof. The large arrows depict the particulate shuttle and unrestricted marine pathways of Mo and U deposition in marine sediments. Similar Mo/U ratios between Lake Superior (3.3) and average seawater (3.4) allow us to use this marine approach (after Algeo and Tribovillard, 2009) with the lacustrine sediments.

4.5.3 Implications for Biological Productivity and Atmospheric Oxygen

Based upon sediment Mo geochemistry in the Mesoproterozoic Stoer Group, Parnell et al. (2015) hypothesized that high atmospheric pO_2 in the Mesoproterozoic would have increased delivery of sulfate, resulting in (1) sulfate reduction and significant Mo burial via sulfides in lakes (*i.e.*, widespread euxinia) and (2) no nutrient limitation and therefore high levels of biological productivity. While the Stoer Group is marine-influenced, and not strictly lacustrine (Stüeken et al., 2017), Parnell et al. (2015) provide a testable hypothesis for Mesoproterozoic lake environments. The Stoer Group Mo contents are greater than both those of the Nonesuch Formation and the modern systems (Figure 4.3) and could be the result of post depositional processes remobilizing and enriching Mo (*e.g.*, Ardakani et al., 2016). When combining our

different approaches (Fe speciation and Mo-U covariation), there is no evidence that euxinia was widespread across terrestrial environments during the Mesoproterozoic, nor any clear indicators for abundant nutrient availability that would help to sustain biological activity (Figures 4.2 and 4.4). The Nonesuch Formation sediments feature organic C contents similar to a modern biologically productive environment (LH; Figure 4.3) and experienced a relatively mild thermal history (<150 °C; Gallagher et al., 2017) suggesting that their C contents are not substantially lower than they were at the time of deposition. However, it is unclear whether this organic C burial can be attributed to an increase in biological productivity or a shift to greater carbon preservation. Well-preserved eukaryotic remains are most abundant and diverse in discrete horizons, which may indicate that pelagic productivity occurred in episodic bursts (Wellman and Strother, 2015), but do not correspond to the observed Mo enrichments. This would be consistent with intermittent nutrient limitation, impacting the extent of biological productivity, and ultimately contrasting with the model of Parnell et al. (2015). Without high enough Mo to indicate significant sulfate weathering, this study provides no clear indicator of Mesoproterozoic atmospheric oxygenation levels. Differences were observed in Fe geochemistry between various Nonesuch Formation rift basin lakes and in the apparent degree of oxygenation from anoxic to oxic. This variability occurred in sediments that were formed penecontemporaneously and therefore under approximately the same atmospheric pO_2, indicating that oxygen availability was locally controlled in the water column and sediments (*e.g.*, by biological production and consumption of oxygen or physically via stratification) rather than by the atmosphere. In the modern analogue setting, an oxygenated atmosphere coexists with both oxic and ferruginous sediment chemistry (Table 4.1). Taking all of this together, the most parsimonious explanation of the Nonesuch Formation Mo geochemistry is that it reflects fluctuating redox conditions and

intense cycling of Fe and Mn oxyhydroxides within the water column, raising questions about attempts to use ancient lakes to reconstruct atmospheric oxygen levels. Indeed, the modern analogue system records ferruginous conditions reflective of a steep redoxcline at depth even in a fully oxygenated atmosphere and thus reflects only a portion of the water column, and not the part that is in contact with the atmosphere.

4.6 Conclusions

It has been proposed that Mo enrichments in Mesoproterozoic lake deposits would indicate widespread euxinia, no nutrient limitation in terrestrial systems, and high levels of atmospheric oxygen. Iron speciation, low Mo contents, and Mo-U covariation of the 1.1 Ga old Nonesuch Formation contradict this model of widespread lacustrine euxinia and do not provide any indication of enhanced biological productivity or provide a useful constraint on atmospheric oxygenation during the Mesoproterozoic. Sediment geochemistry of Proterozoic terrestrial environments may only demonstrate in situ water column and sediment chemistry. Whether or not Mo geochemistry of Mesoproterozoic lakes record biological productivity and global atmospheric oxygenation remains unresolved.

4.7 Acknowledgements

We acknowledge the National Oceanic Administration Thunder Bay National Marine Sanctuary (NOAA TBNMS) scuba divers for their expertise and assistance in the collection of sediment cores at MIS and LH. We would also like to thank both the Wisconsin Geologic and Natural History Survey and the Northern Michigan Geological Repository for providing access to core material. This work was supported by National Science Foundation Graduate Student

Research Fellowships to K. I. R. and T. M. G. and a Sokol Foundation grant to N. D. S. Data supporting the conclusions (for Figures 2-4) can be obtained from Figures S1–S3 and Tables S1–S4.

4.8 References

Algeo, T.J., Tribovillard, N., 2009. Environmental analysis of paleoceanographic systems based on molybdenum-uranium covariation. Chem. Geol. 268, 211–225. https://doi.org/10.1016/j.chemgeo.2009.09.001

Ardakani, O.H., Chappaz, A., Sanei, H., Mayer, B., 2016. Effect of thermal maturity on remobilization of molybdenum in black shales. Earth Planet. Sci. Lett. 449, 311–320. https://doi.org/10.1016/j.epsl.2016.06.004

Blank, C.E., 2013. Origin and early evolution of photosynthetic eukaryotes in freshwater environments: Reinterpreting Proterozoic paleobiology and biogeochemical processes in light of trait evolution. J. Phycol. 49, 1040–1055. https://doi.org/10.1111/jpy.12111

Blank, C.E., Sánchez-Baracaldo, P., 2010. Timing of morphological and ecological innovations in the cyanobacteria - A key to understanding the rise in atmospheric oxygen. Geobiology 8, 1–23. https://doi.org/10.1111/j.1472-4669.2009.00220.x

Blättler, C.L., Claire, M.W., Prave, A.R., Kirsimäe, K., Higgins, J.A., Medvedev, P. V., Romashkin, A.E., Rychanchik, D. V., Zerkle, A.L., Paiste, K., Kreitsmann, T., Millar, I.L., Hayles, J.A., Bao, H., Turchyn, A. V., Warke, M.R., Lepland, A., 2018. Two-billion-year-old evaporites capture Earth's great oxidation. Science 360, 320–323. https://doi.org/10.1126/science.aar2687

Canfield, D.E., Raiswell, R., Westrich, J.T., Reaves, C.M., Berner, R. A., 1986. The use of chromium reduction in the analysis of reduced inorganic sulfur in sediments and shales. Chem. Geol. 54, 149–155. https://doi.org/10.1016/0009-2541(86)90078-1

Chappaz, A., Glass, J., Lyons, T. W., 2018. Molybdenum. In Encyclopedia of Geochemistry V. 1, eds. White, W. M., Casey, W. H., Casey, B., Marty, H., and Yurimoto, H. Cham, Switzerland: Springer International.

Chappaz, A., Gobeil, C., Tessier, A., 2008. Geochemical and anthropogenic enrichments of Mo in sediments from perennially oxic and seasonally anoxic lakes in Eastern Canada. Geochim. Cosmochim. Acta 72, 170–184. https://doi.org/10.1016/j.gca.2007.10.014

Chappaz, A., Lyons, T.W., Gregory, D.D., Reinhard, C.T., Gill, B.C., Li, C., Large, R.R., 2014. Does pyrite act as an important host for molybdenum in modern and ancient euxinic

sediments? Geochim. Cosmochim. Acta 126, 112–122. https://doi.org/10.1016/j.gca.2013.10.028

Cumming, V.M., Poulton, S.W., Rooney, A.D., Selby, D., 2013. Anoxia in the terrestrial environment during the late Mesoproterozoic. Geology 41, 583–586. https://doi.org/10.1130/G34299.1

Elmore, R.D., 1983. Precambrian non-marine stromatolites in alluvial fan deposits, the Copper Harbor Conglomerate, upper Michigan. Sedimentology 30, 829–842. https://doi.org/10.1111/j.1365-3091.1983.tb00713.x

Elmore, R. D., Milavec, G. J., Imbus, S. W., Engel, M. H., 1989. The Precambrian nonesuch formation of the North American mid-continent rift, sedimentology and organic geochemical aspects of lacustrine deposition. Precambrian Res. 43, 191–213. http://doi.org/10.1016/0301-9268(89)90056-9

Erickson, B.E., Helz, G.R., 2000. Molybdenum(VI) speciation in sulfidic waters: Stability and lability of thiomolybdates. Geochim. Cosmochim. Acta 64, 1149–1158. https://doi.org/10.1016/S0016-7037(99)00423-8

Farquhar, J., Bao, H., Thiemens, M., 2000. Atmospheric Influence of Earth's Earliest Sulfur Cycle. Science (80). 289, 756–758. https://doi.org/10.1126/science.289.5480.756

Fedorchuk, N.D., Dornbos, S.Q., Corsetti, F.A., Isbell, J.L., Petryshyn, V.A., Bowles, J.A., Wilmeth, D.T., 2016. Early non-marine life: Evaluating the biogenicity of Mesoproterozoic fluvial-lacustrine stromatolites. Precambrian Res. 275, 105–118. https://doi.org/10.1016/j.precamres.2016.01.015

Gallagher, T.M., Sheldon, N.D., Mauk, J.L., Petersen, S. V., Gueneli, N., Brocks, J.J., 2017. Constraining the thermal history of the North American Midcontinent Rift System using carbonate clumped isotopes and organic thermal maturity indices. Precambrian Res. 294, 53–66. https://doi.org/10.1016/j.precamres.2017.03.022

Glass, J.B., Axler, R.P., Chandra, S., Goldman, C.R., 2012. Molybdenum limitation of microbial nitrogen assimilation in aquatic ecosystems and pure cultures. Front. Microbiol. 3, 1–11. https://doi.org/10.3389/fmicb.2012.00331

Goldman, C. R., 1960. Primary productivity and limiting factors in three lakes of the Alaska peninsula. Ecol. Mono. 30, 207– 230. https://doi.org/10.2307/1948552

Hardisty, D. S., Lyons, T. W., Riedinger, N., Isson, T. T., Owens, J. D., Aller, R. C., Rye, D. M., Planavsky, N. J., Reinhard, C. T., Gill, B. C., Masterson, A. L., Asael, D., & Johnston, D. T., 2018. An evaluation of sedimentary molybdenum and iron as proxies for pore fluid paleoredox conditions. Amer. J. of Sci. 318, 527– 556. http://doi.org/10.2475/05.2018.04

Helz, G.R., Vorlicek, T.P., 2019. Precipitation of molybdenum from euxinic waters; role of organic matter. Chem. Geol. 509, 178–193. https://doi.org/10.1016/j.chemgeo.2019.02.001

Howarth, R.W., Cole, J.J., 2010. Molybdenum availability, nitrogen limitation, and phytoplankton growth in natural waters. Science 318, 527–556. https://doi.org/10.1126/science.229.4714.653

Johnston, D.T., Wolfe-Simon, F., Pearson, A., Knoll, A. H., 2009. Anoxygenic photosynthesis modulated Proterozoic oxygen and sustained Earth's middle age. Proc. Natl. Acad. Sci. 106, 16925–16929. https://doi.org/10.1073/pnas.0909248106

Kinsman-Costello, L.E., Sheik, C.S., Sheldon, N.D., Burton, G. A., Costello, D., Marcus, D.N., Uyl, P. Den, Dick, G.J., 2017. Groundwater shapes sediment biogeochemistry and microbial diversity in a submerged sinkhole. Geobiology 15, 225–239. https://doi.org/10.1038/nature04068

Lyons, T.W., Reinhard, C.T., Planavsky, N.J., 2014. The rise of oxygen in Earth's early ocean and atmosphere. Nature 506, 307–15. https://doi.org/10.1038/nature13068

Nold, S.C., Bellecourt, M.J., Kendall, S.T., Ruberg, S. A., Sanders, T.G., Klump, J.V., Biddanda, B. A., 2013. Underwater sinkhole sediments sequester Lake Huron's carbon. Biogeochemistry 115, 235–250. https://doi.org/10.1007/s10533-013-9830-8

Olson, S.L., Reinhard, C.T., Lyons, T.W., 2016. Limited role for methane in the mid-Proterozoic greenhouse. Proc. Natl. Acad. Sci. 113, 11447–11452. https://doi.org/10.1073/pnas.1608549113

Parnell, J., Boyce, A.J., Mark, D., Bowden, S., Spinks, S., 2010. Early oxygenation of the terrestrial environment during the Mesoproterozoic. Nature 468, 290–293. https://doi.org/10.1038/nature09538

Parnell, J., Spinks, S., Andrews, S., Thayalan, W., Bowden, S., 2015. High Molybdenum availability for evolution in a Mesoproterozoic lacustrine environment. Nat. Commun. 6, 6996. https://doi.org/10.1038/ncomms7996

Planavsky, N.J., Slack, J.F., Cannon, W.F., O'Connell, B., Isson, T.T., Asael, D., Jackson, J.C., Hardisty, D.S., Lyons, T.W., Bekker, A., 2018. Evidence for episodic oxygenation in a weakly redox-buffered deep mid-Proterozoic ocean. Chem. Geol. 483, 581–594. https://doi.org/10.1016/j.chemgeo.2018.03.028

Poulton, S., Canfield, D., 2005. Development of a sequential extraction procedure for iron: implications for iron partitioning in continentally derived particulates. Chem. Geol. 214, 209–221. https://doi.org/10.1016/j.chemgeo.2004.09.003

Raiswell R., Canfield D.E., 2012. The iron biogeochemical cycle past and present. Geochem. Persp. 1, 1–220.

Raiswell, R., Hardisty, D.S., Lyons, T.W., Canfield, D.E., Owens, J.D., Planavsky, N.J., Poulton, S.W., Reinhard, C.T., 2018. The iron paleoredox proxies: A guide to the pitfalls, problems and proper practice. Am. J. Sci. 318, 491–526. https://doi.org/10.2475/05.2018.03

Rico, K.I., Sheldon, N.D., 2019. Nutrient and iron cycling in a modern analogue for the redoxcline of a Proterozoic ocean shelf. Chem. Geol. 511, 42–50. https://doi.org/10.1016/j.chemgeo.2019.02.032

Ruberg, S.A., Kendall, S.T., Biddanda, B.A., Black, T., Nold, S.C., Lusardi, W.R., Green, R., Casserly, T., Smith, E., Sanders, T.G., Lang, G.A., Constant, S.A., 2008. Observations of the Middle Island Sinkhole and Glacial Creation of 400 Million Years. Mar. Technol. Soc. J. 42, 12–21.

Scott, C., Lyons, T.W., 2012. Contrasting molybdenum cycling and isotopic properties in euxinic versus non-euxinic sediments and sedimentary rocks: Refining the paleoproxies. Chem. Geol. 324–325, 19–27. https://doi.org/10.1016/j.chemgeo.2012.05.012

Shen, Y., Canfield, D.E., Knoll, A.H., 2002. Middle Proterozoic Ocean Chemistry: Evidence from the McArthur Basin, Northern Australia. Am. J. Sci. 302, 1–27. https://doi.org/10.1126/science.3.53.32

Slotznick, S.P., Swanson-Hysell, N.L., Sperling, E.A., 2018. Oxygenated Mesoproterozoic lake revealed through magnetic mineralogy. Proc. Natl. Acad. Sci. 201813493. https://doi.org/10.1073/pnas.1813493115

Sperling, E. A., Rooney, A. D., Hays, L., Sergeev, V.N., Vorob'eva, N.G., Sergeeva, N.D., Selby, D., Johnston, D.T., Knoll, A. H., 2014. Redox heterogeneity of subsurface waters in the Mesoproterozoic ocean. Geobiology 12, 373–386. https://doi.org/10.1111/gbi.12091

Strother, P.K., Battison, L., Brasier, M.D., Wellman, C.H., 2011. Earth's earliest non-marine eukaryotes. Nature 473, 505–509. https://doi.org/10.1038/nature09943

Stüeken, E.E., Bellefroid, E.J., Prave, A., Asael, D., Planavsky, N.J., Lyons, T.W., 2017. Not so non-marine? Revisiting the Stoer Group and the Mesoproterozoic biosphere. Geochemical Perspect. Lett. 3, 221–229. https://doi.org/10.7185/geochemlet.1725

Suszek, T., 1997. Petrography and sedimentation of the middle Proterozoic (Keweenawan) Nonesuch Formation, western Lake Superior region, Midcontinent Rift System. In Middle Proterozoic to Cambrian Rifting, Central North American., eds. Ojakangas, R.W., Dickas, A.B. and Green, J. C. Geological Society of America Special Papers. pp. 195–210.

Taylor, S. R., McLennan, S. M., 1985. The continental crust: Its composition and evolution, Oxford, UK: Blackwell.

Tessin, A., Chappaz, A., Hendy, I., Sheldon, N., 2018. Molybdenum speciation as a paleo-redox proxy: A case study from Late Cretaceous Western Interior Seaway black shales. Geology 47, 59–62. https://doi.org/10.1130/g45785.1

Tessin, A., Sheldon, N.D., Hendy, I., Chappaz, A., 2016. Iron limitation in the Western Interior Seaway during the Late Cretaceous OAE 3 and its role in phosphorus recycling and enhanced organic matter preservation. Earth Planet. Sci. Lett. 449, 135–144. https://doi.org/10.1016/j.epsl.2016.05.043

Tribovillard, N., Algeo, T.J., Baudin, F., Riboulleau, A., 2012. Analysis of marine environmental conditions based on molybdenum-uranium covariation-Applications to Mesozoic paleoceanography. Chem. Geol. 324–325, 46–58. https://doi.org/10.1016/j.chemgeo.2011.09.009

Van der Weijden, C.H., 2002. Pitfalls of normalization of marine geochemical data using a common divisor. Mar. Geol. 184, 167–187.

Voorhies, A.A., Biddanda, B.A., Kendall, S.T., Jain, S., Marcus, D.N., Nold, S.C., Sheldon, N.D., Dick, G.J., 2012. Cyanobacterial life at low O(2): community genomics and function reveal metabolic versatility and extremely low diversity in a Great Lakes sinkhole mat. Geobiology 10, 250–67. https://doi.org/10.1111/j.1472-4669.2012.00322.x

Vorlicek, T.P., Chappaz, A., Groskreutz, L.M., Young, N., Lyons, T.W., 2015. A new analytical approach to determining Mo and Re speciation in sulfidic waters. Chem. Geol. 403, 52–57. https://doi.org/10.1016/j.chemgeo.2015.03.003

Wagner, M., Chappaz, A., Lyons, T.W., 2017. Molybdenum speciation and burial pathway in weakly sulfidic environments: Insights from XAFS. Geochim. Cosmochim. Acta 206, 18–29. https://doi.org/10.1016/j.gca.2017.02.018

Wellman, C.H., Strother, P.K., 2015. The terrestrial biota prior to the origin of land plants (embryophytes): A review of the evidence. Palaeontology 58, 601–627. https://doi.org/10.1111/pala.12172

Wilmeth, D.T., Dornbos, S.Q., Isbell, J.L., Czaja, A.D., 2014. Putative domal microbial structures in fluvial siliciclastic facies of the Mesoproterozoic (1.09 Ga) Copper Harbor Conglomerate, Upper Peninsula of Michigan, USA. Geobiology 12, 99–108. https://doi.org/10.1111/gbi.12071

CHAPTER V

Conclusions

5.1 Summary of Results

In Chapter II, I explore the differences in macronutrient burial and Fe geochemistry between the sediments of the low-oxygen Middle Island Sinkhole (MIS) and the fully oxygenated Lake Huron control site (LH). Stable C isotopes and C:N ratios demonstrate that the organic C buried with MIS sediments is the same as that of LH—Lake Huron phytoplankton. The MIS microbial mats present at the sediment-water interface are not one of the main sources of C being buried in MIS sediments; C:N ratios also indicate that the microbial mats are also not controlling overall C and N cycling in MIS sediments. With organic C stemming from the same source between LH and MIS, the enhanced macronutrient burial in MIS must not be attributable to differences in productivity, but instead to differences in preservation (*i.e.*, redox); iron speciation is used to explore this further.

Iron speciation indicates that MIS is ferruginous and that LH is oxic, which is consistent with the known water chemistry of the two locales. Notably, Fe speciation records the strong redoxcline of the MIS site (<3 m of water column), and not the ~20 m of oxygenated water column above. These results indicate that we should take caution when interpreting Fe speciation results to indicate entire water column processes in the fossil record. Altogether, nutrient and Fe geochemistry in the analogue MIS site demonstrates that Proterozoic biogeochemical cycling in

surficial sediments may be driven primarily by redoxcline—not microbial or water column—processes.

In Chapter III, I use sediment redox-sensitive trace metal (*e.g.,* Mn, Mo, and U) contents and microbial community composition to infer abiotic and biotic controls on trace metal burial in MIS and LH, and to test whether or not trace metal covariation with organic C can be used as biosignature for microbial mats. I demonstrate that relationships between trace metals and organic C in MIS and LH are not consistent with our expectations of how the different trace metals are buried. Given that some of the metals analyzed in Chapter III are considered to be robust paleoproxies for redox, these results have major implications for our interpretations of metal abundance and metal isotope systematics in ancient systems. In particular, this work suggests a burial mechanism for Mo—often considered one of the most robust trace metal proxies for water column euxinia—that is related to organic matter burial, and independent of free sulfide availability. Additionally, significant overlap between LH and MIS microbial assemblages make it difficult to correlate sediment trace metal geochemistry to microbial groups or metabolisms, with the possible exception that Mn enrichment correlates well with oxygenated LH sediment geochemistry. Ultimately, Chapter III concludes that bulk sediment trace metal abundance cannot be used as a biosignature for the community composition of microbial mats under low oxygen conditions.

Chapter IV directly compares MIS Fe and Mo geochemistry to that of Nonesuch Formation (~1.1 billion years old; USA) sediments to constrain the redox chemistry of Mesoproterozoic lacustrine environments. The Nonesuch Formation Fe speciation data mostly indicate oxic or possibly anoxic conditions, with no evidence for euxinia. Similarly, both the modern systems and the Nonesuch Formation exhibit Mo contents far below what is anticipated

for euxinic conditions. Some Nonesuch Formation samples exhibit Mo enrichments relative to the modern systems; the burial mechanisms for these moderate Mo enrichments in the Nonesuch Formation sediments are explored using Mo-U covariation.

Mo-U covariation for both the modern and ancient environments indicate Mo enrichments via the "particulate shuttle" pathway of Mo burial—the first record of a lacustrine particulate Mo shuttle in the geologic record— wherein authigenic Mo is scavenged by metal hydroxides (*e.g.*, Mn and Fe) in the water column. Euxinic conditions are not directly causing Mo enrichments in the ancient sediments nor its modern analogue, directly contrasting the model of Parnell et al. (2015). Additionally, there is no evidence for enhanced biological productivity within the Nonesuch Formation. Finally, without high enough Mo to indicate significant sulfate weathering, this study provides no clear indicator of Mesoproterozoic atmospheric oxygenation levels. The Nonesuch Formation Fe and Mo geochemistry primarily reflects fluctuating redox conditions and intense cycling of metals within the water column.

Together, Chapters II–IV help to constrain the abiotic and biotic burial pathways of nutrients and metals within the MIS sediments, with implications for how to interpret the geochemistry of these elements in the fossil record (*e.g.*, in Proterozoic sediments). This work indicates that the dynamic microbial mat at the sediment-water interface within MIS has no clear influence on the burial of major nor trace elements within the sediments, implying that the presence of Proterozoic aquatic microbial mats in may not have made a significant imprint on sediment geochemistry, or that much of the biogeochemical cycling was cryptic (*a la* Canfield et al., 2010), and not readily preserved. Importantly, with Fe speciation only capturing partial water column redox chemistry, and unexpected trace metal and organic C covariation patterns, Chapters II and III highlight the need to examine the burial mechanisms for metals critically in

modern oxic and low-oxygen environments in order to interpret sediment geochemistry in the geologic record. Finally, Chapter IV highlights the need to use multiple redox proxies in tandem with one another (*e.g.*, iron speciation and Mo-U covariation) to best interpret geochemical results. A careful consideration for metal burial pathways in the future will have major implications for how we use these metals as redox proxies, not just for interpreting the oxygenation of Proterozoic environments, but also at other periods in geologic history wherein constraining water column oxygenation is critical: the evolution of animals within the Phanerozoic, Oceanic Anoxic Events in the Cretaceous, and even considering the development of modern oxygen minimum zones.

5.2 Future Research Directions

5.2.1 How does Sediment Metal Geochemistry Reflect Water Column and/or Porewater Chemistry?

Chapters II and III broadly consider the impact of water column oxygenation and Fe on sediment metal geochemistry, but the impact of water column and porewater trace metal contents on sediment geochemistry remains unclear. Preliminary results paint a complicated picture for interpreting sediment trace metal geochemistry. For example, the trace metal Zn is incorporated into organic matter in oxic sediments, released into the water column under reducing conditions, and complexed with free sulfide under euxinic conditions (Huerta-Diaz and Morse, 1992; Lepp, 1992; Calvert and Pederson, 1993). As a paleoredox proxy, Zn is often considered to have "strong euxinic affinity" (*e.g.*, Algeo and Maynard, 2004). Therefore, Zn enrichments in the geologic record—in tandem with enrichments in organic C, S, and other trace metals with an affinity for euxinia (*e.g.*, Mo)—are interpreted to depict euxinic conditions (*e.g.*, Hatch and

Leventhal, 1992; März et al., 2008). As evident in Chapter II, MIS is ferruginous and not euxinic, making the absence of a significant Zn enrichment in MIS sediments (Figure 5.2) consistent with how Zn is used as a paleoredox proxy. This directly contradicts the conclusions drawn from Chapter III, which demonstrates that Zn-C_{org} covariation is consistent across all LH and MIS sediments, regardless of oxygen and free sulfide availability in the sediments. These discrepancies raise interesting questions about which trace metals, and under what redox regimes, trace metal enrichments versus trace metal covariations with C_{org} are the most appropriate paleoredox proxies.

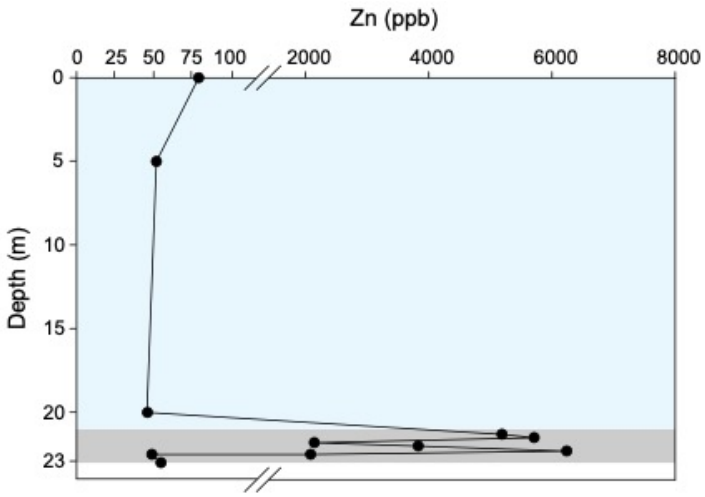

Figure 5.1 Water column Zn concentrations in MIS, spanning the overlying Lake Huron water and the chemocline. Zn concentrations were measured by ICP-MS with ICP Science certified standards at the STARLAB, Central Michigan University.

Notably, MIS sediment Zn enrichments do not reflect the water column enrichments. In the MIS water column, Zn is elevated by nearly two orders of magnitude in comparison to the overlying Lake Huron water on the ppb scale (Figure 5.1). Despite this, MIS sediment Zn contents are only moderately enriched (~2x) relative to those of LH, on the ppm scale (Figure 5.2). These discrepancies in scale demonstrate that, in ancient aquatic systems, sediment geochemistry may not reflect the availability of micronutrients (*e.g.*, Cd, Ni, Zn) in the water

column. This implies that sediment trace contents alone may not be appropriate measures micronutrient availability in paleoenvironments.

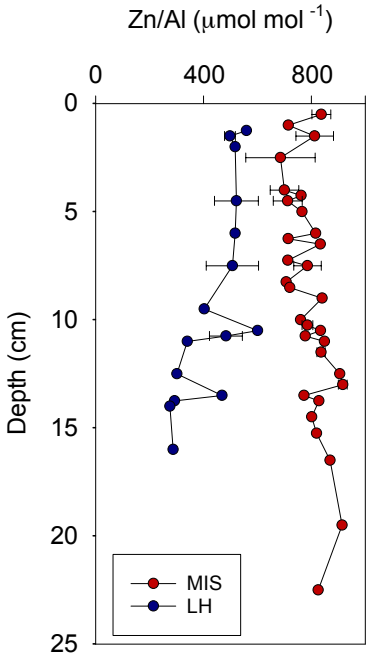

Figure 5.2 Depth profiles of Zn for Middle Island Sinkhole (MIS) and Lake Huron (LH). Values for a given depth are reported as means, with error bars representing variability (1σ) between different cores at particular depths (n = 9 for MIS, and n = 8 for LH). Zn is normalized to Al content in order to represent authigenic concentrations of target elements; Al was chosen because Al contents across MIS and LH had lower variability than other immobile elements for this dataset. Data from Chapter III.

For ancient systems, sediment trace metal contents are typically considered to be attributed to water column chemistry, not porewater chemistry (*e.g.* Algeo and Maynard, 2004; Sperling et al., 2014; Miller et al., 2017). However, it is clear that sediment trace metal contents do not reflect the water column trace metal contents for Zn in MIS (Figures 5.1 and 5.2). Complicating this further, sediment and porewater Zn contents exhibit a modest correlation ($r = 0.59$; $p < 0.05$; Figure 5.3), indicating some equilibrium between sediment and porewater Zn, and therefore posing some challenges to how we interpret sediment geochemistry in the geologic record. For example, Zn enrichments have been used to interpret euxinia throughout the Phanerozoic, including Upper Pennsylvanian marine black shales (Hatch and Leventhal, 1992;

Algeo and Maynard, 2004), the Late Devonian-Early Mississippian Bakken Formation (Scott et al., 2017), and during Oceanic Anoxic Event 3 (März et al., 2008). However, the correlation between sediment and porewater Zn in MIS indicate that Zn contents in aquatic systems may also be influenced by porewater (not water column) free sulfide availability, at least in some basins at some times. Ultimately, identifying all controls on sediment trace metal geochemistry in a variety of modern aquatic systems will allow for a more holistic interpretation of these data in the fossil record.

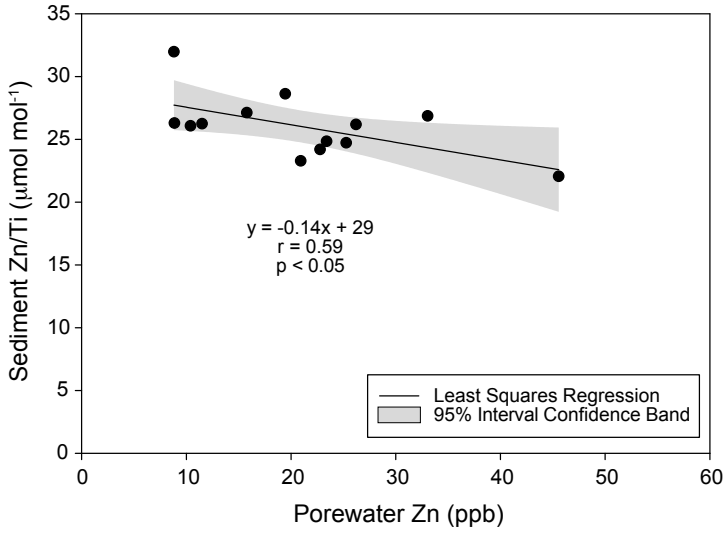

Figure 5.3 MIS sediment Zn contents vs porewater Zn contents (n = 13). Zn concentrations of all samples were measured by ICP-MS with ICP Science certified standards at the STARLAB, Central Michigan University. Sediment Zn is normalized to Ti content in order to represent authigenic concentrations of target elements; Ti was chosen because Ti contents across MIS sediments had lower variability than other immobile elements for this dataset.

5.2.2 Mercury Burial in a Low-Oxygen Great Lakes Environment

Given the importance of water in the Great Lakes Basin to millions of North Americans today, and its potential as a critical freshwater source in other parts of the country in the future, understanding stressors such as metal toxicity is critical. Trace metals have been deposited

historically up through the present in the Great Lakes through industrial effluent (Dolan & Bierman, 1982; Yuan et al., 2018). In Chapter III, I demonstrate that MIS has an increased trace metal load relative to the Lake Huron control site. Preliminary results suggest that MIS also buried more Hg than Lake Huron, with overlap in the surficial sediments (<5 cm depth; Figure 5.4). While a difference in preservation (*e.g.*, redox) between the two locales could account for the different trends seen in Figure 5.4 (just as redox chemistry impacts macronutrient and metal burial in Chapters II and III), groundwater may also be a source of Hg to these sites, with the burial of Hg dependent on differences how each site is influenced by regional groundwater (*e.g.*, Kinsman-Costello et al., 2017).

Especially in low-oxygen environments (*i.e.*, in environments such as MIS), Hg can be methylated (creating MeHg), resulting in a bioavailable and toxic form of this metal that biomagnifies in Great Lakes biota (Regnell, 1994; Pak and Bartha, 1998; Fleming et al., 2006; Zananski et al., 2011). There are a number of sulfate- and iron- reducing bacteria that have been confirmed to methylate Hg in low-oxygen aquatic systems, from the genera *Desulfobulbus*, *Desulfovibria*, and *Geobacter* (Pak and Bartha, 1998; Kerin et al., 2006; Fleming et al., 2006; Parks et al., 2013). These genera, and sulfate- and iron- reduction metabolic capabilities, have all been identified in the microbial community amongst sinkhole sediments (Kinsman-Costello, 2017; Medina, 2018; Grim, 2019). However, despite abiotic and biotic conditions in MIS being ideal for MeHg, only six out of the 23 samples the bulk of the samples (n = 23) were able to be analyzed for MeHg via acid dissolution, while the rest had matrix effects that made analysis difficult; use of a distillation method could improve MeHg for the rest of the samples. Of the six samples wherein MeHg was extracted, MIS had low MeHg (<0.5% of total), and in fact there is more MeHg in LH than in MIS (Table 5.1). MeHg in MIS may be limited by the presence of free

sulfides in the sediments (Kinsman-Costello et al., 2017), which can out-compete other ligands for Hg complexation (Dyrssen and Wedborg, 1991; Benoit et al., 1999), or hinder methylation by sulfate-reducing bacteria (Gilmour et al., 1992; Liu et al., 2009). Further work is needed to constrain the biogeochemical cycling of Hg in the Great Lakes as a whole, including considering additional methods to extract tightly bound MeHg prior to analysis, and to understand why Hg is not being methylated in an environment primed for Hg methylation.

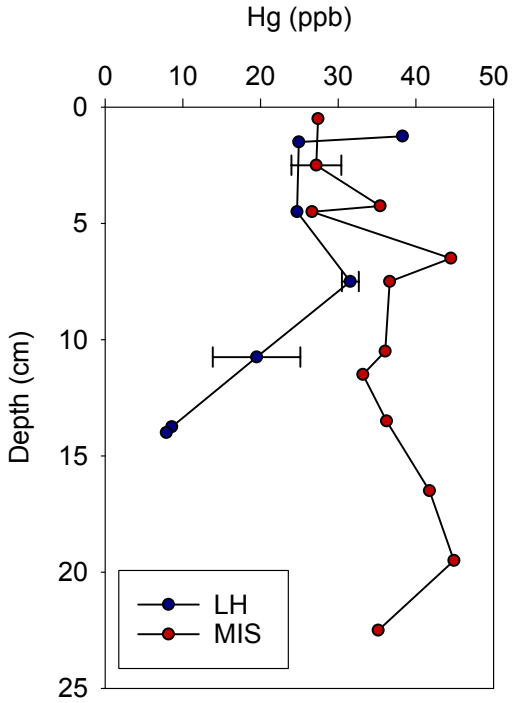

Figure 5.4 Total Hg profiles for MIS sediments (n = 13) and LH sediments (n = 9). Error bars represent variability (1σ) between two cores at particular depths. Samples were analyzed via a combustion furnace attached to an Atomic Absorption Spectrometer (combustion-AAS), with NRCC MESS-3 and TORT-3 standard reference materials run in tandem with the samples.

Table 5.1 Total Hg contents, MeHg contents, and %MeHg for LH and MIS sediments. Samples were acid digested analyzed with Methyl Hg Gas Chromatography and Pyrolysis, with NRCC MESS-3 and TORT-3 standard reference materials run in tandem with the samples.

Sample ID	ng Hg/g sediment	pg MeHg/g sediment	%MeHg of THg
LH2015.006-1A	38.29	179.03	0.47%
LH2015.008-2	32.34	113.25	0.37%
MIS0914.3-2	34.41	69.81	0.20%
MIS0914.3-3	44.51	42.76	0.10%
MIS2015.011-6	41.76	43.48	0.10%
MIS2015.011-7	44.91	70.22	0.16%

5.2.3 Gaps in our Knowledge for Interpreting Sediment Trace Metal Geochemistry

Results from Chapters II–IV demonstrate the need for a more comprehensive assessment of the metal burial mechanisms in aquatic systems. Research considering trace metal burial mechanisms in non-marine, non-euxinic environments such as lakes, and ferruginous and sub-oxic environments, would vastly improve our understanding of the abiotic controls on trace metal burial. For example, using Fe, Mo, and U geochemistry in the Nonesuch Formation, I identified a Proterozoic lacustrine particulate Mo shuttle in Chapter IV. In addition to considering abiotic mechanisms for trace metal burial, identifying how microbial species use trace metals on a nano- to micro-scale, and considering how these transformations are or are not reflected within bulk sediment geochemistry, could elucidate new biotic controls on trace metal burial.

In Chapter II, I demonstrate that, although many trace metals are used as micronutrients for microbiota (*e.g.*, Cd, Ni, Zn; Lepp ,1992), there is no evidence of significant enrichments or depletions in these profiles where the microbial mat is present (*e.g.*, Figure 5.2). For example, despite an abundance Zn in the MIS water column (Figure 5.1), an abundance of Epsilonproteobacteria in the MIS microbial mat (Kinsman-Costello et al., 2017), and considering that all of the Epsilonproteobacteria sulfate oxidizers in the MIS mat have transporters for Zn,

there is still no evidence of microbial transformations of Zn within the bulk sediment Zn chemistry (Figure 5.2). Because bulk sediment geochemistry has not provided a clear indicator of microbial mat presence in our modern analogue system, approaches considering different scales and interactions between metals and organic matter—metal speciation (*e.g.*, Ardakani et al., 2016), lipid biomarker analysis (*e.g.*, Willers et al., 2015), and/or quantification of the quality/lability of organic C (*e.g.*, Strauss and Lamberti, 2002)— may be necessary for interpreting trace metal data in a biological context, ultimately improving how we use sediments to define the chemistry of ancient environments.

5.3 References

Algeo, T.J., Maynard, J.B., 2004. Trace-element behavior and redox facies in core shales of Upper Pennsylvanian Kansas-type cyclothems. Chem. Geol. 206, 289–318. https://doi.org/10.1016/j.chemgeo.2003.12.009

Ardakani, O.H., Chappaz, A., Sanei, H., Mayer, B., 2016. Effect of thermal maturity on remobilization of molybdenum in black shales. Earth Planet. Sci. Lett. 449, 311–320. https://doi.org/10.1016/j.epsl.2016.06.004

Benoit, J.M., Gilmour, C.C., Mason, R.P., Heyes, A., 1999. Sulfide controls on mercury speciation and bioavailability to methylating bacteria in sediment pore waters. Environ. Sci. Technol. 33, 951–957. https://doi.org/10.1021/es9808200

Calvert, S.E., Pedersen, T.F., 1993. Geochemistry of Recent oxic and anoxic marine sediments: Implications for the geological record. Mar. Geol. 113, 67–88. https://doi.org/10.1016/0025-3227(93)90150-T

Canfield, D.E., Stewart, F.J., Thamdrup, B., De Brabandere, L., Dalsgaard, T., Delong, E.F., Revsbech, N.P., Ulloa, O., 2010. A Cryptic Sulfur Cycle in. Science2 330, 1375–1378. https://doi.org/10.1126/science.1196889

Cohen, M., Artz, R., Draxler, R., Miller, P., Poissant, L., Niemi, D., Ratté, D., Deslauriers, M., Duval, R., Laurin, R., Slotnick, J., Nettesheim, T., McDonald, J., 2004. Modeling the atmospheric transport and deposition of mercury to the Great Lakes. Environ. Res. 95, 247–265. https://doi.org/10.1016/j.envres.2003.11.007

Dolan, D.M., Bierman, V.J., 1982. Mass Balance Modeling of Heavy Metals in Saginaw Bay, Lake Huron. J. Great Lakes Res. 8, 676–694. https://doi.org/10.1016/S0380-1330(82)72008-8

Dyrssen, D., Wedborg, M., 1991. The sulphur-mercury(II) system in natural waters. Water, Air, Soil Pollut. 56, 507–519. https://doi.org/10.1007/BF00342295

Fleming, E.J., Mack, E.E., Green, P.G., Nelson, D.C., 2006. Mercury methylation from unexpected sources: Molybdate-Inhibited freshwater sediments and an iron-reducing bacterium. Appl. Environ. Microbiol. 72, 457–464. https://doi.org/10.1128/AEM.72.1.457

Gilmour, C.C., Henry, E.A., Ralph, M., 1992. Sulfate Stimulation of Mercury Methylation in Freshwater Sediments. Environ. Sci. Technol. 26, 2281–2287. https://doi.org/10.1021/es00035a029

Grim, S., 2019. "Genomic and functional investigations into seasonally-impacted and morphologically-distinct anoxygenic photosynthetic cyanobacterial mats." Doctoral dissertation, University of Michigan.

Hamelin, S., Amyot, M., Barkay, T., Wang, Y., Planas, D., 2011. Methanogens: Principal methylators of mercury in lake periphyton. Environ. Sci. Technol. 45, 7693–7700. https://doi.org/10.1021/es2010072

Hatch, J.R., Leventhal, J.S., 1992. Relationship between inferred redox potential of the depositional environment and geochemistry of the Upper Pennsylvanian (Missourian) Stark Shale Member of the Dennis Limestone, Wabaunsee County, Kansas, U.S.A. Chem. Geol. 99, 65–82. https://doi.org/10.1016/0009-2541(92)90031-Y

Huerta-Diaz, M.A., Morse, J.W., 1992. Pyritization of trace metals in anoxic marine sediments. Geochim. Cosmochim. Acta 56, 2681–2702. https://doi.org/10.1016/0016-7037(92)90353-K

Kerin, E.J., Gilmour, C.C., Roden, E., Suzuki, M.T., Coates, J.D., Mason, R.P., 2006. Mercury methylation by dissimilatory iron-reducing bacteria. Appl. Environ. Microbiol. 72, 7919–7921. https://doi.org/10.1128/AEM.01602-06

Kinsman-Costello, L.E., Sheik, C.S., Sheldon, N.D., Burton, G. a., Costello, D., Marcus, D.N., Uyl, P. Den, Dick, G.J., 2017. Groundwater shapes sediment biogeochemistry and microbial diversity in a submerged sinkhole. Geobiology 15, 225–239. https://doi.org/10.1038/nature04068

Lepp, N. W., 1992. Uptake and accumulation of metals in bacteria and fungi. In: Biogeochemistry of Trace Metals, ed. Adriano, D. C. Boca Raton, FL: Lewis Publishers. pp. 277–298

Liu, J., Valsaraj, K.T., Delaune, R.D., 2009. Inhibition of Mercury Methylation by Iron Sulfides in an Anoxic Sediment. Environ. Eng. Sci. 26, 833–840. https://doi.org/10.1089/ees.2008.0243

März, C., Poulton, S.W., Beckmann, B., Küster, K., Wagner, T., Kasten, S., 2008. Redox sensitivity of P cycling during marine black shale formation: Dynamics of sulfidic and anoxic, non-sulfidic bottom waters. Geochim. Cosmochim. Acta 72, 3703–3717. https://doi.org/10.1016/j.gca.2008.04.025

Medina, M, 2016. "Genomic and transcriptomic evidence for niche partitioning among sulfate-reducing bacteria in redox-stratified cyanobacterial mats of the Middle Island Sinkhole." Master's thesis, University of Michigan.

Miller, A.J., Strauss, J. V., Halverson, G.P., Macdonald, F.A., Johnston, D.T., Sperling, E.A., 2017. Tracking the onset of Phanerozoic-style redox-sensitive trace metal enrichments: New results from basal Ediacaran post-glacial strata in NW Canada. Chem. Geol. 457, 24–37. https://doi.org/10.1016/j.chemgeo.2017.03.010

Pak, K.R., Bartha, R., 1998. Mercury Methylation and Demethylation in Anoxic Lake Sediments and by Strictly Anaerobic Bacteria. Appl. Environ. Microbiol. 64, 1013–1017.

Parks, J.M., Johs, A., Podar, M., Bridou, R., Jr, R.A.H., Smith, S.D., Tomanicek, S.J., Qian, Y., Brown, S.D., Brandt, C.C., Palumbo, A. V, Smith, J.C., Wall, J.D., Elias, D.A., Liang, L., 2013. The Genetic Basis for Bacterial Mercury Methylation 339, 1332–1336. https://doi.org/10.1126/science.1230667

Regnell, O., 1994. The effect of pH and dissolved oxygen levels on methylation and partitioning of mercury in freshwater model systems. Environ. Pollut. 84, 7–13. https://doi.org/10.1016/0269-7491(94)90064-7

Rico, K.I., Sheldon, N.D., 2019. Nutrient and iron cycling in a modern analogue for the redoxcline of a Proterozoic ocean shelf. Chem. Geol. 511, 42–50. https://doi.org/10.1016/j.chemgeo.2019.02.032

Scott, C., Slack, J.F., Kelley, K.D., 2017. The hyper-enrichment of V and Zn in black shales of the Late Devonian-Early Mississippian Bakken Formation (USA). Chem. Geol. 452, 24–33. https://doi.org/10.1016/j.chemgeo.2017.01.026

Sperling, E. a., Rooney, a. D., Hays, L., Sergeev, V.N., Vorob'eva, N.G., Sergeeva, N.D., Selby, D., Johnston, D.T., Knoll, A. H., 2014. Redox heterogeneity of subsurface waters in the Mesoproterozoic ocean. Geobiology 12, 373–386. https://doi.org/10.1111/gbi.12091

Strauss, E.A., Lamberti, G.A., 2002. Effect of dissolved organic carbon quality on microbial decomposition and nitrification rates in stream sediments. Freshw. Biol. 47, 65–74.

Willers, C., Jansen van Rensburg, P.J., Claassens, S., 2015. Microbial signature lipid biomarker analysis - an approach that is still preferred, even amid various method modifications. J. Appl. Microbiol. 118, 1251–1263. https://doi.org/10.1111/jam.12798

Yuan, F., Chaffin, J.D., Xue, B., Wattrus, N., Zhu, Y., Sun, Y., 2018. Contrasting sources and mobility of trace metals in recent sediments of western Lake Erie. J. Great Lakes Res. 44, 1026–1034. https://doi.org/10.1016/j.jglr.2018.07.016

Zananski, T.J., Holsen, T.M., Hopke, P.K., Crimmins, B.S., 2011. Mercury temporal trends in top predator fish of the Laurentian Great Lakes. Ecotoxicology 20, 1568–1576. https://doi.org/10.1007/s10646-011-0751-9

APPENDIX A

Supplemental Figures and Tables for Chapter II

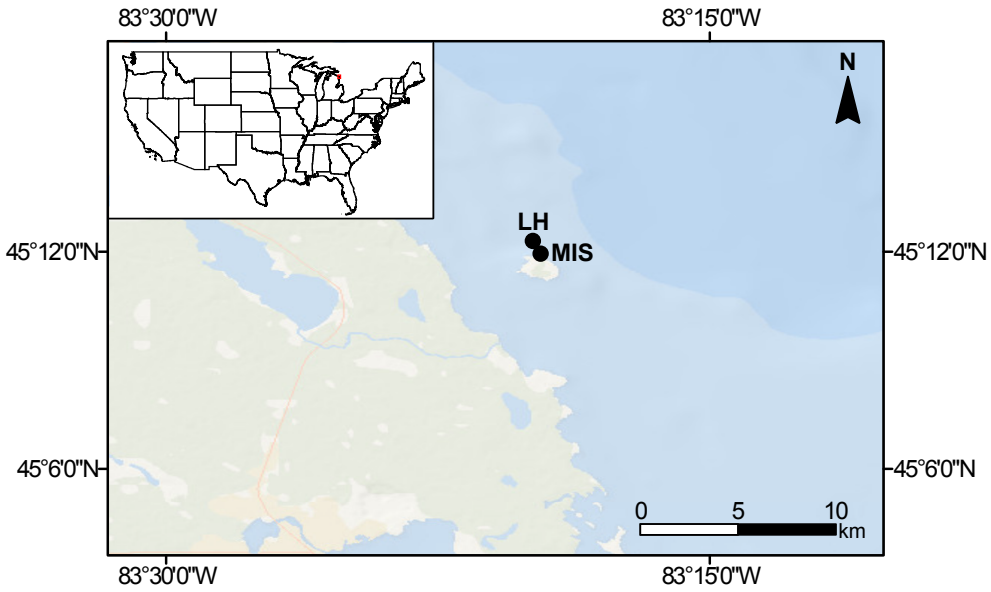

Figure A1 Location map of the Middle Island Sinkhole (MIS) and Lake Huron site (LH).

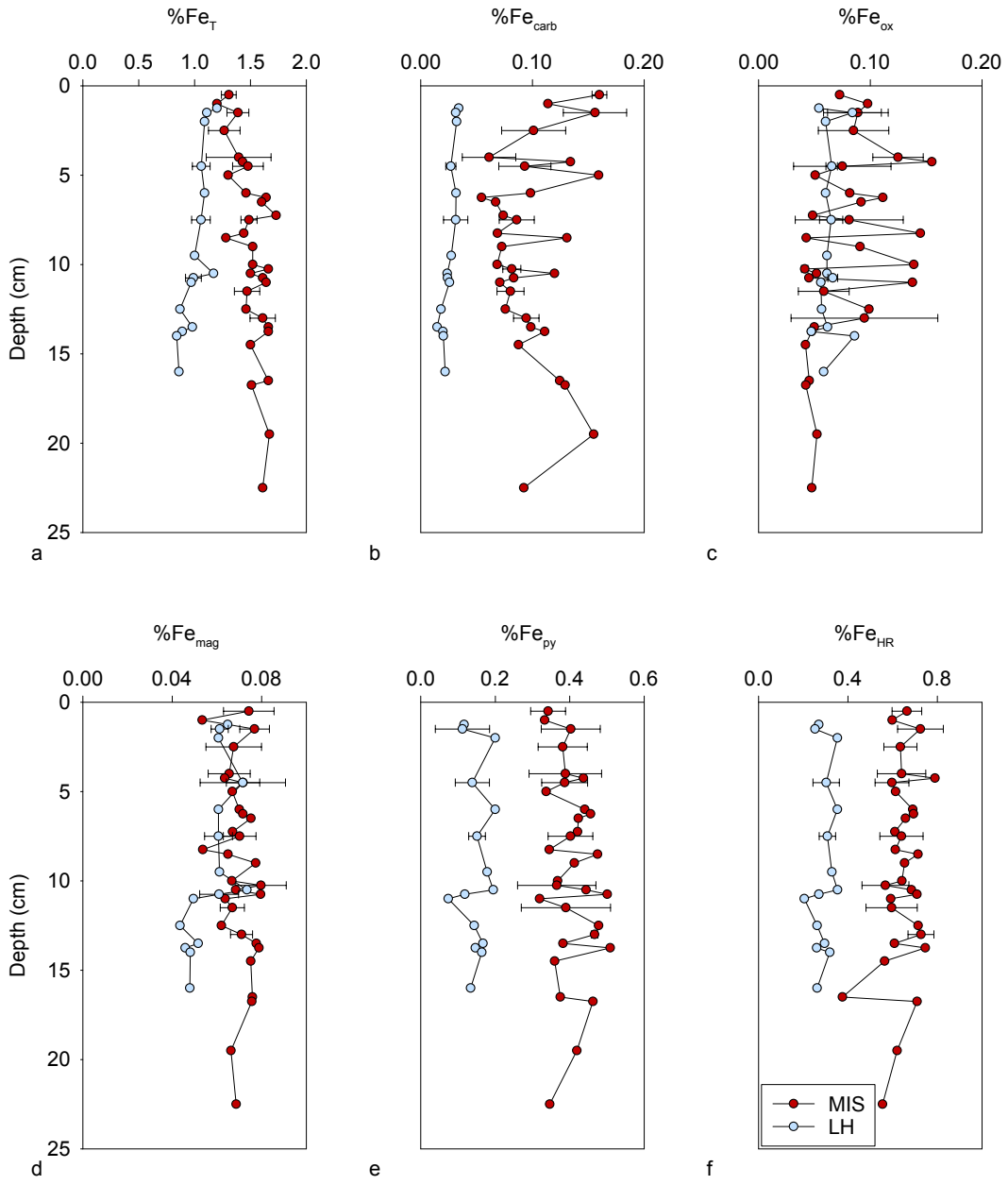

Figure A2 Average (a) $\%Fe_T$, (b) $\%Fe_{carb}$, (c) $\%Fe_{ox}$, (d) $\%Fe_{mag}$, (e) Fe_{py}, and (f) $\%Fe_{HR}$. Error bars represent variability (1σ) between different cores at particular depths (n = 9 for Middle Island Sinkhole, MIS; and n = 5 for Lake Huron, LH).

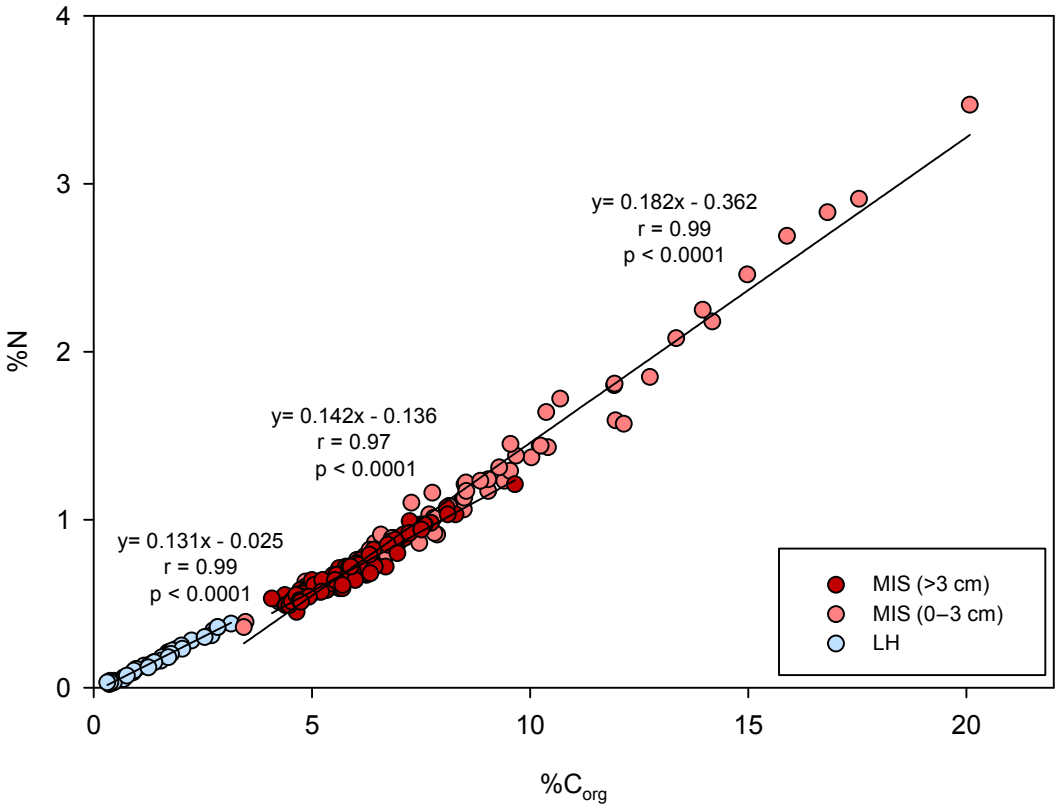

Figure A3 Cross plot of the %N versus $\%C_{org}$ for Middle Island Sinkhole (MIS) sediments (n = 102), MIS mat (n = 71), and Lake Huron (LH) sediments (n = 27).

Table A1 Sample collection information and sediment macronutrient geochemistry for Middle Island Sinkhole (MIS) and Lake Huron (LH).

Location	Month	Year	Sample	Depth	$\%C_{org}$	%N	Molar C:N	$\delta^{13}C$	%S	%P
MIS	May	2013	MIS0513.1-1	1.5	11.96	1.59	8.79	-22.7		
MIS	May	2013	MIS0513.1-2	4.5	9.65	1.21	9.31	-22.38		
MIS	May	2013	MIS0513.1-3	7.5	8.11	1.03	9.18	-21.97		
MIS	May	2013	MIS0513.1-4	10.5	7.57	0.97	9.12	-22.77		
MIS	May	2013	MIS0513.2-1	1.5	12.15	1.57	9.08	-22.68		
MIS	May	2013	MIS0513.2-2	4.5	8.29	1.03	9.41	-22.53		
MIS	May	2013	MIS0513.2-3	7.5	7.59	0.97	9.19	-22.31		
MIS	May	2013	MIS0513.2-4	10.5	7.23	0.92	9.2	-21.66		
MIS	May	2013	MIS0513.3-1	1.5	9.54	1.29	8.69	-22.64		
MIS	May	2013	MIS0513.3-2	4.5	7.73	0.98	9.26	-21.8		
MIS	May	2013	MIS0513.4-1	1.5	10.03	1.37	8.53	-22.7		
MIS	May	2013	MIS0513.4-2	4.5	6.81	0.87	9.26	-22.55		
MIS	May	2013	MIS0513.4-3	7.5	5.99	0.71	9.78	-22.2		
MIS	May	2013	MIS0513.4-4	10.5	7.51	0.94	9.33	-21.31		
MIS	July	2013	MIS0713.3-1	1.5	6.49	0.83	9.16	-22.65		
MIS	July	2013	MIS0713.3-2	4.5	4.9	0.59	9.66	-22.54		
MIS	July	2013	MIS0713.3-3	7.5	6.1	0.75	9.59	-21.76		
MIS	July	2013	MIS0713.3-4	10.5	5.44	0.62	10.39	-22.36		
MIS	July	2013	MIS0713.6-1	1.5	6.2	0.78	9.39	-22.82		
MIS	July	2013	MIS0713.6-2	4.5	6.32	0.77	9.49	-22.23		
MIS	July	2013	MIS0713.6-3	7.5	5.98	0.71	9.91	-22.36		
MIS	July	2013	MIS0713.6-4	10.5	5.81	0.7	9.64	-22.25		
MIS	July	2013	MIS0713.7-1A	0.5	6.62	0.81	7.4	-24.15		
MIS	July	2013	MIS0713.7-1B	1.5	6.09	0.74	8.56	-22.92		
MIS	July	2013	MIS0713.7-1C	2.5	10.37	1.64	9.02	-22.66		
MIS	July	2013	MIS0713.7-2	4.5	7.24	0.99	9.59	-22.24		
MIS	July	2013	MIS0713.7-3	7.5	7.1	0.91	9.55	-22		
MIS	July	2013	MIS0713.8-1A	0.5	5.7	0.71	8.34	-23.42		
MIS	July	2013	MIS0713.8-1B	1.5	4.25	0.51	9.16	-22.67		
MIS	July	2013	MIS0713.8-1C	2.5	6.58	0.91	9.08	-22.47		
MIS	July	2013	MIS0713.8-2	4.5	6.41	0.82	9.33	-22.57		
MIS	July	2013	MIS0713.8-3	7.5	6.91	0.88	9.93	-22.36		
MIS	July	2013	MIS0713.9-1	1.5	6.44	0.86	8.66	-23.45		
MIS	July	2013	MIS0713.9-2	4.5	5.62	0.71	9.23	-22.93		
MIS	July	2013	MIS0713.9-3	7.5	4.97	0.61	9.51	-22.33		
MIS	July	2013	MIS0713.9-4	10.5	5.05	0.61	9.75	-22.72		
MIS	July	2013	MIS0713.11-1A	0.5	20.08	3.47	6.76	-25.98		

Location	Month	Year	Sample	Depth	$\%C_{org}$	%N	Molar C:N	$\delta^{13}C$	%S	%P
MIS	July	2013	MIS0713.11-1B	1.5	10.69	1.72	7.22	-24.97		
MIS	July	2013	MIS0713.11-1C	2.5	6.83	0.89	9	-23.06		
MIS	July	2013	MIS0713.11-2	4.5	4.38	0.55	9.3	-22.96		
MIS	July	2013	MIS0713.11-3	7.5	4.96	0.6	9.62	-22.69		
MIS	July	2013	MIS0713.13-1	1.5	4.98	0.63	9.24	-23.72		
MIS	July	2013	MIS0713.13-2	4.5	5.13	0.62	9.53	-23.26		
MIS	July	2013	MIS0713.13-3	7.5	6.74	0.85	9.27	-22.21		
MIS	July	2013	MIS0713.13-4	10.5	6.11	0.76	9.31	-23.24		
MIS	September	2014	MIS0914.1-1A	1	6.86	0.89	8.85		0.5	0.068
MIS	September	2014	MIS0914.1-1B	2.5	6.32	0.82	9.04		0.55	0.051
MIS	September	2014	MIS0914.1-2	4.5	4.08	0.53	8.85		0.58	0.048
MIS	September	2014	MIS0914.1-3	7.5	5	0.64	9.12		0.54	0.044
MIS	September	2014	MIS0914.1-4	10	5.06	0.59	10.06		0.56	0.047
MIS	September	2014	MIS0914.1-5	13	6.32	0.79	9.23		0.66	0.053
MIS	September	2014	MIS0914.2-1A	0.5	9.04	1.17	9.03			
MIS	September	2014	MIS0914.2-1B	1.5	7.54	0.97	9.07			
MIS	September	2014	MIS0914.2-1C	2.5	4.85	0.63	9		0.42	0.045
MIS	September	2014	MIS0914.2-2	4	6.14	0.71	10.13		0.63	0.048
MIS	September	2014	MIS0914.2-3	6	6.32	0.78	9.57		0.63	0.048
MIS	September	2014	MIS0914.2-4	8.25	4.76	0.56	10.04		0.53	0.046
MIS	September	2014	MIS0914.2-5	11	6.03	0.74	9.51		0.66	0.052
MIS	September	2014	MIS0914.2-6	12.5	5.93	0.7	9.97		0.62	0.051
MIS	September	2014	MIS0914.3-1A	0.5	6.96	0.88	9.27		0.72	0.068
MIS	September	2014	MIS0914.3-1B	1.5	6.03	0.76	9.23			
MIS	September	2014	MIS0914.3-1C	2.5	5.14	0.61	9.71		0.45	0.054
MIS	September	2014	MIS0914.3-2	4.25	4.73	0.58	9.4		0.58	0.045
MIS	September	2014	MIS0914.3-3	6.5	5.76	0.71	9.51		0.64	0.05
MIS	September	2014	MIS0914.3-4	8.75	5.01	0.58	10.01			
MIS	September	2014	MIS0914.3-5	11.5	4.64	0.55	9.98		0.62	0.051
MIS	September	2014	MIS0914.4-1A	0.5	10.22	1.44	8.26			
MIS	September	2014	MIS0914.4-1B	1.5	7.69	1.03	8.67		0.63	0.074
MIS	September	2014	MIS0914.4-1C	2.5	4.29	0.52	9.57		0.39	0.046
MIS	September	2014	MIS0914.4-2	4	5.54	0.65	10.15		0.44	0.044
MIS	September	2014	MIS0914.4-3	6.25	5.72	0.67	10.03		0.62	0.051
MIS	September	2014	MIS0914.4-4	9	6.02	0.73	9.57		0.64	0.052
MIS	September	2014	MIS0914.5-1A	0.5	8.46	1.12	8.7			
MIS	September	2014	MIS0914.5-1B	1.5	6.87	0.89	8.99			
MIS	September	2014	MIS0914.5-1C	2.5	4.97	0.59	9.99			
MIS	September	2014	MIS0914.5-2	4	5.99	0.73	9.52			

Location	Month	Year	Sample	Depth	%C_{org}	%N	Molar C:N	$\delta^{13}C$	%S	%P
MIS	September	2014	MIS0914.5-3	6.25	4.92	0.58	9.98			
MIS	September	2014	MIS0914.5-4	9	5.71	0.64	10.46			
MIS	September	2014	MIS0914.5-5	12.5	4.72	0.52	10.62			
MIS	September	2014	MIS0914.6-1A	0.5	9.41	1.23	8.81			
MIS	September	2014	MIS0914.6-1B	1.5	7.48	0.97	9.04			
MIS	September	2014	MIS0914.6-1C	2.5	4.85	0.6	9.36			
MIS	September	2014	MIS0914.6-2	4.25	6.41	0.73	10.22			
MIS	September	2014	MIS0914.6-3	6.75	5	0.59	9.88			
MIS	September	2014	MIS0914.6-4	9.5	5.32	0.58	10.72			
MIS	September	2014	MIS0914.6-5	12	6.07	0.73	9.58			
MIS	September	2014	MIS0914.6-6	14.5	5.89	0.72	9.58			
MIS	September	2014	MIS0914.7-1A	0.5	12.75	1.85	8			
MIS	September	2014	MIS0914.7-1B	1.5	8.53	1.22	8.18			
MIS	September	2014	MIS0914.7-1C	2.5	8.14	1.08	8.86			
MIS	September	2014	MIS0914.7-2	4	5.86	0.69	9.99			
MIS	September	2014	MIS0914.7-3	6	5.34	0.59	10.43			
MIS	September	2014	MIS0914.7-4	8.5	4.65	0.45	12.12			
MIS	September	2014	MIS0914.7-5	11.25	4.54	0.51	10.11			
MIS	September	2014	MIS0914.7-6	13.5	5.24	0.64	9.48			
MIS	September	2014	MIS0914.8-1A	0.5	14.98	2.46	7.12			
MIS	September	2014	MIS0914.8-1B	1.5	11.94	1.81	7.74			
MIS	September	2014	MIS0914.8-1C	2.5	8.54	1.17	8.5			
MIS	September	2014	MIS0914.8-2	4	5.7	0.71	9.28			
MIS	September	2014	MIS0914.8-3	6	5.63	0.59	11.01			
MIS	September	2014	MIS0914.8-4	8.5	6.69	0.72	10.81			
MIS	September	2014	MIS0914.8-5	11	5.49	0.67	9.53			
MIS	September	2014	MIS0914.8-6	13.5	5.99	0.64	10.98			
MIS	June	2015	MIS2015.011-1A	0.5	8.48	1.06	9.37			
MIS	June	2015	MIS2015.011-1B	1.5	7.87	0.91	10.08			
MIS	June	2015	MIS2015.011-1C	2.5	7.46	0.86	10.26		0.7	0.069
MIS	June	2015	MIS2015.011-2	4.5	6.17	0.75	11.78		0.61	0.058
MIS	June	2015	MIS2015.011-3	7.5	5.34	0.58	11.83		0.58	0.047
MIS	June	2015	MIS2015.011-4	10.5	6.44	0.72	10.65		0.65	0.052
MIS	June	2015	MIS2015.011-5	13.5	5.21	0.57	11.8		0.6	0.054
MIS	June	2015	MIS2015.011-6	16.5	5.7	0.61	10.48		0.63	0.057
MIS	June	2015	MIS2015.011-7	19.5	6.34	0.68	11		0.69	0.058
MIS	June	2015	MIS2015.011-8	22.5	4.75	0.51	10.79		0.6	0.055
MIS	June	2015	MIS2015.012-1A	0.5	14.18	2.18	7.59			
MIS	June	2015	MIS2015.012-1B	1.5	9.29	1.31	8.28			

Location	Month	Year	Sample	Depth	$\%C_{org}$	%N	Molar C:N	$\delta^{13}C$	%S	%P
MIS	June	2015	MIS2015.012-1C	2.5	7.81	0.92	9.96			
MIS	June	2015	MIS2015.012-2	4.5	7.12	0.89	9.35			
MIS	June	2015	MIS2015.012-3	7.5	5.54	0.66	9.76			
MIS	June	2015	MIS2015.012-4	10.5	6.1	0.72	9.94			
MIS	June	2015	MIS2015.012-5	13.5	5.58	0.63	10.4			
MIS	June	2015	MIS2015.013-1A	0.5	11.93	1.8	7.69			
MIS	June	2015	MIS2015.013-1B	1.5	7.79	1.01	9.05			
MIS	June	2015	MIS2015.013-1C	2.5	6.7	0.8	9.77			
MIS	June	2015	MIS2015.013-2	4.5	4.75	0.54	10.26			
MIS	June	2015	MIS2015.013-3	7.75	6.2	0.68	10.73			
MIS	June	2015	MIS2015.013-4	11.25	4.77	0.54	10.33			
MIS	June	2015	MIS2015.014-1A	0.5	13.35	2.08	7.46			
MIS	June	2015	MIS2015.014-1B	1.5	9.04	1.24	8.48			
MIS	June	2015	MIS2015.014-1C	2.5	5.28	0.64	9.64			
MIS	June	2015	MIS2015.014-2	4.5	4.4	0.49	10.53			
MIS	June	2015	MIS2015.014-3	7.75	5.19	0.57	10.53			
MIS	June	2015	MIS2015.014-4	11.25	5.59	0.65	10.08			
MIS	June	2015	MIS2015.015-1A	0.5	17.54	2.91	7.04			
MIS	June	2015	MIS2015.015-1B	1.5	9.68	1.38	8.24			
MIS	June	2015	MIS2015.015-1C	2.5	9.55	1.45	7.7			
MIS	June	2015	MIS2015.015-2	4.5	8.09	1.07	8.83			
MIS	June	2015	MIS2015.015-3	7.5	4.41	0.49	10.53			
MIS	June	2015	MIS2015.015-4	10.25	5.28	0.6	10.1			
MIS	June	2015	MIS2015.015-5	13	5.85	0.71	9.63			
MIS	June	2015	MIS2015.016-1A	0.5	16.82	2.83	6.91			
MIS	June	2015	MIS2015.016-1B	1.5	10.41	1.43	8.49		0.85	0.113
MIS	June	2015	MIS2015.016-1C	2.5	6.96	0.85	9.55		0.62	0.071
MIS	June	2015	MIS2015.016-2	5	6.91	0.86	9.25		0.64	0.063
MIS	June	2015	MIS2015.016-3	8.5	5.26	0.62	9.86		0.51	0.049
MIS	June	2015	MIS2015.016-4	11.5	5.56	0.67	9.54		0.6	0.049
MIS	June	2015	MIS2015.016-5	14.5	5.53	0.64	10.08		0.59	0.052
MIS	June	2015	MIS2015.016-6	16.75	5.78	0.72	9.41		0.6	0.053
MIS	June	2015	MIS2015.017-1A	0.5	13.96	2.25	7.26			
MIS	June	2015	MIS2015.017-1B	1.5	10.24	1.44	8.33			
MIS	June	2015	MIS2015.017-1C	2.5	7.28	1.1	7.67			
MIS	June	2015	MIS2015.017-2	4.5	6.93	0.83	9.82			
MIS	June	2015	MIS2015.017-3	7.5	5.79	0.65	10.41			
MIS	June	2015	MIS2015.017-4	10.75	6.96	0.8	10.15			
MIS	June	2015	MIS2015.018-1A	0.5	15.89	2.69	6.9			

Location	Month	Year	Sample	Depth	$\%C_{org}$	%N	Molar C:N	$\delta^{13}C$	%S	%P
MIS	June	2015	MIS2015.018-1B	1.5	8.86	1.23	8.39		0.82	0.112
MIS	June	2015	MIS2015.018-1C	2.5	7.76	1.16	7.76		0.66	0.084
MIS	June	2015	MIS2015.018-2	4.5	4.55	0.52	10.34		0.52	0.049
MIS	June	2015	MIS2015.018-3	7.25	5.18	0.61	9.74		0.67	0.052
MIS	June	2015	MIS2015.018-4	10.25	4.82	0.56	10.07		0.61	0.057
MIS	June	2015	MIS2015.018-5	13.75	4.93	0.54	10.59		0.67	0.054
MIS	June	2015	MIS2015.019-1A	0.5	8.5	1.21	8.16		0.98	0.112
MIS	June	2015	MIS2015.019-1B	1.5	6.62	0.87	8.82		0.68	0.075
MIS	June	2015	MIS2015.019-1C	2.5	3.48	0.39	10.28		0.52	0.052
MIS	June	2015	MIS2015.019-2	4.5	4.76	0.53	10.42		0.64	0.045
MIS	June	2015	MIS2015.019-3	7.5	5.7	0.59	11.2		0.66	0.048
MIS	June	2015	MIS2015.019-4	10.75	4.48	0.49	10.5		0.61	0.052
MIS	June	2015	MIS2015.019-5	13	5.79	0.65	10.3		0.72	0.057
MIS	June	2015	MIS2015.020-1A	0.5	8.49	1.13	8.71		0.91	0.096
MIS	June	2015	MIS2015.020-1B	1.5	6.66	0.77	10.16		0.67	0.073
MIS	June	2015	MIS2015.020-1C	2.5	3.44	0.36	11.02		0.37	0.04
MIS	June	2015	MIS2015.020-2	4.5	4.71	0.52	10.46		0.59	0.047
MIS	June	2015	MIS2015.020-3	7.5	6.25	0.67	10.68		0.68	0.051
MIS	June	2015	MIS2015.020-4	10.25	5.09	0.57	10.35		0.63	0.052
LH	June	2015	LH2015.004-1A	1.5	1.7	0.21	9.37	-22.33		
LH	June	2015	LH2015.004-1B	4.5	1.15	0.13	9.65	-22.72	0.06	0.036
LH	June	2015	LH2015.004-2	7.5	0.97	0.11	10.15	-23.25	0.05	0.035
LH	June	2015	LH2015.004-3	10.5	1.71	0.18	11.15	-25.18	0.08	0.032
LH	June	2015	LH2015.004-4	13.5	0.76	0.07	12.65	-25.28	0.07	0.026
LH	June	2015	LH2015.004-5	16	0.31	0.03	10.2	-25.23	0.04	0.022
LH	June	2015	LH2015.005-1A	2	3.15	0.38	9.38	-23.27	0.2	0.048
LH	June	2015	LH2015.005-1B	6	1.26	0.13	10.99	-23.7	0.14	0.035
LH	June	2015	LH2015.005-2	9.5	0.92	0.1	10.39	-23.35	0.11	0.032
LH	June	2015	LH2015.005-3	12.5	0.37	0.04	11.27	-25.39	0.07	0.025
LH	June	2015	LH2015.006-1A	1.25	2.74	0.34	9.33	-22.77	0.1	0.053
LH	June	2015	LH2015.006-1B	4	2.24	0.28	9.16	-23.24		
LH	June	2015	LH2015.006-2	7.25	2.54	0.3	9.73	-23.12	0.14	0.045
LH	June	2015	LH2015.006-3	10.75	1.38	0.15	10.32	-23.9	0.13	0.035
LH	June	2015	LH2015.006-4	14	0.38	0.03	15.92	-24.93	0.06	0.024
LH	June	2015	LH2015.007-1A	1.5	1.75	0.21	9.72	-23.12	0.07	0.041
LH	June	2015	LH2015.007-1B	4.5	1.54	0.16	10.89	-24.34	0.07	0.037
LH	June	2015	LH2015.007-2	7.5	0.9	0.09	11.71	-23.94	0.07	0.031
LH	June	2015	LH2015.007-3	11	0.46	0.03	17.83	-25.08	0.06	0.029
LH	June	2015	LH2015.008-1A	1.5	1.75	0.21	9.37	-22.85	0.07	0.044

Location	Month	Year	Sample	Depth	$\%C_{org}$	%N	Molar C:N	$\delta^{13}C$	%S	%P
LH	June	2015	LH2015.008-1B	4.5	2.01	0.25	9.3	-23.29	0.08	0.04
LH	June	2015	LH2015.008-2	7.5	2.03	0.23	9.85	-23.06	0.08	0.04
LH	June	2015	LH2015.008-3	10.75	0.68	0.05	16.14	-25.14	0.05	0.025
LH	June	2015	LH2015.008-4	13.75	0.36	0.02	18.74	-24.83	0.05	0.025
LH	June	2015	LH2015.009-1A	1.5	1.9	0.23	9.74	-22.43		
LH	June	2015	LH2015.009-1B	5	0.4	0.03	13.9	-24.99		
LH	June	2015	LH2015.009-2	8.5	1.77	0.2	10.22	-23.36		
LH	June	2015	LH2015.009-3	11.75	1.39	0.15	10.76	-23.98		
LH	June	2015	LH2015.010-1A	1.25	2.84	0.36	9.13	-22.67		
LH	June	2015	LH2015.010-1B	3.75	2.7	0.31	9.83	-22.99		
LH	June	2015	LH2015.010-2	6.25	1.8	0.22	9.66	-23.35		
LH	June	2015	LH2015.010-3	9.25	0.69	0.06	12.68	-23.93		
LH	June	2015	LH2015.010-4	12.5	2.84	0.36	9.21	-22.69		
LH	June	2015	LH2015.011-1A	1.75	1.56	0.18	10.1	-23.28		
LH	June	2015	LH2015.011-1B	5	1.31	0.14	10.74	-23.89		
LH	June	2015	LH2015.011-2	8	0.47	0.04	13.35	-25.03		
LH	June	2015	LH2015.011-3	11.75	1.25	0.12	11.66	-24.15		

Table A2 Sample collection information and sediment iron geochemistry for Middle Island Sinkhole (MIS) and Lake Huron (LH).

Location	Month	Year	Core	Section	Sample	Depth	$\%Fe_{carb}$	$\%Fe_{ox}$	$\%Fe_{mag}$	$\%Fe_{py}$	$\%Fe_{T}$
MIS	September	2014	1	1A	MIS0914.1-1A	1	0.114	0.098	0.053	0.333	1.2
MIS	September	2014	1	1B	MIS0914.1-1B	2.5	0.086	0.102	0.06	0.503	1.34
MIS	September	2014	1	2	MIS0914.1-2	4.5	0.089	0.15	0.059	0.445	1.3
MIS	September	2014	1	3	MIS0914.1-3	7.5	0.062	0.148	0.06	0.332	1.32
MIS	September	2014	1	4	MIS0914.1-4	10	0.068	0.139	0.067	0.368	1.52
MIS	September	2014	1	5	MIS0914.1-5	13	0.086	0.141	0.068	0.473	1.53
MIS	September	2014	2	1C	MIS0914.2-1C	2.5	0.071	0.085	0.072	0.326	1.22
MIS	September	2014	2	2	MIS0914.2-2	4	0.078	0.109	0.072	0.457	1.6
MIS	September	2014	2	3	MIS0914.2-3	6	0.098	0.082	0.07	0.441	1.46
MIS	September	2014	2	4	MIS0914.2-4	8.25	0.069	0.145	0.054	0.345	1.44
MIS	September	2014	2	5	MIS0914.2-5	11	0.071	0.138	0.064	0.32	1.64
MIS	September	2014	2	6	MIS0914.2-6	12.5	0.076	0.099	0.062	0.478	1.46
MIS	September	2014	3	1C	MIS0914.3-1C	2.5	0.085	0.127	0.057	0.299	1.21
MIS	September	2014	3	2	MIS0914.3-2	4.25	0.134	0.155	0.064	0.437	1.43
MIS	September	2014	3	3	MIS0914.3-3	6.5	0.067	0.092	0.075	0.424	1.6
MIS	September	2014	3	5	MIS0914.3-5	11.5	0.072	0.075	0.063	0.305	1.55
MIS	September	2014	4	1B	MIS0914.4-1B	1.5	0.117	0.134	0.069	0.386	1.4
MIS	September	2014	4	1C	MIS0914.4-1C	2.5	0.091	0.128	0.055	0.336	1.08
MIS	September	2014	4	2	MIS0914.4-2	4	0.044	0.141	0.059	0.32	1.19
MIS	September	2014	4	3	MIS0914.4-3	6.25	0.054	0.111	0.072	0.456	1.64
MIS	September	2014	4	4	MIS0914.4-4	9	0.073	0.091	0.077	0.413	1.52
MIS	June	2015	11	1C	MIS2015.011-1C	2.5	0.153	0.087	0.082	0.397	1.47
MIS	June	2015	11	2	MIS2015.011-2	4.5	0.133	0.074	0.073	0.391	1.45
MIS	June	2015	11	3	MIS2015.011-3	7.5	0.093	0.048	0.073	0.374	1.52
MIS	June	2015	11	4	MIS2015.011-4	10.5	0.12	0.052	0.068	0.444	1.5
MIS	June	2015	11	5	MIS2015.011-5	13.5	0.099	0.05	0.078	0.382	1.66
MIS	June	2015	11	6	MIS2015.011-6	16.5	0.125	0.045	0.076	0.375	1.67
MIS	June	2015	11	7	MIS2015.011-7	19.5	0.155	0.052	0.066	0.419	1.65
MIS	June	2015	11	8	MIS2015.011-8	22.5	0.092	0.048	0.069	0.347	1.61
MIS	June	2015	16	1B	MIS2015.016-1B	1.5	0.197	0.087	0.081	0.499	1.54
MIS	June	2015	16	1C	MIS2015.016-1C	2.5	0.142	0.083	0.086	0.374	1.3
MIS	June	2015	16	2	MIS2015.016-2	5	0.159	0.051	0.067	0.337	1.3
MIS	June	2015	16	3	MIS2015.016-3	8.5	0.131	0.043	0.065	0.475	1.28
MIS	June	2015	16	4	MIS2015.016-4	11.5	0.089	0.042	0.071	0.475	1.39
MIS	June	2015	16	5	MIS2015.016-5	14.5	0.088	0.042	0.075	0.36	1.5
MIS	June	2015	16	6	MIS2015.016-6	16.75	0.129	0.042	0.076	0.463	1.51
MIS	June	2015	18	1B	MIS2015.018-1B	1.5	0.16	0.073	0.073	0.304	1.27

Location	Month	Year	Core	Section	Sample	Depth	$\%Fe_{carb}$	$\%Fe_{ox}$	$\%Fe_{mag}$	$\%Fe_{py}$	$\%Fe_{T}$
MIS	June	2015	18	1C	MIS2015.018-1C	2.5	0.111	0.069	0.078	0.385	1.34
MIS	June	2015	18	2	MIS2015.018-2	4.5	0.086	0.045	0.073	0.305	1.3
MIS	June	2015	18	3	MIS2015.018-3	7.25	0.074	0.048	0.067	0.421	1.73
MIS	June	2015	18	4	MIS2015.018-4	10.25	0.087	0.043	0.072	0.44	1.67
MIS	June	2015	18	5	MIS2015.018-5	13.75	0.111	0.047	0.079	0.509	1.66
MIS	June	2015	19	1A	MIS2015.019-1A	0.5	0.155	0.073	0.081	0.308	1.25
MIS	June	2015	19	1B	MIS2015.019-1B	1.5	0.149	0.089	0.086	0.466	1.36
MIS	June	2015	19	1C	MIS2015.019-1C	2.5	0.083	0.046	0.065	0.348	1.39
MIS	June	2015	19	2	MIS2015.019-2	4.5	0.07	0.053	0.079	0.446	1.62
MIS	June	2015	19	3	MIS2015.019-3	7.5	0.094	0.043	0.072	0.456	1.51
MIS	June	2015	19	4	MIS2015.019-4	10.75	0.083	0.045	0.08	0.501	1.61
MIS	June	2015	19	5	MIS2015.019-5	13	0.103	0.048	0.075	0.461	1.69
MIS	June	2015	20	1A	MIS2015.020-1A	0.5	0.165	0.07	0.081	0.395	1.38
MIS	June	2015	20	1B	MIS2015.020-1B	1.5	0.157	0.062	0.076	0.359	1.37
MIS	June	2015	20	1C	MIS2015.020-1C	2.5	0.087	0.038	0.052	0.463	1.04
MIS	June	2015	20	2	MIS2015.020-2	4.5	0.088	0.053	0.074	0.346	1.54
MIS	June	2015	20	3	MIS2015.020-3	7.5	0.094	0.085	0.076	0.448	1.6
MIS	June	2015	20	4	MIS2015.020-4	10.25	0.076	0.039	0.088	0.291	1.65
LH	June	2015	4	1B	LH2015.004-1B	4.5	0.023	0.065	0.054	0.091	0.97
LH	June	2015	4	2	LH2015.004-2	7.5	0.02	0.069	0.059	0.12	0.98
LH	June	2015	4	3	LH2015.004-3	10.5	0.024	0.061	0.073	0.195	1.17
LH	June	2015	4	4	LH2015.004-4	13.5	0.015	0.062	0.052	0.167	0.98
LH	June	2015	4	5	LH2015.004-5	16	0.022	0.058	0.048	0.134	0.86
LH	June	2015	5	1A	LH2015.005-1A	2	0.032	0.065	0.08	0.172	1.35
LH	June	2015	5	1B	LH2015.005-1B	6	0.031	0.06	0.061	0.2	1.09
LH	June	2015	5	2	LH2015.005-2	9.5	0.027	0.061	0.061	0.178	1
LH	June	2015	5	3	LH2015.005-3	12.5	0.018	0.056	0.043	0.144	0.87
LH	June	2015	6	1A	LH2015.006-1A	1.25	0.034	0.054	0.065	0.116	1.2
LH	June	2015	6	2	LH2015.006-2	7.25	0.046	0.074	0.058	0.174	1.09
LH	June	2015	6	3	LH2015.006-3	10.75	0.025	0.063	0.055	0.12	1.04
LH	June	2015	6	4	LH2015.006-4	14	0.02	0.086	0.048	0.164	0.84
LH	June	2015	7	1B	LH2015.007-1B	4.5	0.025	0.071	0.092	0.141	1.09
LH	June	2015	7	2	LH2015.007-2	7.5	0.029	0.05	0.056	0.156	1
LH	June	2015	7	3	LH2015.007-3	11	0.026	0.056	0.05	0.074	0.97
LH	June	2015	8	1A	LH2015.008-1A	1.5	0.031	0.102	0.059	0.06	1.12
LH	June	2015	8	1B	LH2015.008-1B	4.5	0.032	0.06	0.068	0.183	1.12
LH	June	2015	8	2	LH2015.008-2	7.5	0.03	0.066	0.07	0.154	1.16
LH	June	2015	8	3	LH2015.008-3	10.75	0.023	0.069	0.067	0.116	0.94
LH	June	2015	8	4	LH2015.008-4	13.75	0.02	0.047	0.046	0.147	0.89

Table A3 Water column dissolved Fe concentrations with depth, from Lake Huron surface down to the Middle Island Sinkhole sediment-water interface.

Depth (m)	Fe (uM)
0.0	<DL
5.0	<DL
20.0	0.07
22.5	1.14
23.0	1.88

APPENDIX B

Supplemental Methods, References, Figures, and Tables for Chapter III

Methods

For ordination methods, in order to demonstrate true variance in the data, and account for different unit scales, all variables were standardized by z-score (z_i; Equation 1):

Equation 1: $z_i = \frac{x_i - \bar{x}}{\sigma}$

where x_i is the value of a variable, and $\bar{x}$ and σ are the mean and standard deviation of all values for that variable, respectively.

Redundancy Analysis (RDA) was used to consider the ways in Middle Island Sinkhole and Lake Huron microbial assemblages constrain the variability in sediment geochemistry. RDA was carried out with the Vegan package in RStudio software version 1.1.463.

REFERENCES

Oksanen, K., Blanchet, F. G., Kindt, R., Legendre, P., Minchin, P. R., O'hara, R. B., Simpson, G. L., Solymos, P., Stevens, M. H., Wagner, H., Oksanen, M. J., 2013. Package 'vegan'. *Community ecology package, version 2.5-5*.

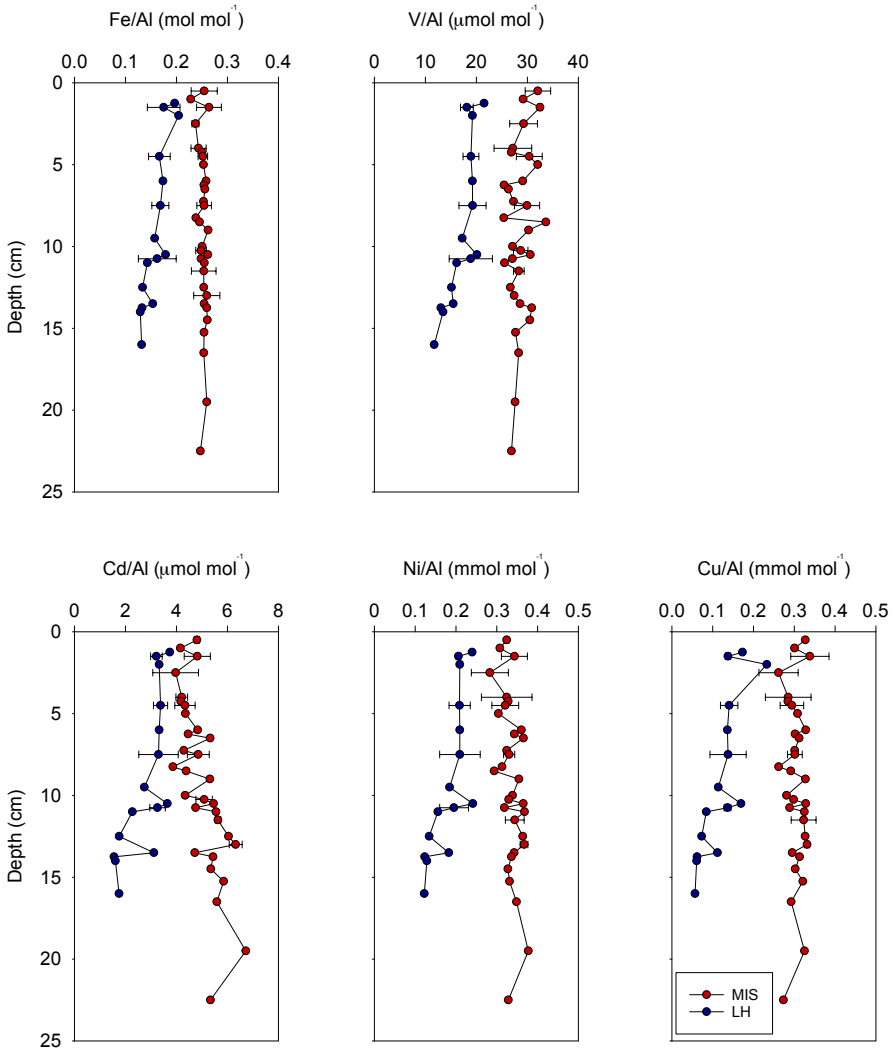

Figure B1 Al-normalized depth profiles of V, Cd, Ni, Cu, and Fe in Middle Island Sinkhole (MIS) and Lake Huron (LH) sediments (wherein the MIS profile includes the surficial microbial mat). Depths are reported as averages, with error bars representing variability (1σ) between different cores at particular depths (n = 9 for MIS, and n = 8 for LH).

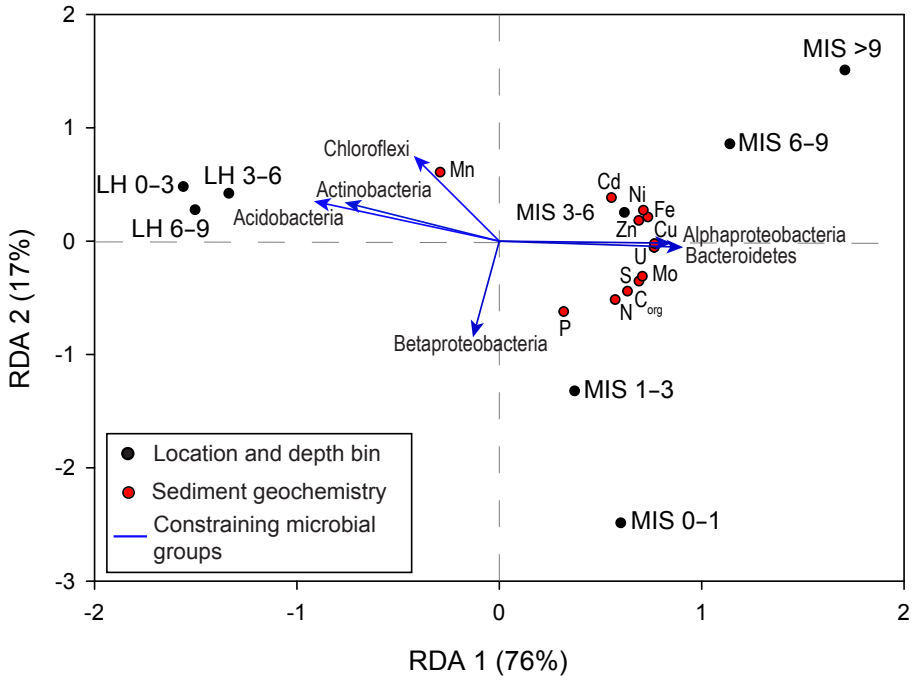

Figure B2 Redundancy analysis demonstrating the major microbial groups that constrain most of the variability in the sediment trace metal and macronutrient geochemistry. LH and MIS sediments grouped by depth bins. Macronutrient and Fe data from Rico and Sheldon (2019). Mo and U data from Rico et al. (2019). Relative abundances of major microbial groups are from Kinsman-Costello et al. (2017).

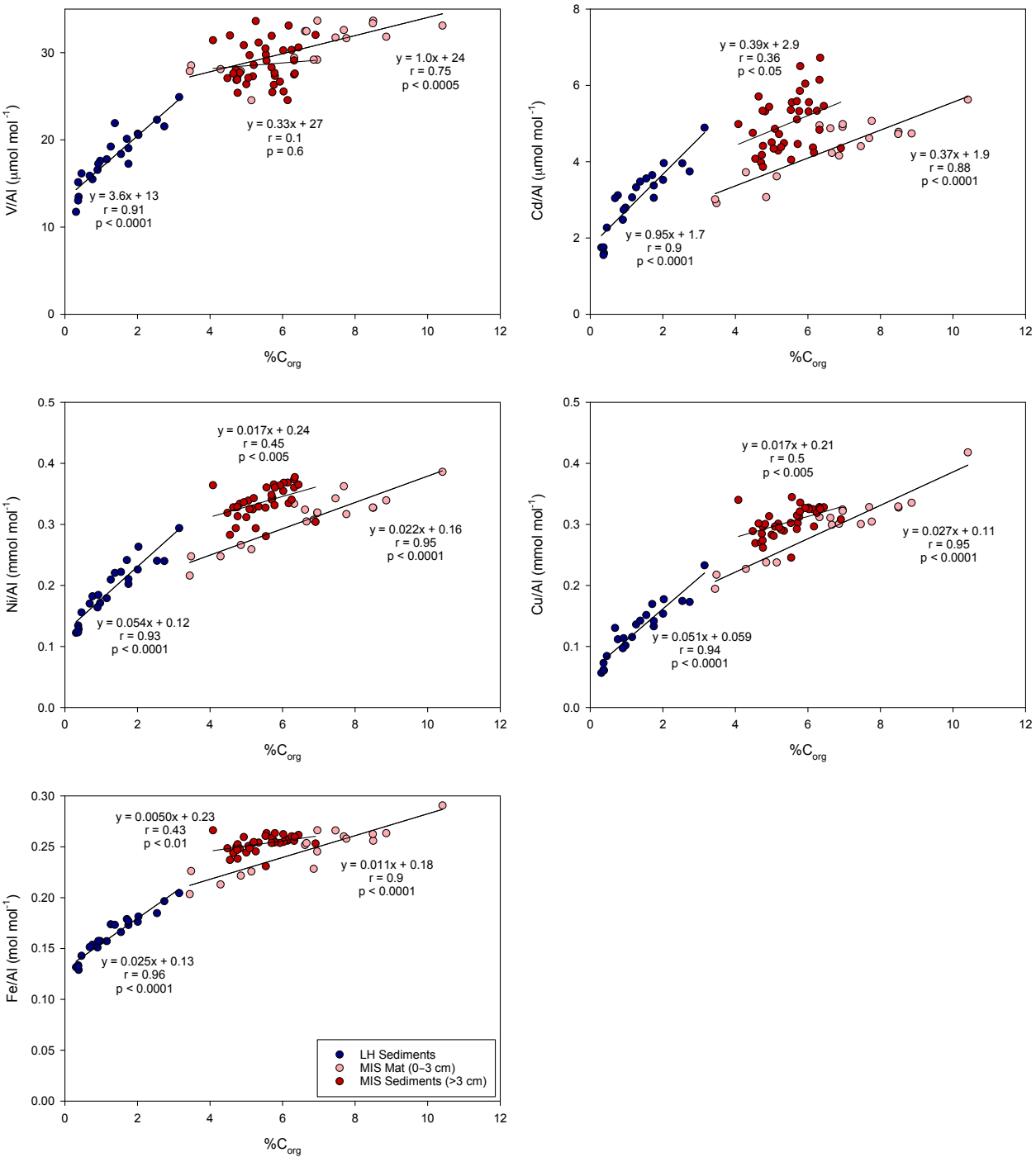

Figure B3 Correlations between Al-normalized trace metals and C_{org} for V, Cd, Ni, Cu, and Fe in Lake Huron (LH) sediments, Middle Island Sinkhole (MIS) sediments, and MIS mat. C_{org} data from Rico and Sheldon (2019).

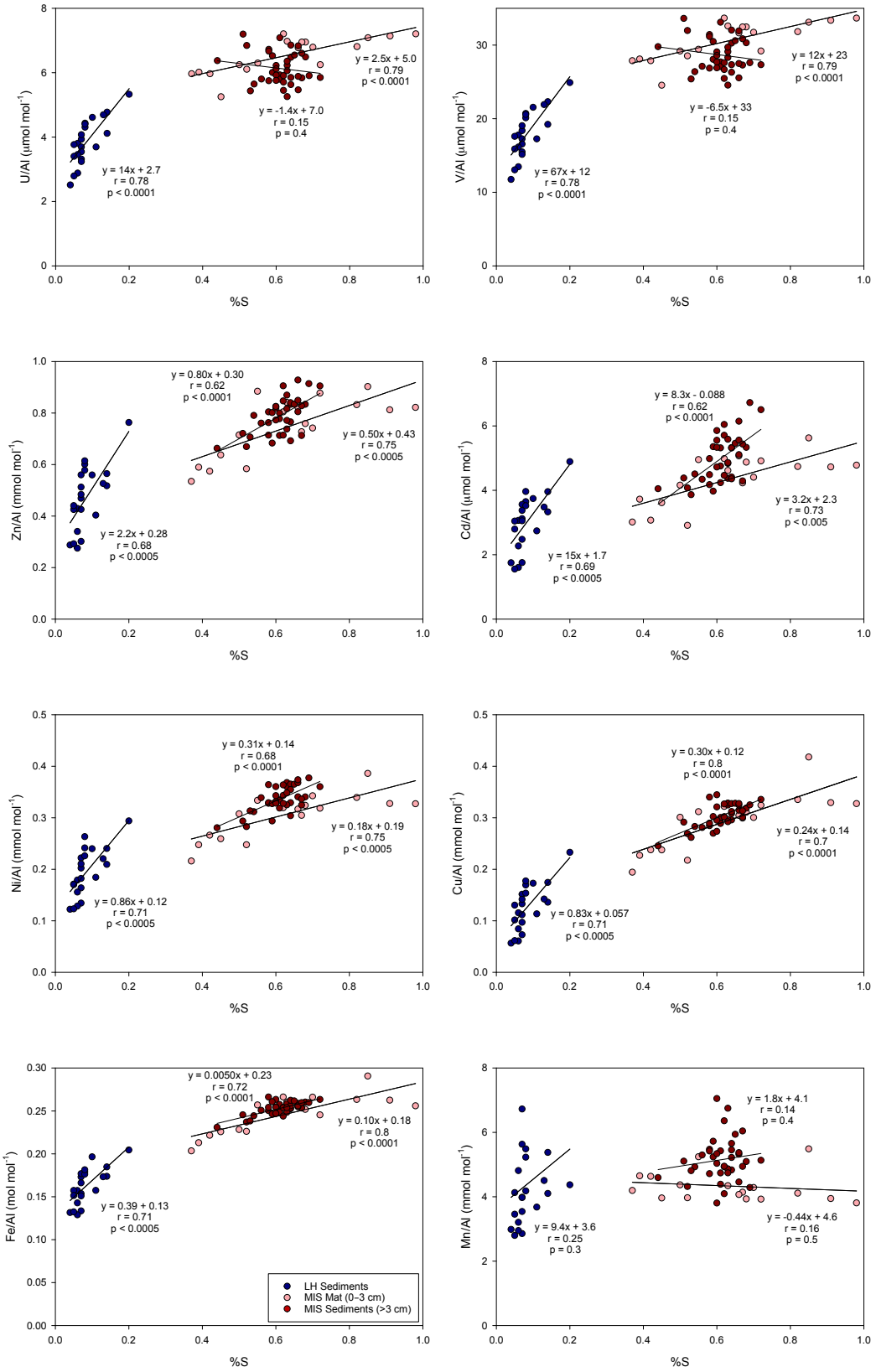

Figure B4 Correlations between Al-normalized trace metals and S for U, V, Zn, Cd, Ni, Cu, Fe, and Mn in Lake Huron (LH) sediments, Middle Island Sinkhole (MIS) sediments, and MIS mat. S data from Rico and Sheldon (2019).

Table B1 Lake Huron and Middle Island Sinkhole sediment U, V, Zn, Cd, Ni, Cu, Mn, Mo, and Al contents.

Sample ID	Depth (cm)	U (ppm)	V (ppm)	Zn (ppm)	Cd (ppm)	Ni (ppm)	Cu (ppm)	Mn (ppm)	Mo (ppm)	Al (%)
LH2015.004-1B	4.5	1	1	31	0.38	11.6	8.1	192	0.26	2.98
LH2015.004-2	7.5	1	1	31	0.35	11.2	7.2	183	0.2	3.01
LH2015.004-3	10.5	1.2	1.2	46	0.48	16.6	12.6	352	0.31	3.16
LH2015.004-4	13.5	0.9	0.9	35	0.4	12.2	8.1	343	0.25	3.08
LH2015.004-5	16	0.7	0.7	22	0.23	8.4	4.2	185	0.16	3.16
LH2015-005-1A	2	1.5	1.5	59	0.65	20.4	17.5	222	0.83	3.19
LH2015-005-1B	6	1.1	1.1	38	0.42	13.8	9.7	230	0.31	3.03
LH2015.005-2	9.5	1	1	30	0.35	12.3	8.2	189	0.27	3.07
LH2015.005-3	12.5	0.9	0.9	23	0.23	9.2	5.4	419	0.17	3.15
LH2015.006-1A	1.25	1.2	1.2	40	0.46	15.4	12	292	0.28	2.95
LH2015.006-2	7.5	1.2	1.2	39	0.47	14.9	11.7	526	0.34	2.85
LH2015.006-3	10.75	1.2	1.2	37	0.42	13.9	9.7	257	0.31	2.9
LH2015.006-4	14	0.8	0.8	21	0.21	8.8	4.5	211	0.17	3.15
LH1015.007-1A	1.5	1	1	36	0.39	13.5	9.6	253	0.25	3.07
LH2015.007-1B	4.5	1.1	1.1	43	0.47	15.3	11.3	284	0.26	3.17
LH2015.007-2	7.5	1	1	33	0.33	11.4	7.3	312	0.25	3.2
LH2015.007-3	11	1	1	27	0.31	11.1	6.5	214	0.22	3.28
LH2015.008-1A	1.5	1.1	1.1	38	0.43	14	10.2	269	0.25	3.06
LH2015.008-1B	4.5	1.2	1.2	43	0.45	15.1	11.1	253	0.25	3.07
LH2015.008-2	7.5	1.2	1.2	46	0.51	17.7	12.9	266	0.31	3.09
LH2015.008-3	10.75	0.9	0.9	32	0.38	11.1	9.2	259	0.21	3
LH2015.008-4	13.75	0.8	0.8	23	0.21	8.7	4.7	329	0.17	3.25
MIS0914.1-1A	1	1.4	1.4	44	0.44	17	18	262	0.48	2.54
MIS0914.1-1B	2.5	1.4	1.4	54	0.52	18.3	18.5	286	0.43	2.52
MIS0914.1-2	4.5	1.4	1.4	46	0.49	18.7	18.9	311	0.48	2.36
MIS0914.1-3	7.5	1.3	1.3	50	0.49	17.7	17.4	237	0.45	2.61
MIS0914.1-4	10	1.5	1.5	54	0.53	21.6	19.4	208	0.42	2.93
MIS0914.1-5	13	1.5	1.5	65	0.74	23.5	22.3	256	0.44	2.89
MIS0914.2-1C	2.5	1.4	1.4	37	0.34	15.4	14.9	337	0.37	2.66
MIS0914.2-2	4	1.4	1.4	54	0.55	24.2	23.1	232	0.47	3.02
MIS0914.2-3	6	1.5	1.5	54	0.55	21.4	21.1	307	0.51	2.73
MIS0914.2-4	8.25	1.4	1.4	50	0.47	19.9	18	324	0.42	2.92
MIS0914.2-5	11	1.5	1.5	64	0.72	24.9	23.8	183	0.47	3.11
MIS0914.2-6	12.5	1.4	1.4	61	0.7	22	21.4	357	0.43	2.78
MIS0914.3-1A	0.5	1.4	1.4	54	0.52	17.6	19.4	226	0.54	2.54
MIS0914.3-1C	2.5	1.2	1.2	40	0.39	14.6	14.5	280	0.43	2.59
MIS0914.3-2	4.25	1.4	1.4	51	0.48	19.7	18.5	404	0.44	2.76
MIS0914.3-3	6.5	1.5	1.5	61	0.67	24	22.2	244	0.43	3.02

Sample ID	Depth (cm)	U (ppm)	V (ppm)	Zn (ppm)	Cd (ppm)	Ni (ppm)	Cu (ppm)	Mn (ppm)	Mo (ppm)	Al (%)
MIS0914.3-5	11.5	1.6	1.6	63	0.73	21.9	21.8	209	0.54	3.07
MIS0914.4-1B	1.5	1.6	1.6	53	0.5	20.5	20.1	316	0.61	2.6
MIS0914.4-1C	2.5	1.3	1.3	35	0.38	13.2	13.1	203	0.37	2.45
MIS0914.4-2	4	1.4	1.4	40	0.42	15.2	14.4	233	0.43	2.49
MIS0914.4-3	6.25	1.5	1.5	54	0.58	23.3	22.2	268	0.44	3.12
MIS0914.4-4	9	1.6	1.6	57	0.62	21.6	21.6	195	0.53	2.8
MIS2015.011-1C	2.5	1.6	1.6	48	0.49	19.9	18.9	209	0.55	2.67
MIS2015.011-2	4.5	1.7	1.7	47	0.48	19.8	19	233	0.61	2.72
MIS2015.011-3	7.5	1.7	1.7	50	0.54	20.7	19.7	244	0.53	2.89
MIS2015.011-4	10.5	1.6	1.6	56	0.63	22	21.4	359	0.56	2.77
MIS2015.011-5	13.5	1.7	1.7	59	0.62	23.5	21.9	324	0.47	3.15
MIS2015.011-6	16.5	1.7	1.7	67	0.74	24.1	21.9	322	0.52	3.18
MIS2015.011-7	19.5	1.6	1.6	68	0.86	25.2	23.5	308	0.61	3.07
MIS2015.011-8	22.5	1.6	1.6	63	0.7	22.5	20.3	318	0.5	3.15
MIS2015.016-1B	1.5	1.6	1.6	56	0.6	21.5	25.2	316	0.54	2.56
MIS2015.016-1C	2.5	1.5	1.5	46	0.49	16.4	17.9	265	0.57	2.36
MIS2015.016-2	5	1.5	1.5	46	0.45	16.4	18	323	0.65	2.48
MIS2015.016-3	8.5	1.6	1.6	44	0.46	16.1	17.3	312	0.45	2.52
MIS2015.016-4	11.5	1.4	1.4	51	0.59	20	20.7	240	0.45	2.55
MIS2015.016-5	14.5	1.6	1.6	54	0.62	19.8	19.8	220	0.42	2.78
MIS2015.016-6	15.25	1.5	1.5	57	0.7	20.7	21.7	211	0.49	2.87
MIS2015.018-1B	1.5	1.4	1.4	47	0.46	17.2	18.4	251	0.48	2.33
MIS2015.018-1C	2.5	1.5	1.5	50	0.53	17.3	18	321	0.55	2.51
MIS2015.018-2	4.5	1.6	1.6	43	0.45	16.3	16.8	243	0.47	2.65
MIS2015.018-3	7.25	1.7	1.7	57	0.59	23.3	23.4	286	0.46	3.3
MIS2015.018-4	10.25	1.7	1.7	63	0.72	23.6	23	233	0.47	3.25
MIS2015.018-5	13.75	1.8	1.8	62	0.7	22.6	22.8	204	0.56	3.09
MIS2015.019-1A	0.5	1.5	1.5	47	0.47	16.8	18.2	269	0.57	2.36
MIS2015.019-1B	1.5	1.6	1.6	48	0.53	18.4	19.1	415	0.57	2.61
MIS2015.019-1C	2.5	1.6	1.6	42	0.36	16	15.2	256	0.49	2.97
MIS2015.019-2	4.5	1.6	1.6	52	0.57	22.2	21.6	319	0.43	3.1
MIS2015.019-3	7.5	1.7	1.7	55	0.6	20.9	20.9	262	0.53	2.82
MIS2015.019-4	10.75	1.6	1.6	59	0.62	21.7	21.3	311	0.47	3.13
MIS2015.019-5	13	1.6	1.6	68	0.84	24.3	24.5	302	0.46	3.1
MIS2015.020-1A	0.5	1.6	1.6	50	0.5	18.1	19.7	263	0.55	2.54
MIS2015.020-1B	1.5	1.6	1.6	46	0.46	17.3	18.4	270	0.59	2.61
MIS2015.020-1C	2.5	1.3	1.3	32	0.31	11.6	11.3	230	0.37	2.47
MIS2015.020-2	4.5	1.6	1.6	50	0.5	19.3	19.2	335	0.42	3.02
MIS2015.020-3	7.5	1.7	1.7	60	0.66	22	22.3	366	0.51	2.97

Sample ID	Depth (cm)	U (ppm)	V (ppm)	Zn (ppm)	Cd (ppm)	Ni (ppm)	Cu (ppm)	Mn (ppm)	Mo (ppm)	Al (%)
MIS2015.020-4	10.25	1.8	1.8	60	0.65	22.7	22.4	406	0.47	3.21

Table B2 Relative abundances of different major biological groups for Middle Island Sinkhole (MIS) and Lake Huron (LH) sediment depth bins. Relative abundances from Kinsman-Costello et al. (2017).

	LH 0–3 cm	LH 3–6 cm	LH 6–9 cm	MIS 0–1 cm	MIS 1–3 cm	MIS 3–6 cm	MIS 6–9 cm	MIS >9 cm
Acidobacteria	0.0558	0.0601	0.0566	0.0095	0.0158	0.0190	0.0193	0.0159
Actinobacteria	0.0193	0.0467	0.0444	0.0031	0.0062	0.0070	0.0112	0.0108
Alphaproteobacteria	0.0180	0.0184	0.0179	0.0236	0.0286	0.0297	0.0324	0.0261
Bacteroidetes	0.0780	0.0428	0.0419	0.1487	0.1985	0.2282	0.1988	0.1955
Betaproteobacteria	0.0980	0.0755	0.0698	0.1118	0.0955	0.0832	0.0700	0.0640
Chloroflexi	0.0334	0.0550	0.0566	0.0101	0.0182	0.0273	0.0368	0.0447
Chloroplast	0.0996	0.0226	0.0200	0.1045	0.0889	0.0344	0.0205	0.0119
Cyanobacteria	0.0066	0.0039	0.0033	0.2296	0.0834	0.0269	0.0263	0.0182
Deltaproteobacteria	0.1876	0.2504	0.2473	0.0861	0.1124	0.1226	0.1185	0.1206
Epsilonproteobacteria	0.0036	0.0040	0.0034	0.0417	0.0308	0.0298	0.0220	0.0241
Euryarchaeota	0.0101	0.0191	0.0242	0.0021	0.0119	0.0311	0.0447	0.0488
Firmicutes	0.0022	0.0020	0.0019	0.0410	0.0421	0.0293	0.0251	0.0227
Gammaproteobacteria	0.1013	0.0823	0.0732	0.0668	0.0779	0.0953	0.1042	0.1059
mitochondria	0.0012	0.0003	0.0004	0.0137	0.0068	0.0012	0.0008	0.0004
Nitrospirae	0.0840	0.1239	0.1364	0.0030	0.0085	0.0158	0.0211	0.0280
Other	0.1042	0.1166	0.1255	0.0395	0.0744	0.1151	0.1520	0.1684
Planctomycetes	0.0332	0.0341	0.0358	0.0087	0.0147	0.0203	0.0257	0.0282
Spirochaetes	0.0077	0.0109	0.0106	0.0272	0.0416	0.0417	0.0363	0.0395
Verrucomicrobia	0.0564	0.0313	0.0307	0.0294	0.0437	0.0420	0.0345	0.0261

APPENDIX C

Supplemental Figures, Tables, and References for Chapter IV

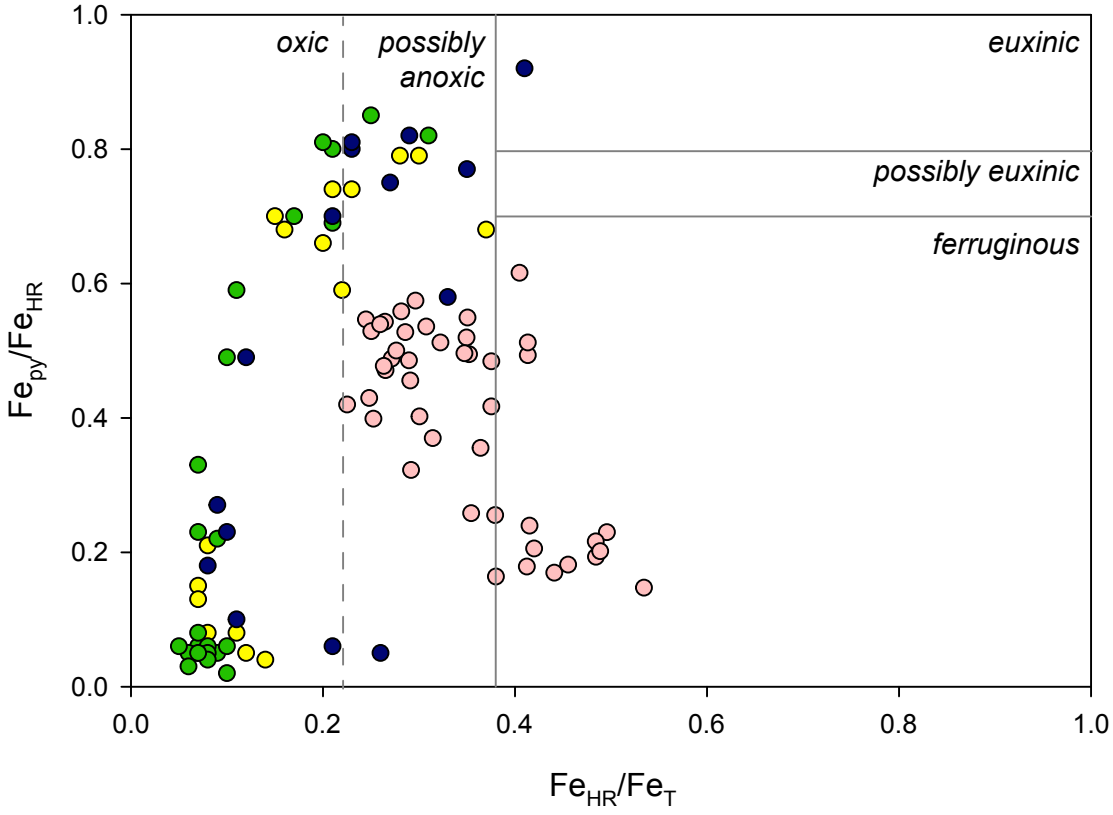

Figure C1 Cross plot of the ratios of iron in pyrite (Fepy) to highly reactive iron (FeHR) versus FeHR to total iron (FeT) for the Nonesuch Formation DO-6 (yellow circles), WPB-4 (green circles), PI-2 (blue circles) sediments. Previously published Nonesuch Formation data of Cumming et al. (2013) is included for comparison (pink circles). Because the Nonesuch Formation includes a series of rift basins (Elmore et al., 1989; Cumming et al., 2013; Gallagher et al., 2017), data from this study likely incorporates separate lake systems than that of previously published data from Cumming et al. (2013). These Fe ratios can distinguish the redox chemistries of aquatic environments as oxic, ferruginous, or euxinic (Raiswell and Canfield, 2012; Raiswell et al., 2018). Solid gray lines are recommended boundaries whereas dashed gray line is suggested only for ancient sediments (after Raiswell et al., 2018).

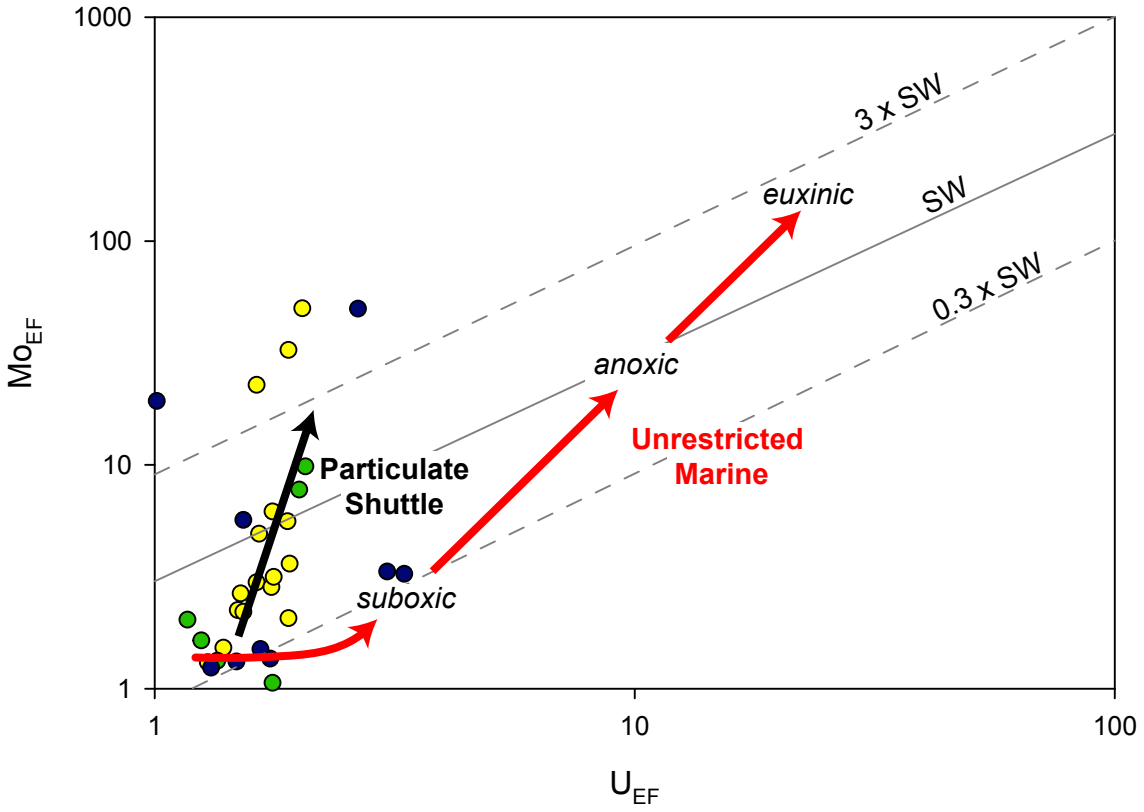

Figure C2 Cross plot of the enrichment factors of Mo and U for the Nonesuch Formation DO-6 (yellow circles), WPB-4 (green circles), PI-2 (blue circles) sediments. Diagonal lines represent the Mo:U ratio of present-day seawater and fractions thereof. Large arrows depict the particulate shuttle and unrestricted marine pathways of Mo and U deposition in marine sediments.

Figure C3. Image of a sediment core taken from the Middle Island Sinkhole (left) and a core taken from Lake Huron (right). The difference in color between the two cores can be attributed to a difference in organic matter burial, with organic C contents for MIS >2x that of LH (Nold et al., 2013; Kinsman-Costello et al., 2017; Rico & Sheldon, 2019).

Table C1 Extraction procedure[1] for the highly reactive pools of Fe.

Extraction	Main Fe minerals extracted	Terminology
(1) Sodium acetate buffered with acetic acid	Carbonate phases, e.g. siderite and ankerite	Fe_{carb}
(2) Sodium dithionite buffered with acetic acid and sodium citrate	Crystalline oxides, e.g. goethite and hematite	Fe_{ox}
(3) Ammonium oxalate buffered with ammonium hydroxide	Magnetite	Fe_{mag}
(4) Chromous chloride sulfur reduction titrated with potassium iodate	Pyrite	Fe_{py}

[1]Fe extraction protocols follow Poulton and Canfield (2005) for (1)–(3) and Canfield et al. (1986) for (4).

Table C2 Middle Island Sinkhole, Lake Huron, and Nonesuch Formation sediment Mo, U, and Al contents; Nonesuch Formation Fe, S, P, and organic C contents

Sample ID	Mo (ppm)	U (ppm)	Al (%)	Fe (%)	S (%)	P (ppm)	Organic C (%)
Middle Island Sinkhole							
MIS0914.1-1A	0.48	1.4	2.54				
MIS0914.1-1B	0.43	1.4	2.52				
MIS0914.1-2	0.48	1.4	2.36				
MIS0914.1-3	0.45	1.3	2.61				
MIS0914.1-4	0.42	1.5	2.93				
MIS0914.1-5	0.44	1.5	2.89				
MIS0914.2-C	0.37	1.4	2.66				
MIS0914.2-2	0.47	1.4	3.02				
MIS0914.2-3	0.51	1.5	2.73				
MIS0914.2-4	0.42	1.4	2.92				
MIS0914.2-5	0.47	1.5	3.11				
MIS0914.2-6	0.43	1.4	2.78				
MIS0914.3-1A	0.54	1.4	2.54				
MIS0914.3-1C	0.43	1.2	2.59				
MIS0914.3-2	0.44	1.4	2.76				
MIS0914.3-3	0.43	1.5	3.02				
MIS0914.3-5	0.54	1.6	3.07				
MIS0914.4-1B	0.61	1.6	2.6				
MIS0914.4-1C	0.37	1.3	2.45				
MIS0914.4-2	0.43	1.4	2.49				
MIS0914.4-3	0.44	1.5	3.12				
MIS0914.4-4	0.53	1.6	2.8				
MIS2015.011-1C	0.55	1.6	2.67				
MIS2015.011-2	0.61	1.7	2.72				
MIS2015.011-3	0.53	1.7	2.89				
MIS2015.011-4	0.56	1.6	2.77				
MIS2015.011-5	0.47	1.7	3.15				
MIS2015.011-6	0.52	1.7	3.18				
MIS2015.011-7	0.61	1.6	3.07				
MIS2015.011-8	0.50	1.6	3.15				
MIS2015.016-1B	0.54	1.6	2.56				
MIS2015.016-1C	0.57	1.5	2.36				
MIS2015.016-2	0.65	1.5	2.48				
MIS2015.016-3	0.45	1.6	2.52				
MIS2015.016-4	0.45	1.4	2.55				
MIS2015.016-5	0.42	1.6	2.78				

Sample ID	Mo (ppm)	U (ppm)	Al (%)	Fe (%)	S (%)	P (ppm)	Organic C (%)
MIS2015.016-6	0.49	1.5	2.87				
MIS2015.018-1B	0.48	1.4	2.33				
MIS2015.018-1C	0.55	1.5	2.51				
MIS2015.018-2	0.47	1.6	2.65				
MIS2015.018-3	0.46	1.7	3.3				
MIS2015.018-4	0.47	1.7	3.25				
MIS2015.018-5	0.56	1.8	3.09				
MIS2015.019-1A	0.57	1.5	2.36				
MIS2015.019-1B	0.57	1.6	2.61				
MIS2015.019-1C	0.49	1.6	2.97				
MIS2015.019-2	0.43	1.6	3.1				
MIS2015.019-3	0.53	1.7	2.82				
MIS2015.019-4	0.47	1.6	3.13				
MIS2015.019-5	0.46	1.6	3.1				
MIS2015.020-1A	0.55	1.6	2.54				
MIS2015.020-1B	0.59	1.6	2.61				
MIS2015.020-1C	0.37	1.3	2.47				
MIS2015.020-2	0.42	1.6	3.02				
MIS2015.020-3	0.51	1.7	2.97				
MIS2015.020-4	0.47	1.8	3.21				
Lake Huron							
LH2015.004-1B	0.26	1	2.98				
LH2015.004-2	0.20	1	3.01				
LH2015.004-3	0.31	1.2	3.16				
LH2015.004-4	0.25	0.9	3.08				
LH2015.004-5	0.16	0.7	3.16				
LH2015-005-1A	0.83	1.5	3.19				
LH2015-005-1B	0.31	1.1	3.03				
LH2015.005-2	0.27	1	3.07				
LH2015.005-3	0.17	0.9	3.15				
LH2015.006-1A	0.28	1.2	2.95				
LH2015.006-2	0.34	1.2	2.85				
LH2015.006-3	0.31	1.2	2.9				
LH2015.006-4	0.17	0.8	3.15				
LH1015.007-1A	0.25	1	3.07				
LH2015.007-1B	0.26	1.1	3.17				
LH2015.007-2	0.25	1	3.2				
LH2015.007-3	0.22	1	3.28				
LH2015.008-1A	0.25	1.1	3.06				

Sample ID	Mo (ppm)	U (ppm)	Al (%)	Fe (%)	S (%)	P (ppm)	Organic C (%)
LH2015.008-1B	0.25	1.2	3.07				
LH2015.008-2	0.31	1.2	3.09				
LH2015.008-3	0.21	0.9	3				
LH2015.008-4	0.17	0.8	3.25				
Nonesuch Formation							
DO-6-51-2	0.44	3.1	7.2	5.49	0.99	630	1.46
DO-6-51-3-B	0.52	3	7.5	5.41	1.10	640	0.72
DO-6-51-5	2.25	3.7	6.24	4.46	1.39	730	1.09
DO-6-51-9	2.15	1.9	3.48	2.34	0.91	510	0.26
DO-6-52-3	4.11	4.3	7.35	4.69	1.44	750	1.70
DO-6-52-6	1.6	3.3	7.13	4.59	0.77	810	0.39
DO-6-52-9	2.24	3.8	7.52	4.65	0.91	750	1.63
DO-6-53-3	1.93	3.4	7.27	4.45	0.42	710	0.30
DO-6-53-6	1.48	3.2	6.73	4.43	0.64	820	0.28
DO-6-53-9	1.99	3.8	7	4.82	0.68	820	0.45
DO-6-54-3	0.85	2.4	5.59	4.00	0.57	840	0.33
DO-6-54-6	0.91	2.6	4.42	3.08	0.59	810	0.64
DO-6-54-7-B	1.44	2.5	4.57	3.44	0.79	920	0.52
DO-6-54-9	23	2.9	4.6	3.28	0.83	770	0.55
DO-6-55-3	11.6	2.1	3.56	2.81	0.93	740	0.36
DO-6-55-6	0.21	2.7	6.11	4.21	0.03	840	0.02
DO-6-55-9	0.2	2.4	6.58	4.59	0.02	770	0.03
DO-6-56-3	0.19	2.2	6.42	3.83	0.01	800	0.06
DO-6-56-6	0.25	3	6.32	4.57	0.02	930	0.03
DO-6-56-9	0.21	2.3	6.97	4.96	0.03	740	0.04
DO-6-57-3	0.28	2.7	7.17	5.10	0.04	830	0.04
DO-6-57-6	0.26	2.5	6.97	5.41	0.02	800	0.03
DO-6-57-9	3.27	3.4	6.66	4.75	0.80	860	0.37
DO-6-58-4	0.18	2	6.02	4.19	0.01	700	0.04
DO-6-58-6	0.17	1.9	5.97	3.57	0.01	690	0.03
DO-6-58-9	0.19	2.3	6.92	4.72	0.01	780	0.03
DO-6-59-2	0.12	1.8	5.26	2.65	0.10	660	0.04
DO-6-59-4-B	0.17	1.9	6.61	4.29	0.06	770	0.04
DO-6-59-6	0.23	2.2	6.46	4.04	0.09	780	0.04
DO-6-59-9	0.3	2.5	7.27	4.87	0.33	790	0.13
DO-6-60-3	0.23	2.4	7.41	6.06	0.05	840	0.05
DO-6-60-6	0.43	2.8	7.31	5.83	0.22	850	0.09
DO-6-60-9	0.23	1.7	6.49	4.87	0.02	640	0.02
DO-6-61-3	0.3	2.4	7.04	5.17	0.13	780	0.06
DO-6-61-6	0.95	2.9	7.26	5.91	0.51	830	0.08
DO-6-61-9	16.65	3.7	7.31	5.60	1.92	880	0.61

Sample ID	Mo (ppm)	U (ppm)	Al (%)	Fe (%)	S (%)	P (ppm)	Organic C (%)
DO-6-62-3	0.27	2.3	6.7	4.72	0.03	750	0.02
WPB-4-6-1	0.35	3	6.95	4.24	0.01	650	0.05
WPB-4-6-5	0.25	2.8	6.51	4.12	0.01	730	0.05
WPB-4-7-3	0.25	3.3	7.17	4.23	0.01	750	0.04
WPB-4-8-1	1.4	3.3	8.54	5.16	0.03	570	0.11
WPB-4-8-2	1.56	2.8	7.7	4.76	0.88	730	0.58
WPB-4-8-5	0.27	3.1	8.53	6.07	0.01	770	0.04
WPB-4-9-3	0.34	4	4.71	3.69	0.05	1050	0.02
WPB-4-10-1	0.24	2.9	6.83	5.19	0.01	740	0.03
WPB-4-10-5	0.31	3.2	7.85	4.94	0.01	720	0.04
WPB-4-11-3	0.35	3.1	7.84	4.53	0.01	780	0.04
WPB-4-12-1	0.34	3.2	8.01	5.00	0.01	750	0.05
WPB-4-12-5	0.25	2.7	6.28	3.75	0.01	810	0.03
WPB-4-13-3	0.45	3.2	8.48	4.67	0.02	800	0.04
WPB-4-14-1	0.82	3.8	8.38	5.40	0.86	700	0.32
WPB-4-14-5	8.14	5.3	8.29	6.98	2.44	820	2.03
WPB-4-15-3	0.3	3.1	8.38	5.38	0.01	830	0.04
WPB-4-16-1	0.24	3.1	8.33	4.14	0.05	820	0.12
WPB-4-16-5	0.27	3	7.09	5.22	0.01	940	
WPB-4-17-3	0.25	2.8	7.74	4.61	0.00	830	0.04
WPB-4-18-1	0.3	3.2	6.73	4.79	0.01	990	0.04
WPB-4-18-5	0.27	3.2	6.77	3.67	0.01	940	0.03
WPB-4-19-3	0.31	3.4	8.89	5.85	0.02	800	0.08
WPB-4-20-1	0.25	2.9	6.97	4.40	0.01	890	0.04
WPB-4-20-5	0.3	3.7	8.1	3.84	0.04	1050	0.06
WPB-4-21-3	0.52	5.3	8.16	5.73	0.49	890	0.13
WPB-4-22-2	0.19	2.5	6.47	3.56	0.01	690	0.04
WPB-4-22-5	0.26	3.2	8.52	5.35	0.01	780	0.05
WPB-4-23-3	0.22	2.8	6.86	3.58	0.01	830	0.04
WPB-4-24-1	0.7	3.6	6.6	4.02	0.76	720	0.16
WPB-4-24-5	5.75	4.6	7.43	5.19	1.49	850	0.52
WPB-4-25-3	0.26	3.1	7.56	5.09	0.05	900	0.07
WPB-4-26-1	0.49	3.1	8.47	5.99	0.19	990	0.17
WPB-4-26-3	0.61	3.4	7.31	5.61	1.17	740	0.50
WPB-4-26-5	1.05	3.3	7.91	5.99	1.22	760	0.33
WPB-4-27-3	0.4	2.5	8.01	7.68	0.05	920	0.08
WPB-4-28-1	0.24	3.2	7.76	4.82	0.31	750	0.16
WPB-4-28-5	0.27	2.3	7.6	7.03	0.02	1000	0.03
WPB-4-29-3	0.3	2.7	8.07	6.26	0.04	940	0.08
WPB-4-30-1	0.38	2.8	7.41	5.35	0.03	1080	0.08
WPB-4-30-5	0.25	2.8	7.96	6.90	0.06	960	0.00

Sample ID	Mo (ppm)	U (ppm)	Al (%)	Fe (%)	S (%)	P (ppm)	Organic C (%)
WPB-4-31-3	0.3	2.2	7.11	6.11	0.02	910	0.05
WPB-4-32-1	0.58	1.5	7.08	9.39	0.01	1470	0.03
WPB-4-32-5	0.33	2.2	7.57	6.81	0.06	910	
WPB-4-33-3	0.31	2.4	7.44	8.51	0.03	970	0.09
WPB-4-34-2	0.36	1.8	6.9	7.14	0.01	1070	0.03
WPB-4-34-5	0.53	1.3	6.61	8.19	0.03	1330	0.03
WPB-4-35-3	0.47	1.9	7.63	6.66	0.31	990	0.07
WPB-4-36-1	0.37	2.2	7.7	6.72	0.12	1050	0.13
WPB-4-36-5	0.75	1.4	6.66	10.05	0.11	1280	0.02
WPB-4-37-2	0.47	1.8	6.59	4.52	0.05	1440	0.04
WPB-4-38-1	0.21	2.6	7.55	7.09	0.11	780	0.08
PI-2-6-5	0.25	2.6	7.77	4.25	0.04	1540	0.03
PI-2-8-5	0.23	2.9	10	6.34	0.03	740	0.06
PI-2-10-4-B	16.6	2.7	8.62	7.54	2.57	700	0.48
PI-2-10-5	6.47	2.5	8.31	7.02	2.46	690	0.74
PI-2-13-5	0.28	3.5	6.24	5.18	0.02	990	0.02
PI-2-15-5	0.23	2.7	7.55	4.36	0.01	810	0.03
PI-2-17-5	0.23	2.3	5.56	3.21	0.02	630	0.01
PI-2-20-5	0.22	4.7	6.66	2.75	0.01	950	0.03
PI-2-23-5	0.25	3.3	7.65	4.53	0.01	900	0.03
PI-2-25-5	0.23	2.3	6.75	4.26	0.02	940	0.02
PI-2-27-5	0.23	3.4	9.11	4.36	0.08	730	0.05
PI-2-30-4	0.22	3.2	9.17	5.31	0.01	780	0.05
PI-2-32-5	1.04	3.6	7.87	4.44	0.02	970	0.03
PI-2-35-5	0.58	3.1	9.43	5.51	0.30	650	0.16
PI-2-35-6-B	4.4	3.7	7.78	6.26	1.72	790	0.91
PI-2-36-5	40	6.6	8.03	5.94	2.21	870	1.28
PI-2-37-5	1.66	4.7	4.98	3.63	1.02	840	0.00
PI-2-40-5	0.92	3	7.41	5.26	0.96	730	0.31
PI-2-42-5	0.42	3.8	8.25	6.26	0.53	900	0.24
PI-2-43-4-B	1.11	4.4	8.17	5.66	0.53	960	0.44
PI-2-44-5	0.27	2.3	8.58	7.53	0.03	1020	0.08
PI-2-47-5	2.5	7.9	7.7	5.91	1.50	820	0.75
PI-2-48-2-B	0.9	3.1	6.02	4.83	1.29	940	0.35
PI-2-49-3	0.52	2.5	7.62	6.62	0.03	1110	0.05
PI-2-52-2	0.35	2.4	5.9	4.79	0.03	960	0.04

Table C3 Nonesuch Formation sediment Fe speciation data.

Sample ID	Fe_{carb} (%)	Fe_{ox} (%)	Fe_{mag} (%)	Fe_{py} (%)	Fe_T (%)
Nonesuch Formation					
DO6-50-6	0.01	0.47	0.48	0.04	6.89
DO6-51-2	0.06	0.20	0.12	0.74	5.49
DO6-51-3B	0.05	0.15	0.10	0.84	5.41
DO6-52-3	0.03	0.09	0.16	1.05	4.69
DO6-53-3	0.04	0.11	0.07	0.47	4.45
DO6-53-9	0.04	0.12	0.06	0.52	4.82
DO6-54-7B	0.05	0.09	0.07	0.60	3.44
DO6-55-3	0.10	0.09	0.14	0.72	2.81
DO6-56-6	0.06	0.12	0.11	0.08	4.57
DO6-57-6	0.05	0.15	0.13	0.06	5.41
DO6-57-9	0.04	0.16	0.22	0.62	4.75
DO6-59-4B	0.08	0.12	0.22	0.04	4.29
DO6-60-3	0.07	0.20	0.14	0.02	6.06
DO6-61-3	0.07	0.16	0.13	0.03	5.17
DO6-61-9	0.05	0.23	0.08	1.35	5.60
DO6-62-3	0.06	0.12	0.13	0.04	4.72
DO6-62-9	0.01	0.15	0.18	0.02	2.94
WPB4-6-1	0.06	0.12	0.10	0.02	4.24
WPB4-8-1	0.06	0.15	0.09	0.02	5.16
WPB4-8-2	0.07	0.17	0.08	0.69	4.76
WPB4-9-3	0.06	0.12	0.15	0.02	3.69
WPB4-11-3	0.05	0.15	0.16	0.02	4.53
WPB4-13-3	0.04	0.16	0.15	0.02	4.67
WPB4-14-1	0.05	0.14	0.09	0.66	5.40
WPB4-14-5	0.06	0.20	0.10	1.61	6.38
WPB4-15-3	0.05	0.20	0.16	0.02	5.38
WPB4-17-3	0.05	0.11	0.14	0.01	4.61
WPB4-19-3	0.03	0.16	0.17	0.01	5.85
WPB4-21-3	0.06	0.10	0.10	0.37	5.73
WPB4-23-3	0.03	0.10	0.10	0.02	3.58
WPB4-24-5	0.05	0.08	0.06	1.12	5.19
WPB4-25-3	0.07	0.08	0.08	0.11	5.09
WPB4-26-3	0.06	0.09	0.08	0.95	5.61
WPB4-26-5	0.07	0.09	0.07	0.97	5.99
WPB4-28-1	0.06	0.11	0.08	0.23	4.82
WPB4-28-5	0.09	0.10	0.14	0.02	7.03
WPB4-30-5	0.09	0.16	0.14	0.12	6.90

Sample ID	Fe_{carb} (%)	Fe_{ox} (%)	Fe_{mag} (%)	Fe_{py} (%)	Fe_T (%)
WPB4-32-5	0.08	0.18	0.23	0.14	6.81
WPB4-34-5	0.11	0.28	0.37	0.05	8.19
WPB4-36-5	0.11	0.40	0.47	0.02	10.05
PI2-6-5	0.03	0.00	0.30	0.10	4.25
PI2-8-5	0.04	0.26	0.30	0.07	6.34
PI2-10-4B	0.09	0.15	0.16	1.82	7.54
PI2-10-5	0.08	0.03	0.12	2.63	7.02
PI2-13-5	0.07	0.37	0.57	0.06	5.18
PI2-17-5	0.01	0.25	0.53	0.04	3.21
PI2-20-5	0.02	0.07	0.09	0.04	2.75
PI2-27-5	0.03	0.13	0.12	0.10	4.36
PI2-35-6B	0.08	0.11	0.24	1.28	6.26
PI2-36-5	0.07	0.08	0.32	1.58	5.94
PI2-37-5	0.34	0.09	0.08	0.69	3.63
PI2-40-5	0.08	0.08	0.17	0.77	5.26
PI2-42-5	0.10	0.12	0.16	0.37	6.26
PI2-47-5	0.08	0.09	0.10	1.07	5.91
PI2-48-2B	0.06	0.06	0.09	0.90	4.83

Table C4 Water column Mo and U concentrations at three stations within Lake Superior.

Station	Depth	Mo (ppb)	U (ppb)
1	0	0.134	0.04
1	25	0.128	0.038
1	50	0.129	0.041
1	75	0.144	0.04
1	100	0.158	0.04
1	125	0.149	0.042
1	150	0.13	0.039
1	175	0.134	0.041
1	200	0.128	0.037
1	225	0.148	0.04
2	0	0.129	0.041
2	12	0.13	0.041
2	24	0.13	0.039
2	36	0.15	0.042
2	48	0.155	0.042
2	60	0.126	0.041
2	72	0.149	0.042
2	84	0.133	0.042
2	96	0.145	0.041
2	108	0.127	0.04
3	0	0.132	0.041
3	35	0.129	0.038
3	70	0.127	0.04
3	105	0.127	0.042
3	140	0.127	0.04
3	175	0.134	0.041
3	210	0.125	0.039
3	245	0.127	0.039
3	280	0.128	0.04
3	315	0.133	0.041

REFERENCES

Canfield, D. E., Raiswell, R., Westrich, J. T., Reaves, C. M., Berner, R. A., 1986. The use of chromium reduction in the analysis of reduced inorganic sulfur in sediments and shales. Chem. Geol. 54, 149–155. http://doi.org/10.1016/0009-2541(86)90078-1

Cumming, V. M., Poulton, S. W., Rooney, A. D., Selby, D., 2013. Anoxia in the terrestrial environment during the late Mesoproterozoic. Geology 41, 583–586. http://doi.org/10.1130/G34299.1

Elmore, R. D., Milavec, G. J., Imbus, S. W., Engel, M. H., 1989. The Precambrian nonesuch formation of the North American mid-continent rift, sedimentology and organic geochemical aspects of lacustrine deposition. Precam. Res., 43, 191–213. http://doi.org/10.1016/0301-9268(89)90056-9

Gallagher, T. M., Sheldon, N. D., Mauk, J. L., Petersen, S. V., Gueneli, N., Brocks, J. J., 2017. Constraining the thermal history of the North American Midcontinent Rift System using carbonate clumped isotopes and organic thermal maturity indices. Precam. Res., 294, 53–66. http://doi.org/10.1016/j.precamres.2017.03.022

Kinsman-Costello, L.E., Sheik, C.S., Sheldon, N.D., Burton, G. a., Costello, D., Marcus, D.N., Uyl, P. Den, Dick, G.J., 2017. Groundwater shapes sediment biogeochemistry and microbial diversity in a submerged sinkhole. Geobiology 15, 225–239. https://doi.org/10.1038/nature04068

Nold, S.C., Bellecourt, M.J., Kendall, S.T., Ruberg, S. A., Sanders, T.G., Klump, J.V., Biddanda, B. A., 2013. Underwater sinkhole sediments sequester Lake Huron's carbon. Biogeochemistry 115, 235–250. https://doi.org/10.1007/s10533-013-9830-8

Poulton, S., Canfield, D. E., 2005. Development of a sequential extraction procedure for iron: implications for iron partitioning in continentally derived particulates. Chem. Geol., 214, 209–221. http://doi.org/10.1016/j.chemgeo.2004.09.003

Raiswell R., Canfield D.E, 2012. The iron biogeochemical cycle past and present. Geochem. Persp., 1, 1–220.

Raiswell, R., Hardisty, D.S., Lyons, T.W., Canfield, D.E., Owens, J.D., Planavsky, N.J., Poulton, S.W., Reinhard, C.T., 2018. The iron paleoredox proxies: A guide to the pitfalls, problems and proper practice. Am. J. Sci. 318, 491–526. https://doi.org/10.2475/05.2018.03

Rico, K. I., Sheldon, N. D., 2019. Nutrient and iron cycling in a modern analogue for the redoxcline of a Proterozoic ocean shelf. Chem. Geol., 511, 42–50. http://doi.org/10.1016/j.chemgeo.2019.02.032